2004

Monitoring and modeling human interactions with ecosystems

Cristina Milesi
The University of Montana

Maureen and Mike
MANSFIELD LIBRARY

The University of

Montana

Permission is granted by the author to reproduce this material in its entirety, provided that this material is used for scholarly purposes and is properly cited in published works and reports.

Please check "Yes" or "No" and provide signature

Yes, I grant permission $\checkmark$ Yes

No, I do not grant permission   _____

Author's Signature: _Cristina Tilea_

Date: _April 16, 2004_

Any copying for commercial purposes or financial gain may be undertaken only with the author's explicit consent.

8/98

MONITORING AND MODELING
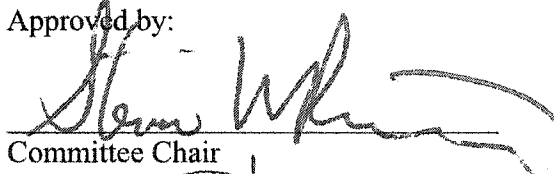# HUMAN INTERACTIONS WITH ECOSYSTEMS

by

Cristina Milesi

B.S. Biological Sciences, University of Trieste

Presented in partial fulfillment of the requirements for the degree of
Doctor of Philosophy
The University of Montana
2004

Approved by:

_____
Committee Chair

_____
Dean, Graduate School

4-28-04
_____
Date

Abstract

CRISTINA MILESI, Ph.D., April 2004, FORESTRY

Monitoring And Modeling Human Interactions With Ecosystems

Committee Chair Dr. Steven W. Running

With rapidly increasing consumption rates and global population, there is a growing interest in understanding how to balance human activities with the other components of the Earth system. Humans alter ecosystem functioning with land cover changes, greenhouse gas emissions and overexploitation of natural resources. On the other side, climate and its inherent interannual variability drive global Net Primary Productivity (NPP), the base of energy for all trophic levels, shaping humans' distribution on the land surface and their sensitivity to natural and accelerated patterns of variation in ecosystem processes.

In this thesis, I analyzed anthropogenic influences on ecosystems and ecosystems impacts on humans through a multi-scale approach. Anthropogenic influences were analyzed with a special focus on urban ecosystems, the living environment of nearly half of the global population and almost 90% of the population in the industrialized countries. A poorly quantified aspect of urban ecosystems is the biogeochemistry of urban vegetation, intensively managed through fertilization and irrigation. In chapter 1, adapting the ecosystem model Biome-BGC, I simulated the growth of turf grasses across the United States, and estimated their potential impact on the continental water and carbon budget. Using a remote sensing-based approach, I also developed a methodology to estimate the impact of land cover changes due to urbanization on the regional photosynthetic capacity (chapter 2), finding that low-density urbanization can retain high levels of net primary productivity, although at the expense of inefficient sprawl. One of the feedbacks of urbanization is the urban heat island effect, which I analyzed in conjunction with a remote sensing based estimate of fractional impervious surface area, showing how this is related to increases in land surface temperatures, independently from geographic location and population density (chapter 3). Finally, in chapter 4, I described the distribution of the global human population as a function of terrestrial NPP and its variability, showing that the median person lives at above average levels of NPP but that almost half of the total population lives in regions significantly affected by climatically induced variability in NPP.

Acknowledgements

My sincere thanks go to my cheerful advisor, Dr. Steve Running, who saved me from a hopeless academic future in Italy and who gave me absolute freedom to pursue my research. I also thank my committee members for their time and advice. The present and past NTSG members I ran across to during these five years all provided a fun and creative environment. In particular, Galina Churkina has been an inspiring first officemate, while Alisa Keyser and Mike White introduced me to the finest aspects of the American lifestyle. I thank Young-ee Cho for her impressive office manager skills and for her friendship. Saxon Holbrook and the computing facility team simplified my life with their prompt and expert support. Many thanks to the numerous friends and colleagues who, at different stages, helped me by editing papers and chapters (Karey Shaffer, Faith Ann Heinsch, Kirsten Schmidt, Eva Karau, Alana Oakins). Ramakrishna Nemani has given me invaluable guidance. Everyone who babysat and entertained Angelica while I was trying to get some work done has provided tremendous help. Last but not least, lots of thanks to my family and friends, here and abroad, for their support during the darkest hours.

Preface

Throughout my PhD I have been interested in the analysis of how people contribute to and are impacted by global environmental change from the point of view of ecosystems processes. Building upon the research of past and present members of the Numerical Terradynamic Simulation Group (NTSG) and other colleagues, I experimented with ways to extend the science of ecosystem analysis, traditionally researching mainly "natural" ecosystems, to the human living environment. Focusing on urbanization and the distribution of population, my research has encompassed a number of spatial scales, ranging from a house's yard to the globe, and presents examples of how humans alter ecosystems, how these alterations feed back upon humans, and how ecosystem dynamics shapes people's living environment and sensitivity to change. In other words, the research here quantifies aspects of people's effects on the environment and of the effects of the environment on people.

Description of Chapter 1

This chapter analyzes an ecological aspect of urbanization common to many Anglo-Saxon countries, but most prevalent in the United States in terms of total surface affected, maintenance industry it generates and amount of time dedicated by individuals: the passion for a lawn.

The pervasive presence of lawns across the suburban American landscape, from residential homes, parks, schools, commercial buildings and golf courses, stems mainly from the combination of two factors: the planning of low density urban development and a culture of neat and clean *curb appeal*. But, if every square meter of surface cultivated with turf grasses in the United States were to look like the perfect lawn, how much water would we need to sprinkle across the 48 states? And if we were to send all the clippings to the landfill, would a lawn be a source or a sink of carbon? And how much surface under turf grasses is there, anyway, in the continental United States? These are the questions that chapter 1 attempts to answer and that supported the last three years of my studies with a NASA Earth System Science funded fellowship.

iv

Description of Chapter 2

In general, urban vegetation is not only made up of lawns. Depending mainly on the climate and the type of dominant vegetation surrounding a certain city, urban vegetation includes also a varying amount of trees, which eventually give the urban areas the appearance of a savanna. Because of the intense fertilization and irrigation management, urban vegetation tends to be characterized by a high productivity, which can compensate, to a certain extent, for the loss in photosynthetic capacity due to the presence of buildings and infrastructure. The extent of this compensation depends on the type of land cover change caused by urbanization, i.e. whether the paving takes place where there used to be cropland or forest.

Chapter 2 takes a regional perspective to propose a remote sensing based methodology for the estimation of the impact of urbanization on ecosystem net primary productivity (NPP), the net amount of carbon fixed by vegetation through the process of photosynthesis. I developed the methodology using as the study area the southeastern United States, a region that in the past decade has undergone one of the fastest growth rates in the nation. I quantified the spatial extent of this growth with the aid of the Defense Meteorological Satellite Program (DMSP) Operational Linescan System (OLS) nighttime citylights, a remote sensing tool that has also been complementary to my research also for chapter 1 and chapter 3, and which main advantage over census statistics is the rapidly updatable mapping of human settlements at moderately high spatial resolution (1 km). The work was published in Milesi et al. (2003).

Description of Chapter 3

From a technical point of view, replacing cropland, grassland, forests or wetlands with buildings, parking lots and infrastructure means replacing pervious surfaces with impervious ones. This type of ecosystem alteration has a number of immediate feedbacks on humans, among them increasing the temperature of cities by up to 10 °C or more than the surrounding rural areas, eventually causing considerable discomfort and increased energy consumption for cooling during summer months. Several papers have described this phenomenon for a large number of urban areas around the globe, both with ground observations and a variety of remote sensing data. In this chapter, I use the 1-km grid fractional impervious surface area for the continental United States

v

described in chapter 1 in conjunction with the recently available land surface temperature data from MODIS (MODerate resolution Imaging Spectroradiometer) to systematically show how the urban-rural difference in temperatures is related to the fractional impervious surface area, independently of the climate and the density of development.

Description of Chapter 4

As humans we have been very successful at adapting to living in a large variety of environments, and through urbanization and technological innovation we have modified Earth's ecosystems to an extent larger than any other species; nevertheless, in our daily life we are highly dependent on a number of ecosystem processes and services. The fact that humans are not distributed homogeneously on the Earth's surface is an indicator of this dependence. Ecosystem processes are regulated by climate and closely follow its fluctuations, in some regions more closely than in others. Growing rates of greenhouse gas emissions as well as changes in the reflective properties of the surface due to land cover changes have been linked to modifications in the present climate average and extreme conditions (IPCC, 2001). In this chapter I describe the distribution of the global population as a function of NPP and dominant climatic limits to NPP. I also compare the rates of population growth between the early 1980s and the late 1990s with the rates of change in NPP observed during the same period, and identify hotspots of population sensitivity to climatically induced changes in NPP.

Table of contents

List of Tables

List of Figures

CHAPTER 1

ANALYSIS OF THE IMPACTS OF TURF GRASS MANAGEMENT PRACTICES ON THE CARBON AND WATER BUDGETS OF THE CONTINENTAL UNITED STATES

Abstract

Despite the ubiquity of turf grasses in the United States, the large-scale functioning of these ecosystems has been largely understudied. Although we know that turf grass systems are sequestering carbon at the expense of a large amount of freshwater resources, a continental carbon and water budget has yet to be attempted. The limited existing information on the total extent and spatial distribution of turf grasses and the variability in management practices are the major factors complicating this assessment. In this study, relating turf grass area to fractional impervious surface area, it was estimated that potentially 165,000 km^2 ($\pm$ 31,500 km^2) of land are cultivated with turf grasses in the continental United States, an area three times larger than that of any irrigated crop. Using the Biome-BGC ecosystem process model, the growth of warm season and cool season turf grasses was modeled for 865 sites across the 48 conterminous states under different management scenarios, including either removal or recycling of the grass clippings, different nitrogen fertilization rates and two alternative water irrigation practices. The simulations portray potential carbon and water fluxes as if the entire turf surface was to be managed like a well-maintained lawn. The results indicate that well watered and fertilized turf grasses act as a carbon sink, even assuming removal and bagging of the grass clippings after mowing. The potential carbon sequestration that could derive from the total surface under turf (up to 17 Tg C/yr with the simulated scenarios) would require a 30% to 70% increase in current domestic and commercial water use, depending on the modeled water irrigation practices. Landscaping water conservation practices such as xeriscaping and irrigation with recycled waste-water may need to be extended as municipalities continue to face increasing pressures on freshwater resources due to continued population growth.

Introduction

Turf grasses, although not native to the U.S., are ubiquitous in the American urban landscape, in residential, commercial, and institutional lawns, parks, most athletic fields and golf courses, often as monocultures, independently of the local climate (Jenkins, 1994). Existing estimates indicate that in the early 1990s the surface cultivated with turf was up to three times larger than that of irrigated corn, the largest irrigated crop in the U.S. (DPRA, Inc., 1992). As the construction of new homes, averaging 1.6 million per year in the late 1990s (U.S. Census Bureau, 1999), continues to expand the American urban landscape, the total surface under turf is expected to further increase.

While turf grasses contribute to soil carbon (C) sequestration (Bandaranayake et al., 2003; Qian and Follett, 2002; Van Dersal, 1936) and, as a component of urban vegetation, to the mitigation of the urban heat island effect (Spronken-Smith et al., 2000), they are also linked with a number of negative environmental impacts. Turf grasses can pose an environmental hazard through the use of lawn chemicals and over-fertilization (Robbins and Birkenholtz, 2003; Robbins et al., 2001). Irrigation of turf grasses sharply increases summer water consumption for residential and commercial use, especially in arid and semiarid regions, where watering lawns can contribute to 75% of the total household water consumption (Mayer et al., 1999).

In spite of the pervading presence of turf grass systems in the urban and suburban landscape and their considerable use of water resources, which often competes with other uses as population and water consumption rates continue to increase, there continues to be little knowledge about the large scale ecological functioning of these systems. If turf grasses are to be considered carbon-sequestering components of the urban ecosystems, what is their contribution to the national carbon sequestration potential? At what expense in potable freshwater resources? The fragmented distribution

2

of residential and commercial lawns and the large variability in management practices adopted to grow the different types of turf surfaces certainly challenges the task of answering these questions.

In this study I attempt a first estimate of the potential impact of turf grasses to the continental U.S. carbon and water budgets by producing a spatially explicit estimate of their distribution within the contiguous 48 states and simulating their growth with an ecosystem process model. Specific objectives of this study are 1) to compare a remote sensing-based estimate with other independent estimates of the total surface under turf grasses, and 2) to evaluate the impact of different turf management practices, such as removal versus on site decomposition of the grass clippings, varying nitrogen fertilization regimes, and alternative irrigation schedules, on the continental C sequestration potential and water budget.

Methods

Estimation of U.S. turf surface

A continental assessment of the carbon and water balances of turf grasses requires their spatial distribution to be mapped. With the exception of golf courses, turf grasses are rarely cultivated on surfaces large enough to be identifiable with moderate resolution remote sensors (~ 1km). Due to excessive costs and time constraints, the use of high-resolution satellite images or aerial photography has been limited. Past attempts to estimate the continental surface of turf grasses used indirect approaches. Vinlove and Torla (1995) estimated the national total home lawn area using methods based on adjusted Federal Housing Authority (FHA) average and median lot sizes by state. These estimates, did not account for turf surfaces of golf courses, parks, schools, roadsides,

3

etc. Moreover, the approach does not depict with sufficient detail the spatial distribution of the areas under turf. DPRA, Inc. (1992), in a report commissioned by the Environmental Protection Agency, estimated the total area under turf on the basis of direct surveys in 12 states, which was extrapolated to the remaining states in proportion to their population. Again, this method provides only a lump estimate for each state rather than higher resolution spatial distribution. In this study, I also adopted an indirect approach, assuming the surface of turf grasses to be inversely related to the extent of impervious surface associated with urban development (roads, roofs, parking lots, sidewalks, etc.).

A 1-km grid of fractional cover of Impervious Surface Area (ISA) for the 48 states was derived using 2001 radiance calibrated nighttime lights and road density (length of road per square kilometer) by Elvidge et al. (*in press*). The road density was calculated using 1998 TIGER (Topologically Integrated Geographic Encoding and Referencing System) road vector data from the U.S. Census Bureau. The nighttime lights data were processed by the National Oceanic and Atmospheric Administration's National Geophysical Data Center using cloud-free portions of DMSP/OLS (Defense Meteorological Satellite Program/Operational Linear Scanner) data with methods described by Elvidge et al. (1999). The nighttime imagery from the DMSP/OLS allow for timely and inexpensive monitoring of human settlements (Elvidge et al., 1999; Elvidge et al., 1997a) and have previously been used to map urbanization in the United States (Imhoff et al., 1997a and 1997b), to estimate population (Sutton et al., 2001; Sutton et al., 1997) and to indicate energy consumption and greenhouse gas emissions (Doll et al., 2000; Elvidge et al., 1997b). At night, the DMSP/OLS sensor operates at high sensitivity in the visible-near infrared portions of the electromagnetic spectrum (0.44-0.94 μm) and is able to detect even faint light emissions from human activity on Earth.

4

Calibration data for estimating fractional ISA was derived from 80 high-resolution (10 cm) color aerial photographs selected along development gradients from thirteen major urban centers. The transects extended from the urban cores out to the sparsely developed (or undeveloped) fringes of the urban centers of Atlanta, Boston, Chicago, Denver, Houston, Las Vegas, Miami, Minneapolis, New York, Phoenix, Portland, Sacramento and Seattle. The aerial photographs were from year 2000 (+/- one year). Square kilometer tiles were extracted from the aerial photography, matching the coverage of specific cells in the reference grid. Overlaying a grid on each photograph (see Figure 1.1 and 1.2 for an example of the aerial photograph over industrial and residential areas of Chicago, respectively), the fraction of ISA per square kilometer was obtained by calculating the proportion of constructed surface (roads, parking lots, buildings) versus the proportion of vegetated (turf grasses and/or trees) or other (undeveloped) surface (Appendix A).

5

Figure 1.1. Detail of aerial photography used to measure fractional ISA over Chicago (infrastructure and commercial buildings).

Figure 1.2. Detail of aerial photography used to measure fractional ISA over Chicago (residential area).

The gridded counts from the aerial photographs were paired to the nighttime lights radiance and road density and linear regression was used to develop the following empirical model for estimating fractional ISA:

Fractional ISA (%) = 0.214 * Radiance + 0.002 * Roads density

7

The regression, forced through the origin, was highly significant, with p-value <

0.0001 and Root Mean Square Error of 13.4. Observed versus predicted values of

fractional ISA are plotted in Figure 1.3. Pearson's coefficient of correlation between

predicted and observed values of fractional ISA was 0.87.
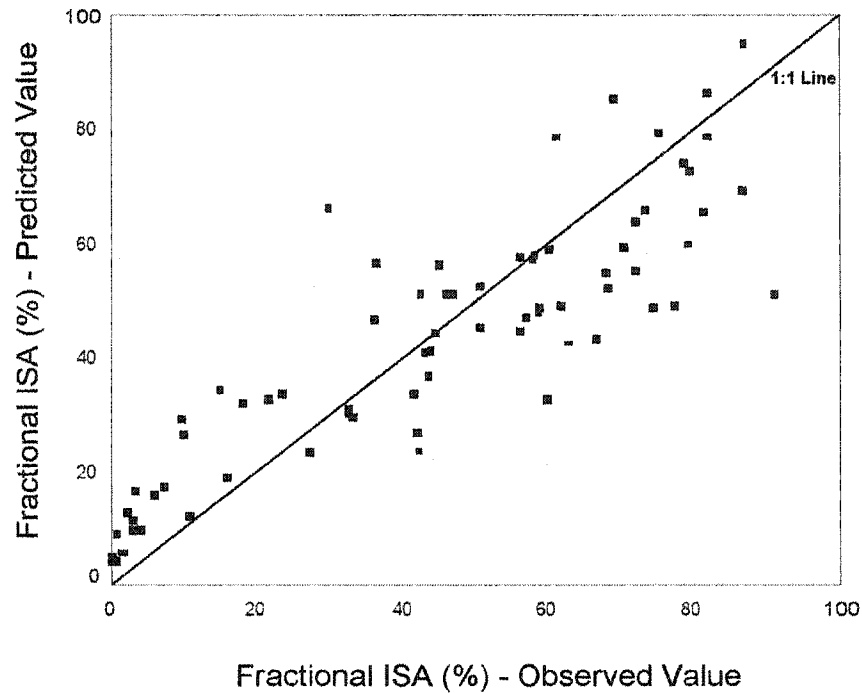
Figure 1.3. Scatter diagram of the observed values of fractional Impervious
Surface Area (ISA) versus the values predicted from linear regression.

The model was applied to the conterminous U.S. to produce a 1-km grid depicting the

spatial distribution of ISA in percentage terms (Figure 1.4). The model was only applied

to areas with lighting detected by the DMSP to reduce the effects of road density found

in certain rural areas. The total ISA for the conterminous U.S. estimated with the above

equation amounted to 106,730 (+/- 12,060) km^2 or 1.3% of the total area.
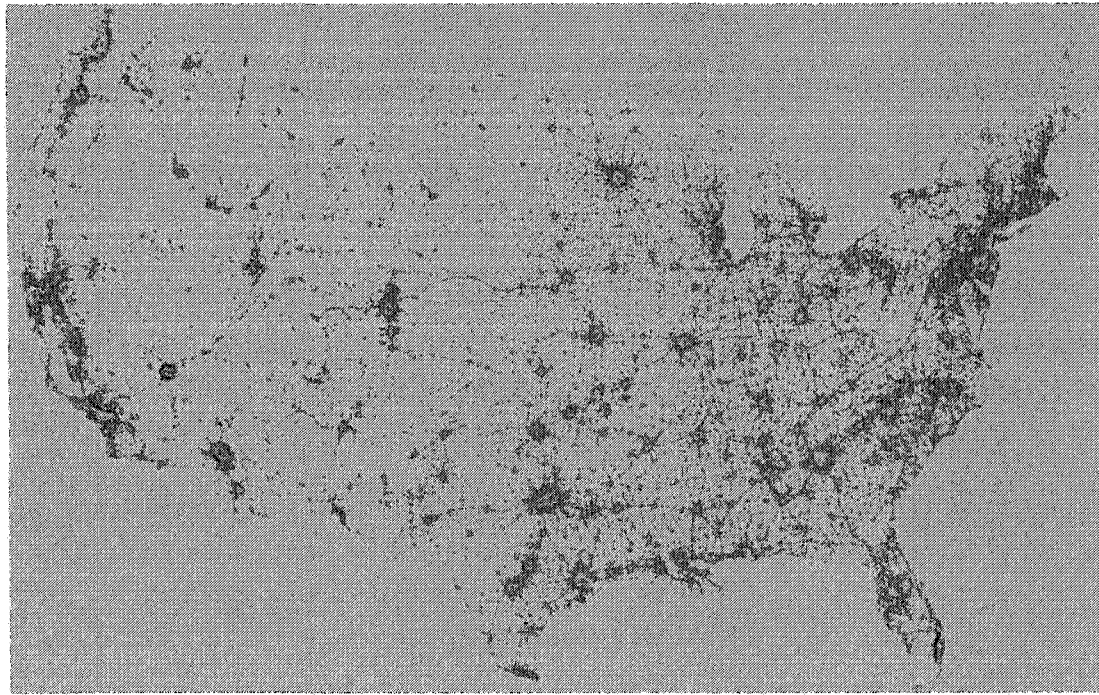
0.0   **Fractional Impervious Surface Area (ISA)**   > .50

Figure 1.4. Distribution of the fractional ISA in the conterminous U.S.

The proportions of impervious versus vegetated surfaces derived from the high resolution aerial photography were then used to develop a predictive relationship between the fractional ISA and the combined fraction of turf and tree surface, given that turf was present under the trees observed in the samples. For this model, only samples over areas with more than 10% fractional ISA were used (denoted with a star symbol in Appendix A), leaving out the sparsely developed urban fringes, where the occurrence of very low development density is often associated with forested and other non-turf vegetated surfaces. The predictive model, forced through the origin, was highly significant (p-value < .0001, RMSE = 11.2, Figure 1.5). The model was applied to the conterminous U.S. to produce a 1-km grid of fractional turf area.

9
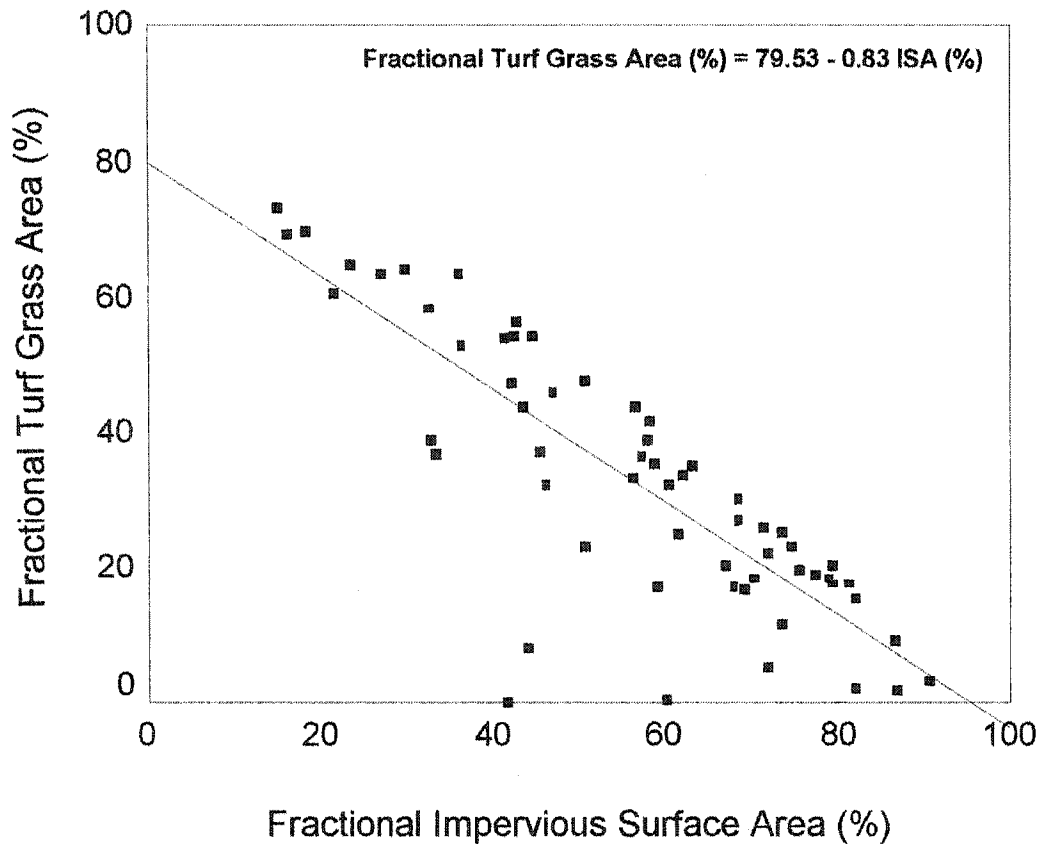
Figure 1.5. Scatter diagram of the direct measurements of fractional turf grass area and fractional Impervious Surface Area (ISA) and equation for the predictive regression model used to estimate the total U.S. surface under turf from the 1-km grid of fractional ISA.

Modeling of turf grasses growth

Management of turf grasses is highly variable, in part because of the different uses for which these surfaces are dedicated. In order to withstand considerable wear, golf courses and athletic fields usually receive much higher doses of nitrogen (N, up to 490 kg/ha/yr). For residential lawns the recommended rates range between 98 and 195 kg/ha/yr (Schultz, 1999) and are lower when the clippings are left to decompose on the turf surface. Many residential lawns are managed by homeowners who do not carefully monitor resource inputs to their lawns. These areas often receive excess water and

10

fertilizer. On the other hand, there also are some areas cultivated with turf grasses that are not adequately watered and fertilized, spending part of the growing season in a dormant stage. Variability also exists in the fate of the clippings, which are either left to decompose on the site (cycled) or removed. The removed clippings are then either bagged and sent to the landfill or composted.

In this study the simulation of the impact of different turf grass management practices on the continental C and water budget was based on the simplifying assumption that, under a given scenario, the entire turf surface is managed homogeneously, such as irrigated with the same criteria, fertilized with the same amount of N and mowed at the same height, whether it is part of a residential lawn or a golf course. This simplification permits a first estimate of the potential continental scale impacts of turf grasses on ecosystem functioning, obtained by asking: how would the continental C and water budgets be affected if all the surface currently under turf was to be managed like a well maintained lawn?

I adapted the Biome-BGC ecosystems process model to predict C and water fluxes of turf ecosystems at 865 sites distributed across the U.S., corresponding to populated places that, according to the 2000 U.S. Census, had a population of at least 40,000 people (the list of populated places is available online at: http://www.census.gov/geo/www/gazetteer/places2k.html).

Biome-BGC, with recent modifications by Thornton (2000), has been extensively documented and validated (White et al., 2000; Kimball et al., 1997; Hunt et al., 1996; Running, 1994; Running and Hunt, 1993; Running and Gower, 1991; Running and Coughlan, 1988). Biome-BGC uses prescribed site conditions, meteorology, and parameter values to simulate daily fluxes and states of C, water, and N for coarsely defined biomes, at areas ranging from 1-m^2 to the entire globe. Biome-BGC can be used to simulate these fluxes for more specifically defined ecosystems when appropriately

11

parameterized. Adapting Biome-BGC for simulating the ecosystem processes of turf grasses required modifying the default parameterization for C3 (cool season) and C4 (warm season) grasses to reflect the higher specific leaf area as well as the lower C:N ratio of leaf, litter and fine roots of fertilized and watered turf grasses. Leaf C:N ratio was assigned to 20 and litter C:N ratio was assigned to 40, as suggested by Bandaranayake et al. (2003). I also modified the lignin, cellulose and labile portions of fine roots to, respectively, 12%, 52%, and 36%, while the specific leaf area was set to 70 m^2/kg C.

Mowing activities were simulated as mortality processes that would take place every time the leaf area index (LAI) reached a critical value of 1.5. The mortality event was assumed to remove one third of LAI and the corresponding amount of fine roots. Removal of the clippings was simulated by removing the portion of C and N associated with the cut leaves from the ecosystem process. In the cycling scenario, the C and N associated with the cut leaves were left on the site to decompose as litter.

N was added to the system at a constant rate, simulating a slow release fertilizer. To evaluate the effect of clippings recycling on grasses N availability, N was applied at two different rates in contrasting simulation runs. Clippings were either removed or cycled in scenarios simulating an application of 146 kg N/ha/yr and cycled in scenarios with an application of 73 kg N/ha/yr.

Irrigation during the growing season was simulated by adding water to the precipitation field in the climate parameterization. The sprinkling season of a certain location was assumed to start when the minimum temperatures remained above 5 °C for seven consecutive days in the spring, and end when minimum temperatures decreased below 5 °C for seven consecutive days in the fall. The simulations assumed water to be sprinkled following two different watering management types. In one type of watering management I followed the common recommendation that during the growing season

12

turf grasses require about 2.54 cm (1 inch) of water per week (Schultz, 1999). To avoid

overestimating water consumption, a conservative approach is adopted in the

simulations, where in the case of rainfall, rain made up for part of this amount. In the real

world, it is common that sprinklers, especially if automated, run also on rainy days. The

alternative watering management scenario, rather than providing a fixed weekly amount

of water, modulated the irrigation based on the potential evapotranspiration (PET), here

calculated according to Priestly and Taylor (1972, Appendix B). In this case, irrigation

was simulated to be triggered when the PET, accumulated since the last watering event,

exceeded 60% of the added water. Irrigation then replaced 20% of the PET, bringing the

water availability to 80% of PET. The effect of the different water management practices

on the C and water balance was evaluated comparing scenarios in which N added

through fertilization was constant and irrigation was either fixed at 2.54 cm of water/week

or modulated according to PET.

For the 865 selected populated places, soil texture information was extracted from

the STATSGO database (Miller and White, 1998) and 18 year of climate data were

obtained from the Daymet dataset (Thornton et al., 1997). The simulation sites were

assumed to grow C3 (cool season) or C4 (warm season) turf grasses based on

adaptation zones (Beard, 1973; Time-Life Books, 2000). In cities located in the C3-C4

transitional region the grasses were assumed to be a mixture of both photosynthetic

models and the simulation was run twice, once for each type of grass. The resulting C

and water fluxes in the transitional region were determined to be an average of the two

runs, assuming that half of the surface was growing C3 grasses and half C4 grasses.

After initializing the state variables with a spin up run, the growth of turf grasses at the

865 sites was simulated for the following five different scenarios:

Control: Turf grasses growth was simulated with no management (no irrigation and no

N fertilization) except for cycling of the clippings;

13

Removed-146N: The grass was irrigated during the growing season so that a total of 2.54 cm of water per week, rainfall included, was provided, fertilized with 146 kg N/ha/yr, and the clippings were removed from the system after each mowing event;

Cycled-146N: The grass was irrigated during the growing season so that a total of 2.54 cm of water per week, rainfall included, was provided, fertilized with 146 kg N/ha/yr, and the clippings were left on the site after each mowing event;

Cycled-73N: The grass was irrigated during the growing season so that a total of 2.54 cm of water per week, rainfall included, was provided, fertilized with 73 kg N/ha/yr, and the clippings were left on the site after each mowing event;

Cycled-73N-PET: Same as Cycled-73N, except for the irrigation management, which was calculated based on Priestly-Taylor PET.

Mann-Whitney U-tests for differences were used to evaluate whether model results under the five scenarios differed significantly from each other.

The net accumulation (sequestration) of C in the ecosystem was estimated by calculating the Net Ecosystem Exchange (NEE), where NEE = Net Primary Productivity (NPP) – heterotrophic respiration – fluxes of C out of the ecosystem. Fluxes of C out of the ecosystem refer to the C removed with the clippings.

The simulation results were extrapolated to the continental surface assuming that turf areas in the vicinity of a simulation site displayed similar C and water fluxes. I divided the continental U.S. into Thiessen polygons centered on the simulation sites to identify individual 'regions of influence' around each of the 865 simulation localities. I then multiplied the output results at each simulation site by the total turf area estimated within the respective polygon.

14

Model Validation

There are only a few studies on the effect of turf grass management on the C budget. The adaptation of Biome-BGC to simulate the growth of turf grasses was validated by comparing the simulated clipping yield with published clipping yield data (C was assumed to represent 48% of the dry yield). Two studies (Kopp and Guillard, 2002; Heckman et al., 2000) presented clipping yields under different N fertilization rates for C3 grasses. Kopp and Guillard, (2002) present yields both for removed clippings and for recycled clippings. Only one value of clipping yield was available for C4 grasses (Harivandi et al., 1996). The measured versus modeled yield data showed a strong and highly significant correlation ($r = 0.83$, $p < 0.0001$) (Figure 1.6).
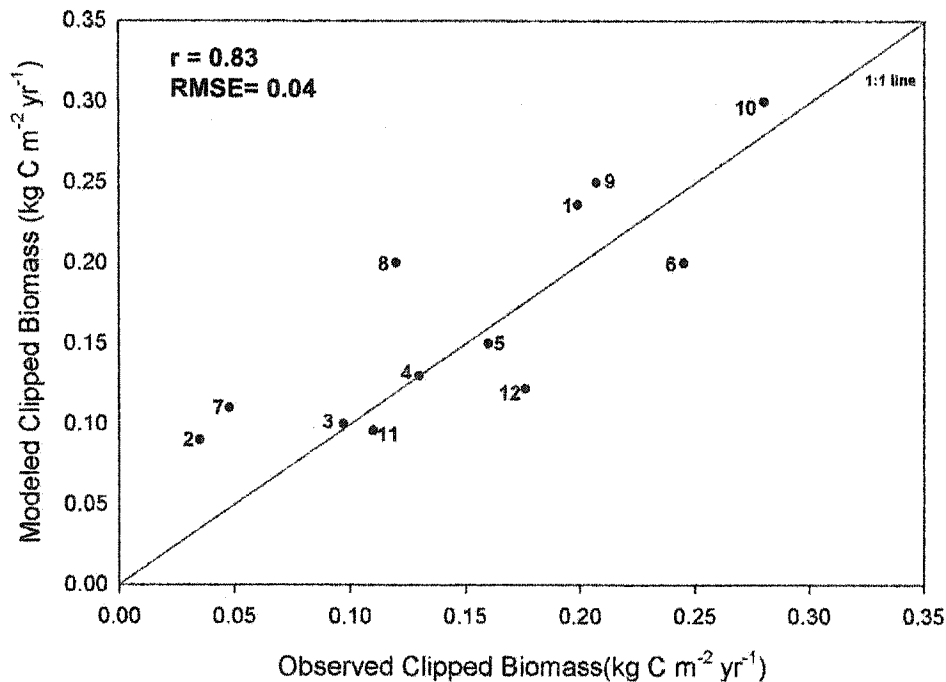
Figure 1.6. Scatter diagram of the modeled versus observed grass clipping yields expressed in C biomass (kg/m²/yr).
1* – Observed and modeled data at Santa Clara, CA, clippings removed, N rate 146.5 kg/ha/yr (Harivandi et al., 1996); 2 – Observed at Spring Manor Farm (SM), Storrs, CT, clippings removed (bagged), N rate 0 kg/ha/yr, modeled at Hartford, CT (Kopp and Guillard, 2002); 3 – Observed at SM, Storrs, CT, clippings removed, N rate 98 kg/ha/yr, modeled at Hartford, CT (Kopp and Guillard, 2002); 4 – Observed at SM, Storrs, CT, clippings removed, N rate 146.5 kg/ha/yr, modeled at Hartford, CT (Kopp and Guillard, 2002); 5 – Observed at SM, Storrs, CT, clippings removed, N rate 196 kg/ha/yr, modeled at Hartford, CT (Kopp and Guillard, 2002); 6 – Observed at SM, Storrs, CT, clippings removed, N rate 392 kg/ha/yr, modeled at Hartford, CT (Kopp and Guillard, 2002); 7 – Observed at SM, Storrs, CT, clippings cycled, N rate 0 kg/ha/yr, modeled at Hartford, CT (Kopp and Guillard, 2002); 8 – Observed at SM, Storrs, CT, clippings cycled, N rate 98 kg/ha/yr, modeled at Hartford, CT (Kopp and Guillard, 2002); 9 – Observed at SM, Storrs, CT, clippings cycled, N rate 196 kg/ha/yr, modeled at Hartford, CT (Kopp and Guillard, 2002); 10 – Observed at SM, Storrs, CT, clippings cycled, N rate 392 kg/ha/yr, modeled at Hartford, CT (Kopp and Guillard, 2002); 11 – Observed at Rutgers, NJ, clippings removed, N rate 97.6 kg/ha/yr, modeled at Edison, NJ (Heckman et al., 2000); 12 – Observed at Rutgers, NJ, clippings removed, N rate 195.2 kg/ha/yr, modeled at Edison, NJ (Heckman et al., 2000).
*Only C4 grass site. Points 2-12 refer to sites growing C3 grasses.

16

Results And Discussion

Estimation of turf grass area

The total turf grass area estimated in this study summed up to 165,058 km^2 ($\pm$ 31,550 km^2 for the upper and lower 95% confidence interval bounds) (Table 1.1). This estimate, intended to include all residential, commercial, and institutional lawns, parks, golf courses and athletic fields, accounts for 1.8% of the total continental U.S. area, which compares with 3.5-4.9% of the total surface estimated to be devoted to urban development (National Association of Realtors, 2001; Nowak et al., 2001) and 1.3% of fractional ISA (as estimated in this study). While it is difficult to validate the estimate of total turf grass area derived from this analysis, it appears to reasonably compare to the estimates of the other studies, in particular when considering the recent growth in population and urban areas in the U.S. (Fulton et al., 2001). DPRA, Incorporated (1992), assuming turf surface to be directly related to the population, estimated a total surface of 188,180 km^2, including 94,090 km^2 of home lawns (Grounds Maintenance, 1996). A 1987 study by Roberts and Roberts (1987) estimated a total surface of 100,000-120,000 km^2. Another study, focusing only on residential lawns, analyzing state-based average lot sizes of single family homes, estimated a total home lawn area ranging between 58,000 km^2 and 71,680 km^2, considerably downsizing DPRA's estimate of home lawns (Vinlove and Torla, 1995). One of the earliest estimates of total turf surface dates back to the late 1960's, when it was reported that 67,000 km^2 of lawn existed nationally (Falk, 1976).

17

Table 1.1. Mean, upper and lower 95% confidence interval (C.I.) estimates of turf grass area for the conterminous states of the U.S. Between parenthesis, the fraction of the State estimated to be occupied by turf grasses.

State	Turf grass area (km^2)		
	Mean	Upper 95% C.I.	Lower 95% C.I.
Alabama	3,739 (2.8%)	4,400 (3.3%)	3,078 (2.3%)
Arizona	2,902 (1.0%)	3,500 (1.2%)	2,305 (0.8%)
Arkansas	2,351 (1.7%)	2,763 (2.0%)	1,941 (1.4%)
California	12,086 (3.0%)	14,681 (3.7%)	9,496 (2.4%)
Colorado	2,414 (0.9%)	2,897 (1.1%)	1,932 (0.7%)
Connecticut	2,118 (17.0%)	2,494 (20.0%)	1,742 (13.9%)
Delaware	560 (11.1%)	664 (13.1%)	456 (9.0%)
District of Columbia	64 (40.0%)	92 (58.0%)	36 (22.6%)
Florida	10,244 (7.3%)	12,289 (4.9%)	8,203 (5.9%)
Georgia	6,230 (4.2%)	7,359 (4.9%)	5,103 (3.4%)
Idaho	787 (0.4%)	931 (0.4%)	643 (0.3%)
Illinois	6,192 (4.3%)	7,450 (5.2%)	4,936 (3.4%)
Indiana	4,114 (4.4%)	4,868 (5.2%)	3,362 (3.6%)
Iowa	2,027 (1.4%)	2,395 (1.7%)	1,660 (1.1%)
Kansas	1,951 (0.9%)	2,324 (1.1%)	1,579 (0.7%)
Kentucky	2,637 (2.6%)	3,110 (3.0%)	2,165 (2.1%)
Louisiana	3,329 (3.0%)	3,955 (3.5%)	2,704 (2.4%)
Maine	614 (0.8%)	718 (0.9%)	510 (0.6%)
Maryland	2,626 (10.4%)	3,139 (12.4%)	2,114 (8.4%)
Massachusetts	3,208 (15.8%)	3,810 (18.8%)	2,607 (12.8%)
Michigan	4,940 (3.4%)	5,879 (4.0%)	4,002 (2.7%)
Minnesota	3,011 (1.5%)	3,579 (1.7%)	2,444 (1.2%)
Mississippi	1,972 (1.6%)	2,316 (1.9%)	1,629 (1.3%)
Missouri	3,679 (2.1%)	4,370 (2.4%)	2,989 (1.7%)
Montana	493 (0.1%)	585 (0.2%)	401 (0.1%)
Nebraska	1,184 (0.6%)	1,413 (0.7%)	955 (0.5%)
Nevada	982 (0.3%)	1,209 (0.4%)	756 (0.3%)
New Hampshire	690 (3.0%)	806 (3.5%)	574 (2.5%)
New Jersey	3,996 (20.8%)	4,804 (25.0%)	3,189 (16.6%)
New Mexico	1,827 (0.6%)	2,157 (0.7%)	1,497 (0.5%)
New York	5,598 (4.6%)	6,748 (5.5%)	4,451 (3.6%)
North Carolina	8,317 (6.7%)	9,767 (7.7%)	6,871 (5.4%)
North Dakota	499 (0.3%)	593 (0.3%)	404 (0.2%)
Ohio	7,339 (6.9%)	8,702 (8.2%)	5,978 (5.6%)
Oklahoma	2,699 (1.5%)	3,202 (1.8%)	2,196 (1.2%)
Oregon	1,928 (0.7%)	2,294 (0.9%)	1,563 (0.6%)
Pennsylvania	7,844 (6.8%)	9,293 (8.0%)	6,398 (5.5%)
Rhode Island	515 (19.0%)	616 (22.7%)	413 (15.3%)
South Carolina	4,154 (5.3%)	4,877 (6.3%)	3,433 (4.4%)
South Dakota	612 (0.3%)	723 (0.4%)	502 (0.3%)
Tennessee	4,780 (4.5%)	5,640 (5.3%)	3,921 (3.7%)
Texas	13,120 (1.9%)	15,746 (2.3%)	10,498 (1.5%)
Utah	1,329 (0.6%)	1,560 (0.7%)	1,059 (0.5%)

18

Vermont	309 (1.3%)	361 (1.5%)	258 (1.1%)
Virginia	4,771 (4.7%)	5,651 (5.5%)	3,893 (3.8%)
Washington	3,070 (1.8%)	3,701 (2.1%)	2,440 (1.4%)
West Virginia	1,537 (2.5%)	1,801 (2.9%)	1,273 (2.0%)
Wisconsin	3,144 (2.2%)	3,723 (2.6%)	2,566 (1.8%)
Wyoming	528 (0.2%)	621 (0.2%)	435 (0.2%)
Total U.S.	**165,058 (1.8%)**	**196,614 (2.1%)**	**133,557 (1.5%)**

Even when the estimate of total surface is considered to be closer to the lower bound of the 95% confidence interval (133,557 km^2), it appears that turf grasses would represent the single largest irrigated "crop" in the U.S., occupying a total area three times larger than the surface of irrigated corn (43,000 km^2 according to the 1997 Census of Agriculture, out of 202,000 km^2 of total irrigated cropland area).

Water budget

The two alternate irrigation methods produced watering requirements that varied widely across the climatic regions of the 48 states, with the yearly total amount of water that needed to be provided through irrigation at each site depending both on the total rainfall and its distribution during the growing season and the length of the sprinkling season. In general, a fixed irrigation management based on turf requirements of 2.54 cm of water per week, including rainfall, resulted in a minimum of no irrigation in Lincoln Park, Michigan (meaning that here rainfall alone is able to satisfy the watering requirements of the turf throughout the growing season) to a maximum of 125 cm of water per year to be added through irrigation in Yuma, Arizona. In contrast, the irrigation management based on PET tended to decrease the amount of water supplied through irrigation in wet regions and increase it in arid and semiarid regions of the U.S., where it was by far larger than 2.54 cm/week. Modulating irrigation according to PET required a minimum of 17 cm/yr of water to be added through irrigation in Pensacola, Florida, to a

19

maximum of 197 cm/yr in Yuma, Arizona. The Mann-Whitney *U*-test for differences indicated that the two irrigation methods would provide significantly different annual amounts of water at 77% of the 865 sites. All but three of the sites with no significant difference between the two irrigation methods were located east of the Great Plains.

cm/yr

-38 -27 -15 -4 7 19 30 41 53 64 72
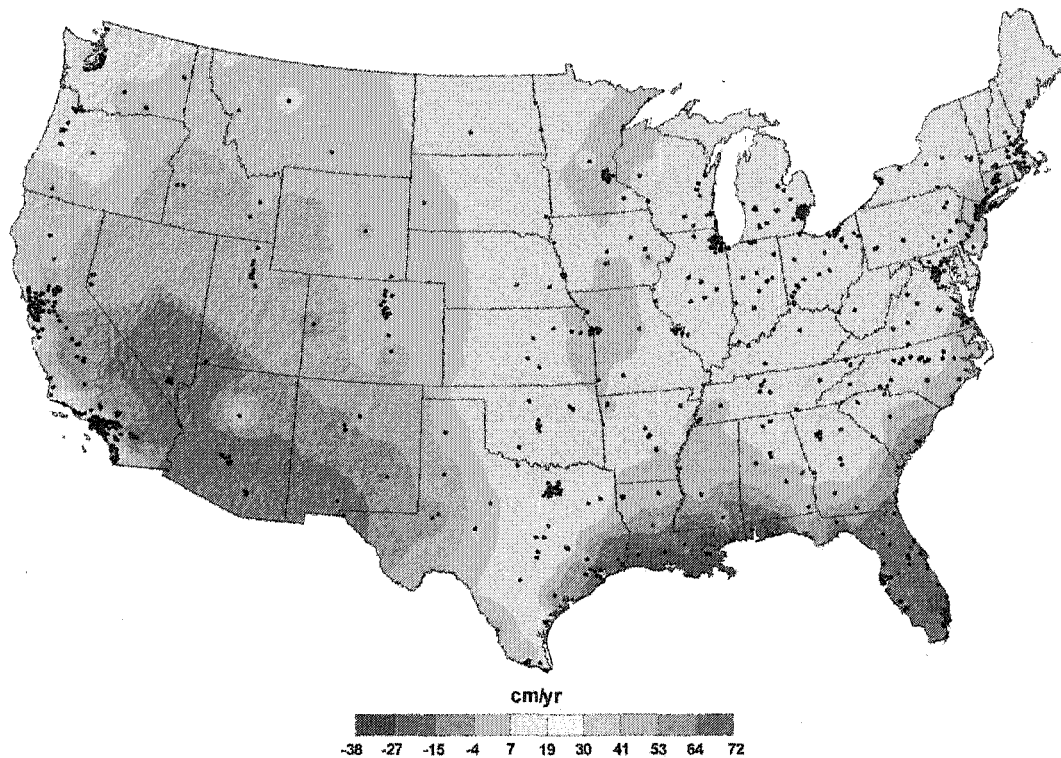
Figure 1.7. Spatially interpolated differences in irrigation water use between the two irrigation scenarios. Turf irrigation with the PET-based method versus the 2.54 cm/week management scenario results in a larger amount of water sprinkled in all the western United States and less water in the southeastern US. No significant difference between irrigation methods is observed in the most of the eastern United States, where the watering recommendation of 1 inch of water per week probably originated.

The spatially interpolated differences in irrigation water use between the two irrigation managements (Figure 1.7) indicates that adopting the PET-based method versus applying constantly 2.54 cm/week would result in a larger amount of water sprinkled in

20

the West, with a maximum difference of up to 72 cm/yr in the Southwest, and less water in the southeastern US, with a reduction in water use of up to 38 cm/yr in southern Florida, where the high relative humidity reduces the evapotranspirational demand.

Extrapolating the water use for irrigation with the two methods at each of the 865 sites to the surface of turf grasses contained in the respective Thiessen polygons yields an average total of 74,900 Mm^3 (Mega cubic meters) of water with the constant 2.54 cm/week method and 97,400 Mm^3 of water with the PET method, while rain contribution during the sprinkling season to the watering of the total estimated turf grass area would amount to 100,500 Mm^3 (Figure 1.8).

Water Budget

Figure 1.8. Water budgets of the total U.S. turf surface for the four management scenarios. Error bars indicate budget values calculated for the 95% confidence interval lower and upper bound estimate of total turf surface.

These estimates indicate that, in the scenario that the entire turf surface in the U.S. was to be irrigated to satisfy the 2.54 cm/week water supply or at 80% of PET, domestic and commercial consumptive water use would be, respectively, 30% and 70% higher than the amount estimated in 1995 (Solley et al., 1998). Noteworthy is that in spite of the

21

elevated irrigation requirements, there appears to be a considerable amount of water leaving the surface as outflow rather than evapotranspiration (58,100 to 57,300 Mm^3 of water, depending on the irrigation management scenarios). 90% of the estimated outflow takes place in the eastern and southern U.S., where it is related to rainfall rather than sprinkling events. In occasion of abundant rainfall, precipitation is larger than the soil water capacity and leaves the soil before the grass can use it for evapotranspiration. In spite of a surplus of available water during the rainy periods, sprinkling is still required during the drier periods.

If irrigation could just replace actual evapotranspirational losses, the water to be added through sprinkling would amount to 24,800 Mm^3 in the case of the 2.54 cm/week method and 51,900 Mm^3 with the PET-based method. The large increase in the water requirements with the PET-based method has to be attributed to the arid western U.S., where grasses can evaporate much more than 2.54 cm of water per week if more irrigation is supplied. Still, part of the water reaching the surface during the growing season, either from precipitation when abundant rainfall occurs, or from the sprinkler, due to Priestly-Taylor PET overestimating actual evapotranspiration, would not be used by the grass and leave the surface as outflow.

Implications of recent climatic changes on turf water requirements

While the water uses for the scenarios analyzed in this paper have been calculated based on 18-year average growing season precipitation (1980-1997) for the 865 modeled sites, we have to consider the potential increase in water use for irrigation during dry years. A measure of the increase in water use during a drought year can be calculated from the water use for 1987-1988 (the driest years in the period analyzed, but with a total precipitation for the U.S. that was still three times higher than that of the

22

record drought years of the past century (Nemani et al., 2002)). A precipitation regime such as the one of the years 1987-88 would have increased water use by an average of 2.9% in the 2.54cm/week management scenario and by 3.8% in the PET-based irrigation.

Precipitation is not the only variable that can increase the water requirements of turf grasses. At constant precipitation, the yearly outdoor use of water for sprinkling can be increased by a longer growing season alone. Recent (1948-1999) observed warming in the U.S. has resulted in a lengthening of the frost-free season from a minimum of 0.3 days per decade (or 1.5 days over five decades) in the southeastern states to up to 5.4 days per decade (or 27 days over five decades!) in California and Nevada (Easterling, 2002).
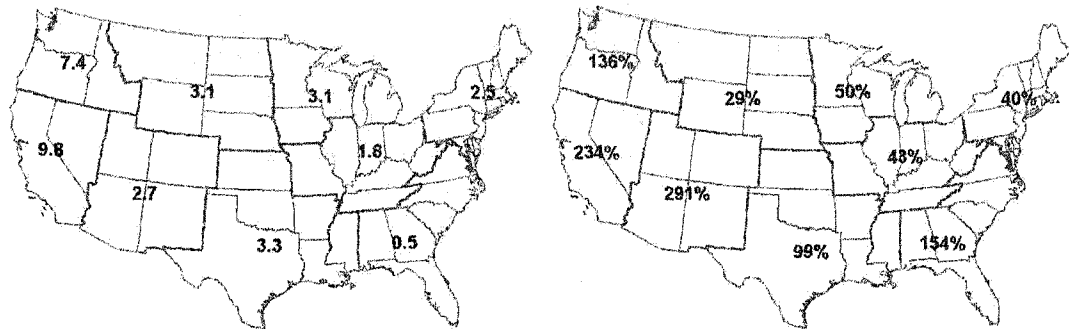
Figure 1.9. Left: change in water requirements (cm/yr) of turf due to the lengthening of the frost-free period illustrated by Easterling (2002). Right: change in population for the period 1950-2000.

Figure 1.9 (left) shows how, over five decades, this increase in the growing season length in the regions used by Easterling (2002) translates into added turf water requirements (in cm per year) under the 2.54 cm of water per week irrigation scenario. Over the same period, also population (and presumably, therefore, the surface cultivated

with turf grasses) increased drastically in most of the U.S. regions (right portion of Figure 1.9). For the entire turf grass surface estimated by this study, the growing season lengthening alone would have increased turf water requirements by 14,412 Mm^3/yr. Of course, part of this increased water demand has been satisfied by increased precipitation trends (Karl and Knight, 1998).

Carbon budget

Table 1.2 reports the ranges in C fluxes and mowing counts for the control and the four management scenarios. In general, the simulation results indicate that the C fluxes of a well-watered grass increase with the amount of available N. For a certain amount of N input through fertilization, the C fluxes were larger when cycling of the grass clippings was simulated, since the onsite decomposition of the mowed grass clippings returned a consistent amount of N to the soil. For each scenario, differences in the maximum–minimum ranges are related mainly to the growing season length.

Table 1.2. Minimum and maximum values of C fluxes and mowing counts recorded for the 865 simulation sites

Carbon fluxes ($g\ C\ m^{-2}\ yr^{-1}$)	Control	Bagged-146N	Cycled-146N	Cycled-73N	Cycled-73N-PET
NPP	22-121	257-641	281-1063	184-604	195-613
Clippings	0-34	79-207	87-348	55-195	58-198
Heterotrophic respiration	31-121	138-392	210-922	140-533	150-542
Mowing counts ($cuts\ yr^{-1}$)	0-7	16-52	22-98	14-55	16-56

24

Figure 1.10. Modeling sites under the control scenario where the number of days between successive turf movings, calculated as the ratio between yearly mowing counts and growing season length, is less than 35. These locations are assumed to allow cultivating turf grasses without the need for irrigation and fertilization.

Unsurprisingly, the control scenario displays the lowest range of C fluxes, and the lowest range of mowing counts, which are both significantly different from all the other scenarios at all 865 sites. The low number of mowing counts simulated in the control scenario permits the inference that in absence of irrigation and fertilization, turf grasses would not be able to grow in most of the U.S. A general guess of where turf grasses could grow with no added resources of N and water can be made by calculating the number of days between successive mowings (ratio of yearly mowing counts to growing season length). Assuming that turf grasses should grow back to an LAI of 1.5 in at least 30-35 days to not be outcompeted by weeds, we can see in Figure 1.10 that turf grasses could probably grow naturally only in a few of the modeling sites, all but one located in the northeastern portion of the country (the site in the western U.S. corresponds to Flagstaff, AZ). If turf grasses reach an LAI of 1.5 only 6-7 times in areas where the

25

growing season is as long as 300-360 days, then it is probable that between subsequent cuts there are several opportunities for weeds to invade the surface and prosper over time. Because the LAI is reduced by 0.3 units every time an LAI equal to 1.5 is reached, the NPP of an unmanaged turf would be considerably lower than that of natural grasslands, which in temperate ecosystems ranges between 320 and 750 $g/m^2/yr$ (Saugier et al., 2001; Schlesinger, 1997).

The largest C fluxes are realized for scenario Cycled-146N, in which Mann-Whitney U-test for differences in C fluxes and mowing count indicates that this scenario is significantly different from the other scenarios for all the variables measured at the 865 sites ($p < 0.01$). Abundant fertilization (146 kg N/ha/yr) and the recycling of the N contained in the leaves left to decompose on the site boosts both the productivity as well as the heterotrophic respiration.

Scenario Removed-146N produces the second highest NPP and clipped biomass ranges. Because the clipped biomass is assumed to be removed from the turf surface, very low on site decomposition activity results in the smallest C fluxes from heterotrophic respiration.

In scenario Cycled-73N, the C fluxes are significantly lower ($p < 0.01$) at all sites when compared to those of Removed-146N and lower in 88-92% of the sites when compared to Cycled-146N.

Scenario Cycled-73N-PET, which differs from Cycled-73N only for the type of water management, modulating irrigation according to PET rather than supplying a weekly fixed amount of water, does not produce significantly different C fluxes from Cycled-73N at any of the 865 sites. Mann-Whitney U-test at 5% significance level indicates a water effect on NPP and clipped C at 7% of the sites, and an effect on heterotrophic respiration at 5% of the sites.

26

An approximated estimation of the total C budget for the continental U.S. turf surface under the five scenarios examined indicates that, if the entire area was well watered and fertilized, we would have a C sequestering system, even when assuming the bagging and removal of the grass clippings (Figure 1.11). The sink is generally stronger when more N is available. N availability can be increased both through increased fertilization or, more efficiently, by leaving the clippings to decompose on the site after mowing. The highest NEE is recorded for the Cycled-146N scenario, amounting to 17 Tg C/yr (Tg = Teragrams, 10^{12} grams). The lowest NEE is recorded for the Removed-146N scenario, for which the removal of the clippings from onsite decomposition reduces the C sink to just 6 Tg C/yr, in spite of the fact that the same amount of N as in Cycled-146N is added through fertilization (a total of 2.42 Tg N/yr for the total estimated surface under turf). Offsite composting of the clippings allows recuperating part of the carbon. On the other hand, the practice, now becoming less common (EPA, 2003), of sending the clippings in trash bags to the landfill leads to their anaerobic decomposition and the production of methane, a greenhouse gas more powerful than carbon dioxide. Reducing the N fertilization by half in scenarios that recycle the clippings (Cycled-73N and Cycled-73N-PET) lowers the NPP by 36-37% and the NEE by 45% compared to the Cycled-146N scenario but also considerably lowers the number of times the grass needs to be cut throughout the growing season. The total C budget for the control scenario, on the other hand, is negligible, with a total NPP of 15.5 Mg C/yr and total amount of clipped C of 4.1 Mg/yr. Heterotrophic respiration (15.6 Mg C/yr) even slightly surpasses the total NPP where climatic constraints on growth are stronger, bringing the NEE for the control scenario close to zero.
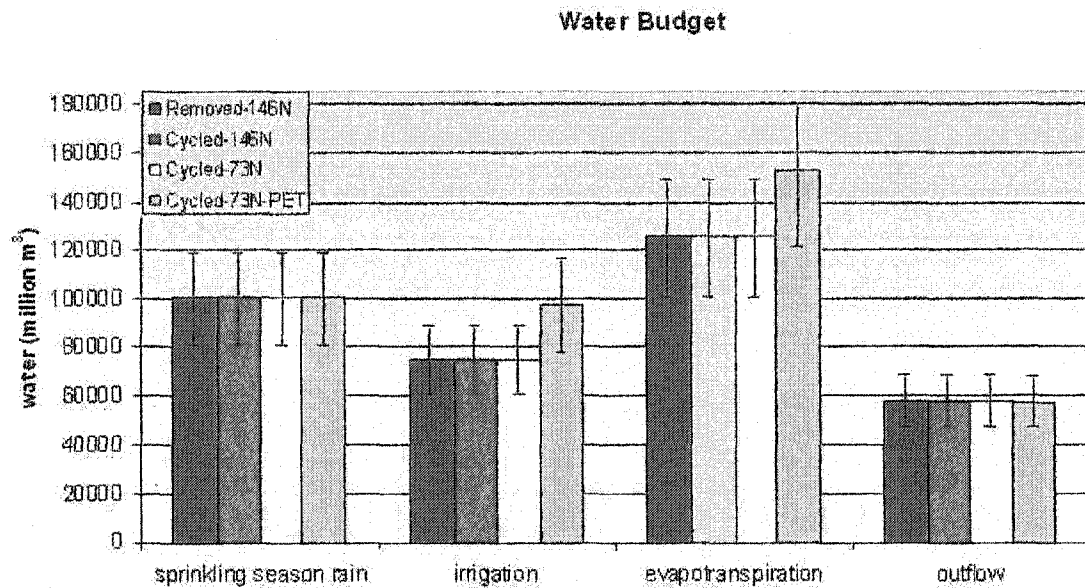
Carbon Budget
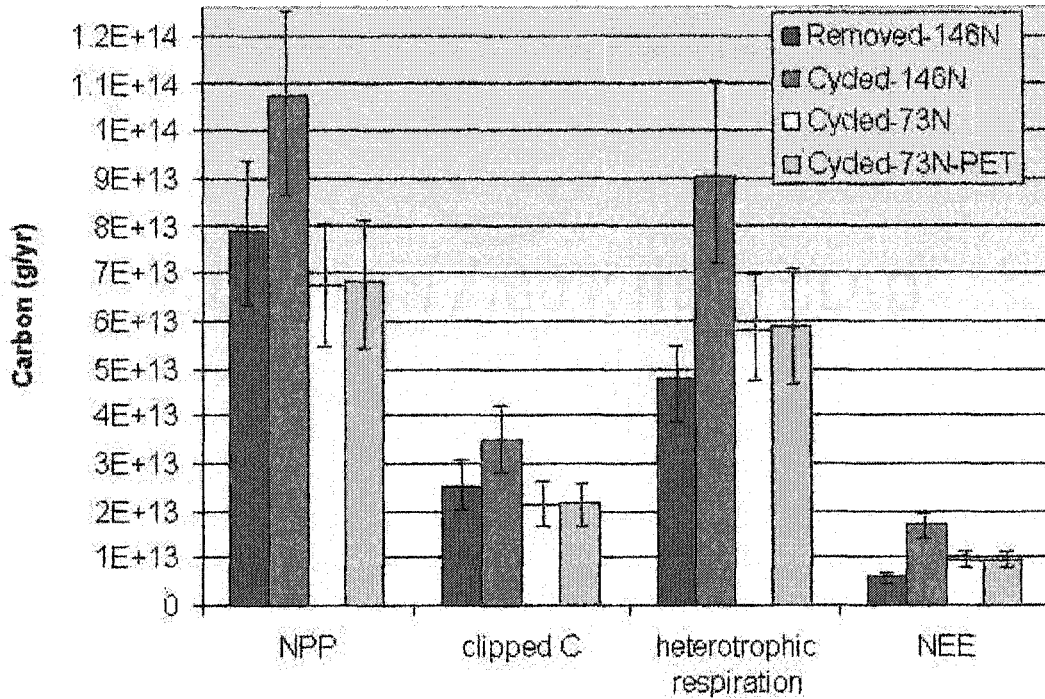
Figure 1.11. Carbon budgets of the total U.S. turf surface for the different simulations. Error bars indicate budget values calculated for the 95% confidence interval lower and upper bound estimate of total turf surface. The carbon budget for the control scenario is negligible and therefore not displayed.

Large differences in total C fluxes can be realized under the same irrigation management of 2.54 cm of water per week, all resulting in very large losses of water through outflow (Figure 1.8). This result is most probably explained by the fact that in all the simulated management scenarios water is not limiting growth, which responds rather to increases in N availability. The large increase in water application observed when modulating irrigation according to PET, on the other hand, results in an insignificant change in C fluxes, indicating that the water is lost in luxury evapotranspiration.

The simulations indicate that in the Cycled-146N turf grasses can contribute up to 2.9-5.7% of the total carbon sink of the continental U.S. (estimated to range between

28

0.30 and 0.58 Pg of carbon per year; Pg = petagram, 10^{15} grams) (Pacala et al., 2001). This contribution is substantial when considering that it is coming from a relatively small portion of the total land. Unfortunately, this sink would come at a very large expense in resources and at the risk, not analyzed here, of watershed pollution due to improper fertilization and use of pesticides (Petrovic, 1990). Beneficial effects of turf grasses, such as a carbon sequestration but also recreation and storm runoff reduction, could be sought by minimizing the application of fertilizers and pesticides, on site decomposition of the grass clippings, and extending the practice of irrigating with waste water rather than with drinking water.

Conclusions

In the present study I tried to estimate the total surface of turf grasses in the continental U.S. and to simulate its potential C and water budget. I also provided a description of how the C and water budgets can be affected by adopting different management practices for irrigation, fertilization and the fate of the clippings. Rather than depicting the present fluxes, I simulated scenarios in which the entire surface was to be managed like a well-maintained lawn, a thick green carpet of turf grasses, watered, fertilized and kept regularly mown. The accuracy of the results is therefore limited by both the uncertainty in the mapping of the total lawn area and by the simplifying assumptions made while modeling turf grasses growth.

The analysis indicates that turf grasses, potentially occupying up to 2% of the surface of the continental U.S., would be the single largest irrigated crop in the country. The study also indicates that a well-maintained lawn is a C sequestering system, although the positive C balance comes at the expense of a very large use of resources such as water, N, and, not quantified in this study, pesticides. The model simulations have

29

assumed a conservative amount of fertilization (146 kg N/ha/yr). In general the rates of N applications are similar to those used for row crops, and N emissions from turf surfaces can contribute to non-point source pollution when fertilization takes place improperly. Proper N fertilization, although boosting C sequestration, also increases the amount of grass clippings due to more frequent cuts. When grass clippings are bagged and sent to the landfill, a practice that fortunately is now becoming less widespread than in the past, the methane release from their anaerobic decomposition probably defeats most of the effects of the field carbon sequestration.

If the entire turf surface was well watered following commonly recommended schedules there would also be an enormous pressure on the U.S. water resources, especially when considering that drinking water is usually sprinkled. At the time of this writing, in most regions outdoor water use already reaches 50-75% of the total residential use. The amount of water used for turf grass irrigation is expected to increase because of demographic growth and because more and more people are moving towards the warmer regions of the country. Several counties in the arid and semiarid regions of the U.S. have already implemented lawn watering restrictions and the recycling of wastewater to replace drinking water for outdoor sprinkling. To protect our water resources as further urban growth takes place in the mostly water limited western U.S., other regions will probably need to extend the practice of recycling wastewater for outdoor use, along with continuing to educate the population on the value of water resources and reducing the surface landscaped with water-thirsty vegetation.

Even where water supply is not limited by climate, taking steps towards wastewater use for outdoor irrigation, reduction of the use of fertilizers and pesticides, increase of people's tolerance towards "weeds" and onsite recycling of the clippings can help increase the ecological and recreational benefits of the large surface under turf in the U.S.

30

Appendix A

Percent fractions and standard deviations of turf, trees, ISA and other surfaces from the 80 samples of high resolution aerial photographs.

SITE	Turf %	Turf st. dev.	Tree %	Tree st. dev.	ISA %	ISA st. dev.	Other %	Other st. dev.	Turf+Tree %
Atlanta 1*	15.41	1.43	11.56	2.04	68.44	2.47	4.59	0.68	26.96
Atlanta 2	4.59	0.51	74.96	1.28	3.26	0.68	17.19	1.80	79.56
Atlanta 3*	8.89	0.44	26.22	0.89	63.11	0.89	1.93	0.26	35.11
Atlanta 4*	23.56	6.90	45.78	1.33	18.22	2.22	12.44	6.17	69.33
Atlanta 5	3.70	1.68	71.26	2.45	3.41	1.68	21.63	2.45	74.96
Atlanta 6*	19.85	2.10	44.00	0.89	29.63	2.19	6.52	0.26	63.85
Atlanta 7*	28.15	5.05	35.26	1.43	26.96	4.45	9.63	0.68	63.41
Atlanta 8*	12.74	2.28	40.00	6.22	36.15	3.78	11.11	0.44	52.74
Atlanta 9*	11.41	2.19	53.33	1.54	23.26	2.28	12.00	0.89	64.74
Atlanta 10*	1.04	0.68	35.56	3.11	33.19	1.56	30.22	2.35	36.59
Atlanta 11	0.89	0.44	83.93	6.45	3.11	1.60	15.41	1.12	84.81
Boston 1	10.37	1.43	82.67	0.89	0.74	0.51	6.22	1.33	93.04
Boston 2*	15.41	2.82	23.41	2.10	57.93	2.60	3.26	1.03	38.81
Boston 3*	18.52	2.60	39.70	4.47	32.44	2.78	9.33	2.31	58.22
Boston 4*	11.41	0.93	14.52	1.36	71.41	2.57	2.67	0.44	25.93
Boston 5	1.48	1.03	90.37	3.83	1.48	1.03	6.67	2.04	91.85
Boston 6*	11.70	0.93	22.07	1.80	61.93	1.56	4.30	0.68	33.78
Chicago 1*	14.23	2.92	18.07	5.66	60.30	2.68	7.41	0.68	32.30
Chicago 2*	44.74	4.54	2.37	0.51	42.07	3.70	10.81	1.43	47.11
Chicago 3*	12.00	1.60	61.19	1.12	14.96	4.32	11.70	1.80	73.19
Chicago 4*	26.07	1.43	27.70	3.15	41.33	3.53	4.89	1.60	53.78
Chicago 5*	26.96	8.34	29.19	10.56	42.67	1.60	1.19	0.68	56.15
Chicago 6*	25.48	4.36	22.22	2.78	50.67	3.56	1.63	0.68	47.70
Chicago 7*	15.26	2.19	9.48	3.83	61.48	1.80	13.78	5.46	24.74
Chicago 8*	9.33	2.70	7.26	0.68	69.04	3.78	14.37	4.96	16.59
Chicago 9*	8.44	2.23	14.82	4.47	74.51	2.23	2.23	2.48	23.26
Chicago 10	18.52	1.36	1.19	0.93	10.81	0.68	69.48	2.00	19.70
Denver 1	10.22	1.78	19.56	4.29	68.30	2.96	1.93	1.36	29.78
Denver 2*	29.63	2.89	14.07	1.12	56.30	2.60	0.00	0.00	43.70
Denver 3*	0.74	0.68	6.07	0.68	1.78	0.77	91.41	0.51	6.81
Denver 4*	8.74	4.47	9.04	2.68	79.26	4.88	2.96	1.03	17.78
Denver 5*	28.74	1.68	17.04	3.39	46.96	3.34	5.04	0.93	45.78
Houston 1*	22.81	4.03	18.52	6.00	58.22	7.32	0.44	0.44	41.33
Houston 2*	0.00	0.00	0.00	0.00	41.63	6.95	58.37	6.95	.00
Houston 3	2.37	1.03	16.59	6.16	9.63	4.01	71.41	2.96	18.96
Houston 4*	1.19	0.26	0.59	0.68	86.81	4.27	11.41	3.78	1.78

31

Houston 5*	15.70	1.85	7.26	0.51	50.67	8.33	26.37	7.14	22.96
Houston 6*	18.67	7.42	13.63	1.43	46.22	3.08	21.48	7.13	32.30
Houston 7	0.00	0.00	57.33	5.57	0.15	0.26	42.52	5.34	57.33
Las Vegas 1*	12.74	2.00	6.22	2.78	77.33	2.78	3.70	4.54	18.96
Las Vegas 2	0.00	0.00	0.00	0.00	7.41	0.51	92.59	0.51	.00
Las Vegas 3*	0.15	0.26	0.15	0.26	60.00	1.33	39.70	1.43	.30
Las Vegas 4*	1.48	0.68	1.48	0.93	90.96	1.36	6.07	1.36	2.96
Las Vegas 5	0.00	0.00	0.00	0.00	0.00	0.00	100.00	0.00	.00
Las Vegas 6*	4.00	0.44	7.70	2.72	73.48	2.86	14.81	1.28	11.70
Las Vegas 7*	6.67	2.35	1.33	0.77	43.85	0.51	48.15	1.43	8.00
Miami 1	0.00	0.00	2.67	0.89	0.00	0.00	97.33	0.89	2.67
Miami 2*	11.70	0.68	10.52	0.26	71.85	1.56	5.93	0.93	22.22
Miami 3*	6.81	2.24	13.48	2.28	79.41	4.13	0.30	0.26	20.30
Miami 4*	24.74	1.36	12.44	1.18	45.19	0.68	17.63	0.68	37.19
Minneapolis 1*	12.74	1.56	56.15	1.12	16.00	0.89	15.11	2.31	68.89
Minneapolis 2*	20.44	3.20	33.48	4.13	42.37	5.56	3.70	1.43	53.93
Minneapolis 3	0.00	0.00	10.96	1.36	0.89	0.77	88.15	1.68	10.96
Minneapolis 4*	8.00	1.94	7.41	2.10	81.93	2.60	2.67	1.33	15.41
Minneapolis 5*	12.00	3.64	5.63	1.43	81.33	2.35	1.04	0.93	17.63
NewYork 1*	0.15	0.26	1.78	0.77	81.93	2.72	16.15	3.34	1.93
NewYork 2*	9.63	0.93	15.41	1.36	73.48	1.56	1.48	0.68	25.04
NewYork 3*	24.44	3.11	38.81	1.80	35.85	1.28	0.89	0.44	63.26
NewYork 4*	18.37	0.51	35.56	1.60	44.59	2.68	1.48	0.68	53.93
NewYork 5	0.00	0.00	100.00	0.00	0.00	0.00	0.00	0.00	100.00
Phoenix 1*	20.59	2.86	14.67	3.85	58.67	1.78	6.07	2.45	35.26
Phoenix 2*	4.59	0.51	4.74	0.93	86.52	1.56	4.15	2.00	9.33
Phoenix 3	0.00	0.00	28.59	6.89	0.00	0.00	71.41	6.89	28.59
Phoenix 4*	9.93	1.36	7.11	0.44	59.11	2.47	23.85	2.24	17.04
Portland 1*	10.96	3.37	7.26	0.68	70.37	4.90	11.41	1.68	18.22
Portland 2*	4.44	1.54	14.07	2.68	78.81	4.45	2.67	3.47	18.52
Portland 3*	15.26	6.42	18.22	4.81	56.15	5.49	10.37	6.69	33.48
Portland 4	5.48	0.68	37.48	4.27	6.07	1.36	50.96	2.86	42.96
Portland 5	1.93	1.68	56.59	1.68	4.15	2.28	37.33	5.24	58.52
Sacramento 1*	3.56	0.44	35.11	4.24	32.59	4.90	28.74	3.28	38.67
Sacramento 2	2.37	1.12	54.22	3.20	9.93	0.68	33.48	4.22	56.59
Sacramento 3	0.00	0.00	79.85	1.80	2.37	0.68	17.78	2.35	79.85
Sacramento 4*	21.93	1.12	21.48	1.36	43.56	4.00	13.04	2.45	43.41
Sacramento 5*	10.81	1.28	25.63	1.56	57.04	1.56	6.52	1.28	36.44
Sacramento 6*	7.11	1.33	9.78	1.60	67.85	3.78	15.26	1.12	16.89
Seattle 1*	0.89	0.44	4.59	1.12	71.85	1.03	22.67	1.18	5.48
Seattle 2*	16.74	2.96	43.70	6.03	21.48	2.45	18.07	2.00	60.44
Seattle 3*	5.33	2.47	14.52	2.45	75.26	3.98	4.89	0.89	19.85
Seattle 4	0.00	0.00	76.15	4.27	0.00	0.00	23.85	4.27	76.15
Seattle 5*	3.26	1.03	17.19	2.05	66.67	3.20	12.89	1.54	20.44

Appendix B

The Priestly-Taylor (Priestley and Taylor, 1972) method provides estimates of potential evaporation without wind and relative humidity inputs. The equation, based only on temperature and radiation, is:

$$E_0 = 1.28 \left(\frac{h_0}{HV} \right) \left(\frac{\delta}{\delta + \gamma} \right)$$

where:

h_0 = the net radiation (from Daymet dataset)

HV = latent heat of vaporization

δ = slope of the saturation vapor pressure

γ = psychometric constant

CHAPTER 2

ASSESSING THE IMPACT OF URBAN LAND DEVELOPMENT ON NET PRIMARY PRODUCTIVITY IN THE SOUTHEASTERN UNITED STATES

Abstract

The southeastern United States has undergone one of the highest rates of landscape changes in the country, due to changing demographics and land use practices over the last few decades. Increasing evidence indicates that these changes have impacted meso-scale weather patterns, biodiversity and water resources. Since the Southeast has one of the highest rates of land productivity in the nation, it is important to monitor the effects of such changes regularly. Here, I propose a remote sensing based methodology to estimate regional impacts of urban land development on ecosystem structure and function. As an indicator of ecosystem functioning I chose net primary productivity (NPP), which is now routinely estimated from the MODerate resolution Imaging Spectroradiometer (MODIS) data. I used the MODIS data, a 1992 Landsat-based land cover map and nighttime data derived from the Defense Meteorological Satellite Program's Operational Linescan System (DMSP/OLS) for the years 1992/93 and 2000 to estimate the extent of urban development and its impact on NPP. The analysis based on the nighttime data indicated that in 1992/93 urban areas amounted to 4.5% of the total land surface of the region. In the year 2000, the nighttime data showed an increase of urban development for the southeastern United States by 1.9%. Estimates derived from the MODIS data indicated that land cover changes due to urban development that took place during the 1992-2000 period reduced annual NPP of the southeastern United States by 0.4%. Despite the uncertainties in sensor fusion and the coarse resolution of the data used in this study, results show that the combination of MODIS products such as NPP with nighttime data could provide rapid assessment of urban land cover changes and their impacts on regional ecosystem resources.

34

Introduction

Land development in the United States is proceeding rapidly, at a rate faster than population growth (U.S. Environmental Protection Agency, 2000; U.S. Department of Housing and Urban Development, 2000; Heimlich and Anderson, 2001), to accommodate the space demands of an affluent society. From an ecological perspective, land development is one of the most disturbing processes since it dramatically alters the natural energy and material cycles of ecosystems (Pielke et al., 1999; McDonnell et al., 1997; Berry, 1990; Oke, 1989). For example, the carbon cycle is altered due to the subtraction of developed land from the photosynthetic process and the increase in CO_2 emissions from fossil energy use in urban areas. On the other hand, intensive management through fertilization and irrigation of the remaining urban vegetation tends to compensate the reduction of the vegetated surface and the net result of urbanization on the photosynthetic capacity depends on the type of ecosystem in which development takes place. In the arid and semiarid western United States, urbanization can even result in an overall increase in vegetation productivity compared to the surrounding rural environment (Imhoff et al., 2000) at a very large expense in water resources (as seen in chapter 1). In contrast, in the less resource-limited regions of the United States (eastern and southeastern), urbanization has the effect of lowering the photosynthetic activity of the landscape (Imhoff et al., 2000). This observation is particularly relevant when considering that urbanization in the United States occurs preferentially where the soils are most productive (Imhoff, 1997a), thereby causing a loss of prime farmland.

In recent years growth in population size and land occupation has been higher than the national average in the southeastern United States (SE-US) where strong economic forces are reshaping the landscape through urbanization (U.S. Bureau of the Census,

35

2001). These forces are significantly fragmenting the landscape of this traditionally rural region, which also hosts among the most productive forests of the United States (Wear and Greis, 2001). Because of its important ecological resources, the SE-US represents the ideal study area in which to develop a remote sensing based methodology for a regional assessment of the effects of land cover changes, in particular urban land development, on ecosystem resources. Earlier studies on the impact of land cover changes on ecosystem resources have been conducted at either global scales (using coarse resolution data sets) or over small regions (Paruelo et al., 2001; Imhoff et al., 2000; DeFries et al., 1999; Houghton et al., 1999). A methodology that is consistent across various spatial scales would provide an ideal tool allowing resource managers to map and monitor the impacts of land cover changes.

The recent availability of remote sensing data from the MODIS sensor on-board TERRA (EOS-AM1) platform offers an improved opportunity to monitor ecosystem resources and functioning at regional to global scales. Similarly, improvements to the Defense Meteorological Satellite Program's Operational Linescan System (DMSP/OLS) nighttime data (Elvidge et al., 2001) also allow us to track changes in human settlements. In this study I explore the combination of the MODIS and DMSP/OLS data sets to assess the impacts of urban development on net primary productivity (NPP) in the SE-US. NPP, the amount of carbon fixed by plants, represents an integrative descriptor of ecosystem functioning and resources because it modulates a number of other ecosystem services ranging from freshwater availability to biodiversity (Field, 2001; McNaughton et al., 1989).

Specifically, the following issues are addressed: 1) what is the extent of recent intensification of urban land development? 2) How has the urban land development impacted regional NPP?

36

Study Area

The region examined in this chapter includes the states of Tennessee, Mississippi, Alabama, North Carolina, South Carolina, Georgia and Florida. These states occupy the southeastern portion of the United States and are characterized by a mild wet climate, with an average annual temperature of 17 °C and annual precipitation greater than 1300 mm. The climate has favored, over time, intense agricultural exploitation, intense timber exploitation and currently, through a strong economic growth, population and urbanization (Alig and Healy, 1987). According to the latest U.S. Census, over 49 million people were living in these seven states in 2000, 20% more than in 1990. It is expected that between 1992 and 2020 urban areas in the South will more than double in extent (Wear and Greis, 2001).

Methods

The methodology used MODIS, DMSP/OLS and Landsat data organized in a geographic information system (GIS). All the data were reproduced at 1 km spatial resolution and projected to Lambert Azimuthal Equal Area. A high resolution land cover map and nighttime imagery from the DMSP/OLS for the years 1992/93 and 2000 were used to describe the land cover changes that have taken place in the SE-US as a consequence of recent urban land development. NPP was calculated from MODIS data, using MODIS derived Leaf Area Index/Fraction of Photosynthetic Active Radiation absorbed by vegetation (LAI/FPAR) and climate data. Using a 1992 land cover as a template I also identified the surface of each land cover type that has been recently converted into urban use, as inferred from 1992/93-2000 nighttime data change

37

detection. Finally, the impact of this recent development on the regional NPP was estimated as a sum of losses in NPP from each land cover type.

Mapping southeastern land cover

Predominant land cover types for the SE-US were derived from the 1992 National Land Cover Data set (NLCD) (Vogelmann et al., 2001). This data set was produced at 30-m spatial resolution from Landsat Thematic Mapper images acquired in the early 1990s and other sources of digital data, mapping 21 land cover classes for the conterminous United States. Overall accuracy for the eastern United States was assessed to be 81% for Anderson level I aggregations (i.e. water, urban, barren land, forest, agricultural land, wetland, rangeland; Anderson et al., 1976), and 60% for all 21 land cover classes (Vogelmann et al., 2001). The NLCD data set exists both in the native 30-m resolution and in a multi-layer 1-km resolution (one layer for each land cover class), in which each pixel reports the percentage land cover type occupied in the square kilometer unit.

A land cover map was required both to track land cover changes due to recent urban sprawl in the SE-US and to guide the estimation of NPP from MODIS data. Since the MODIS algorithm for the calculation of NPP requires a map of canopy functional types, the 21 original land cover types from the 1- km resolution product were grouped into 8 classes, namely: urban, crops, deciduous broadleaf forest, evergreen needleleaf forest, mixed forest (deciduous broadleaf and evergreen needleleaf), grassland, shrubland and barren. Then each square kilometer was assigned to the dominant land cover in the pixel (i.e. to the land cover occupying the largest fraction) (Figure 2.1). The surface fraction occupied by each land cover on a state-by-state basis is reported in Table 2.1.

38
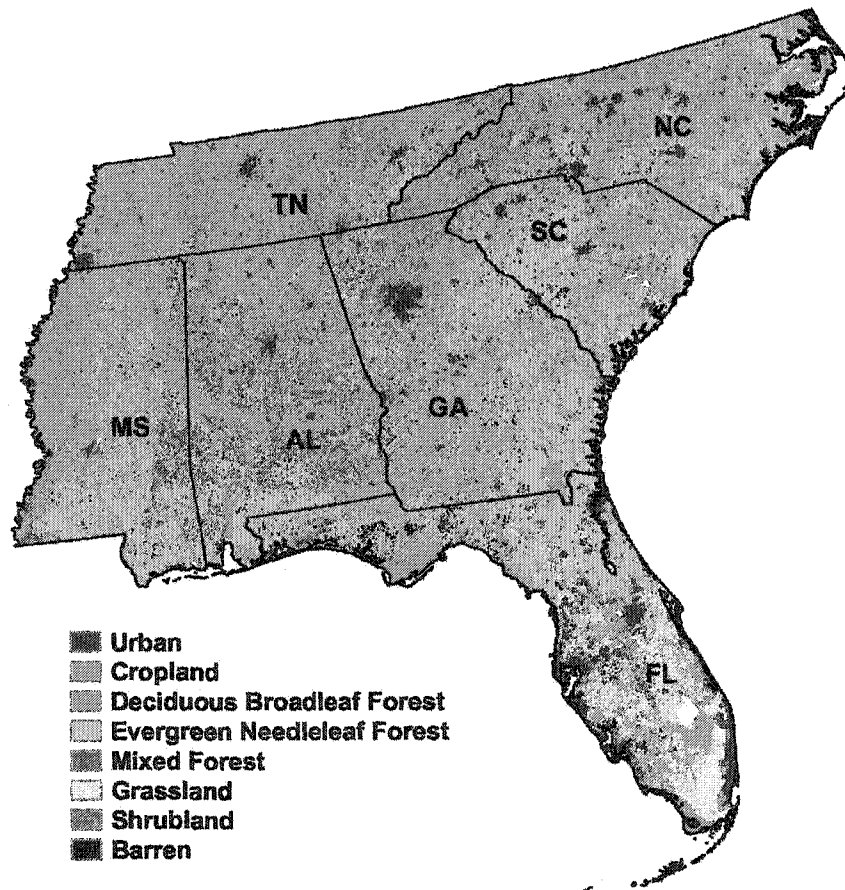
Figure 2.1 A 1-km land cover derived from the 1992 NLCD dataset (30m) by assigning each pixel to the dominant land cover within the 1-km unit. The borders of the seven states included in the SE-US region analyzed in this study are imposed on the land cover. AL = Alabama; FL = Florida; GA = Georgia; MS = Mississippi; NC = North Carolina; SC = South Carolina; TN = Tennessee.

39

Table 2.1. Percent fractions of land cover classes for the seven southeastern states reported from the 1-km land cover

State	Urban (%)	Crops (%)	Deciduous Forest (%)	Evergreen Forest (%)	Mixed Forest (%)	Grassland (%)	Shrubland (%)	Transitional (%)
Alabama	1.8	23.7	35.6	18.8	18.7	0.1	-	1.4
Florida	10.9	13.0	25.8	23.2	1.0	21.6	0.2	3.0
Georgia	3.5	31.2	32.9	25.0	4.4	1.2	-	1.8
Mississippi	1.4	39.3	30.5	21.3	6.1	0.3	-	1.1
N. Carolina	4.9	28.1	47.4	16.1	1.9	0.7	-	0.6
S. Carolina	4.1	27.3	32.2	31.6	0.6	2.3	-	1.5
Tennessee	3.4	35.9	53.5	3.4	3.3	0.1	-	0.3
SE-US	4.4	27.9	36.4	19.8	5.4	4.2	0.02	1.4

40

Mapping developed land with Nighttime data

Land cover data sets such as the NLDC are useful for several regional and national management applications. However the large amount of effort involved in their production limits their updating to not more than once every ten years. While this time scale is more than appropriate for a number of applications, the monitoring of urban growth may require higher frequency assessments in rapidly developing regions.

In this chapter, the extent of recent (1992/93-2000) urban land development in the SE-US was estimated using the DMSP/OLS nighttime. The DN (digital number) of the DMSP/OLS data represented the average nighttime lights from cloud-free portions of orbits collected during the dark portions of the lunar cycles of the months of September, October and November of 1992-93 and 2000. The averaged nighttime lights have a spatial resolution of 1 km. The basic procedure for producing a cloud-free composite for the average DN for lights of each time period (1992/93 and 2000) can be found in Elvidge et al. (1997a).

The resulting average DN nighttime lights could not be used directly to estimate the extent of urban land development in the study area since this would produce an overestimate. The use of the raw average DN data tends to overestimate the size of small towns due to several factors, including: 1) the large size of the OLS pixel footprint; 2) wide overlap in the footprints of adjacent pixels; 3) accumulation of geolocation errors; 4) possible inclusion of scattered light due to fog, clouds or haze. Different DN thresholds, below which all the pixels were zeroed, were applied to the 1992/93 DMSP/OLS data. For each threshold, the total lit area was compared to the total urban area by state from the 1-km land cover derived from the 1-km NLCD data, from the original (30 m) NLCD data and from 1990 U.S. Census tabular data. The statistics obtained for a set of thresholds are reported in Table 2.2.

41

Table 2.2. Comparison of urban area estimates for the 7 states of the Southeastern U.S. from: DMSP data (threshold at digital number (DN) greater or equal to 48, 49, 50, 51 and 52 respectively), from the 1-km land cover, the original NLCD data and from U.S. Bureau of the Census.

	DMSP Threshold $DN{\geq}48$ (km^2)	DMSP Threshold $DN{\geq}49$ (km^2)	**DMSP Threshold $DN{\geq}50$ (km^2)**	DMSP Threshold $DN{\geq}51$ (km^2)	DMSP Threshold $DN{\geq}52$ (km^2)	Land Cover 1km (km^2)	NLCD 30m (km^2)	U.S. Census † (km^2)
1992/93 DMSP data								
Alabama	3967	3821	**3688**	3522	3379	2353	2274.1	7111.6
Florida	13491	13198	**12909**	12617	12294	15947	13086.9	12318
Georgia	6992	6764	**6572**	6376	6149	5297	4364.8	5745.2
Mississippi	1837	1755	**1664**	1584	1484	1696	1770.7	2931
N. Carolina	6362	6127	**5893**	5634	5448	6254	5756.1	4956.5
S. Carolina	3820	3657	**3494**	3338	3189	3275	2954.2	2954.2
Tennessee	5051	4870	**4697**	4524	4346	3656	3709.8	6476.6
SE-US Total	41520	40192	**38917**	37595	36289	38478	33916.5	42493.1
% urban	4.8	4.6	**4.5**	4.3	4.2	4.4	3.9	4.9
*Threshold DMSP vs. Land Cover 1km**								
- b	1.29	1.20	**1.32**	1.34	1.36			
- a	-2042	-1933	**-1817.3**	-1693	-1588.4			
- R^2	0.956	0.9576	**0.9577**	0.958	0.9595			
*Threshold DMSP vs. NLCD 30m**								
- b	1.01	1.02	**1.04**	1.06	1.08			
- a	-1121.7	-1034.7	**-941.7**	-841.6	-759.2			
- R^2	0.949	0.9503	**0.95**	0.9501	0.9512			
*Threshold DMSP vs. U.S. Census**								
- b	0.751	0.77	**0.78**	0.80	0.81			
- a	1607.8	1667.5	**1727.7**	1798.6	1860.9			
- R^2	0.7799	0.7829	**0.7861**	0.7877	0.7885			
t-test, p-value DMSP vs. Land Cover 1km	0.4554	0.6762	**0.9167**	0.838	0.6264			
2000 DMSP data								
Alabama	5838	5624	**5421**	5212	5016			8372.1
Florida	17263	16900	**16538**	16185	15798			15890.9
Georgia	10217	9926	**9662**	9371	9060			7278.6
Mississippi	3242	3099	**2963**	2818	2679			3872.6
N. Carolina	9601	9269	**8933**	8629	8291			7306.1
S. Carolina	5853	5637	**5417**	5202	5004			3390.6
Tennessee	7017	6780	**6542**	6296	6092			7951.0
SE-US Total	59030	57235	**55476**	53713	51940			54061.9
% urban	6.9	6.6	**6.4**	6.2	6.0			6.2
*Threshold DMSP vs. U.S. Census**								
- b	0.80	0.81	**0.83**	0.84	0.86			
- a	969	1063.3	**1157.4**	1264.1	1339.8			
- R^2	0.7918	0.7939	**0.796**	0.7977	0.8011			

† U.S. Census data refer to the year 1990 for the comparison with 1992/93 DMSP data set and to the year 2000 for the comparison with the 2000 DMSP data set.
* b is slope of the linear regression and a is the intercept.

42

The total urban area from the NLCD data was derived aggregating the following

NLCD classes: low-density residential, high-density residential,

commercial/industrial/transportation and urban/recreational grasses. Then, the

percentages of total urban area for each 1-km unit where summed up on a state-by-state

basis. The computation indicated that in 1992 the urban areas in the SE-US occupied

$33,916.5$ m^2 (4% of the total land surface). The total urban area from the 1990 U.S.

Census was obtained from tabular data listing the land area of populated places in 1990

on a state-by-state basis (U.S. Bureau of the Census, 1996). The definition of 'urban' for

the 1990 U.S. Census included all the urbanized areas and places with a population of

more than 2,500. The sum of the land area of all the places with 2,500 or more people

yielded a total urban area for the region of $42,493.1$ km^2 (about 4.9% of the total land

surface).

A number of issues challenged the selection of an appropriate threshold for the

1992/93 DMSP data. One of these issues was the large disagreement (more than 8,500

km^2) between the total urban area estimated from the NLCD data and from the 1990

U.S. Census. The 1992 land cover derived from the NLCD data set, by assigning each

1-km pixel to the dominant land cover in the unit, estimated a total urban area of 38,478

km^2, a value in between the ones estimated from the original NLCD and from the

Census. Since this land cover was used to drive the MODIS algorithms for the

estimation of FPAR/LAI and NPP, it was decided to use it as the reference layer to

compare the total lit area from the DMSP at different thresholds. The threshold that

would produce the best correspondence was identified by linear regression and with a t-

test for significant differences. The best correspondence between the total lit area from

the 1992/93 DMSP data and the current land cover was shown for a threshold at a value

of DN greater than or equal to 50. While lit area estimates from other thresholds all

displayed similar R^2 by linear regression, the estimates from the DMSP with a threshold

43

of DN $\geq$ 50 proved to be the least significantly different from the 1-km land cover

estimates of urban area (paired t-test, hypothesized difference = 0, alpha = 0.05, t-value

= 0.1091, p-value = 0.9167, N=7). The 1992/93 total lit area of all the pixels with a DN $\geq$

50 was 38,917 km^2 (4.5% of the total land surface) and its geographical distribution is

shown in Figure 2.2a. An alternative to this approach would be the selection of a pair of

thresholds, to provide a lower and an upper estimate of the extent of urban area and its

impact on NPP.

Figure 2.2. Average nighttime lights with digital numbers greater or equal to 50 for (a) 1992/93, (b) 2000 and (c) difference between 2000 and 1992/93.
1 = Atlanta, GA; 2 = Nashville, TN; 3 = Atlanta, GA to Greensboro; NC, 4 = Florida.

The extent of total urban area from the 2000 average DN nighttime lights was

estimated by applying the same threshold of DN $\geq$ 50, obtaining a total urbanized

surface of 55,476 km^2 (6.4% of the total surface) (Figure 2.2b). The only data set

available to verify this value was the total land area of all incorporated urban areas and

places with 2,500 or more people from the County and City Data Book 2000 (U.S.

Census Bureau, 2000). According to the U.S. Census data, the total urbanized surface

44

for the SE-US region for the year 2000 is 54,061.9 km^2. While the total estimates are similar for the two methods, wide discrepancies between the state-by-state estimates exist, especially in the case of Alabama.

A difference image between the nighttime averages of 2000 and 1992-93 thresholded at DN $\geq$ 50 was used to estimate the distribution of recent land development in the SE-US. While most of the change in nighttime lights over the study area has taken place in the form of an intensification of human activity in areas already developed by 1992, this study took into account only those pixels that had no nighttime activity in 1992/93 and were lit in 2000. According to this analysis, the total land developed during 1992/93-2000 amounted to 16,559 km^2 (1.9% increase) (Figure 2.2c).

Estimation of land cover change effects on primary productivity

NPP data from MODIS are distributed by the EROS Data Center Distributed Active Archive Center (EDC DAAC) with the product name of MOD17. However, in this data set, urban areas, along with water bodies, are masked out. As a consequence, NPP for the study area needed to be generated from LAI and FPAR (MOD15), which were calculated from the MODIS Normalized Difference Vegetation Index (NDVI) (MOD13) and the MOD15 backup algorithm. MOD13 (NDVI) data for the year 2001 were downloaded from the EDC DAAC. These data represent 16-day composites of atmospherically corrected maximum NDVI and EVI (Enhanced Vegetation Index) at 1-km spatial resolution. For a detailed description of the data see Huete et al. (1999). In order to cover the study area, three MODIS tiles, each covering a ground area of 1200x1200 km, were mosaicked for each of the 20 available bi-weekly composites and reprojected to Lambert Azimuthal Equal Area from the original Integerized Sinusoidal Projection.

45

The MOD15 backup algorithm uses empirical relations between NDVI and LAI and FPAR derived for various land cover types (Knyazikhin et al., 1999; Myneni et al., 1997). The 1992 land cover map was used to guide the estimation of LAI/FPAR after rearranging the classes from the perspective of the radiative transfer theory. While urban areas can have substantial amounts of forest vegetation, at the resolution of 1 square kilometer most of the urban cover is a mosaic of trees with grass underneath and buildings. As a consequence, the urban class was assigned to the savanna biome, defined as a two-layer canopy with an overstory of trees and an understory of grasses (Myneni et al., 1997). The land cover class of mixed forest is also not contemplated as an independent structural type from the radiative transfer theory perspective. Thus, the algorithm was run twice over the pixels classified as mixed forest, once considering them as broadleaf forests and once as needleleaf forests. Assuming that broadleaf and needleleaf species were present in equal proportions in the land cover class of mixed forest, the LAI/FPAR values were calculated as an average of the two runs.

The algorithm used to produce MODIS NPP is shown in Figure 2.3 (Running et al., 2000; Running et al., 1999). The algorithm is based on a light use efficiency logic that relates Absorbed Photosynthetic Active Radiation (APAR) to GPP, where APAR = FPAR * IPAR (IPAR = Incident Photosynthetic Active Radiation). ε_{max} is a biome specific light use efficiency factor that is modified into ε by daily meteorological conditions (minimum temperature and vapor pressure deficit). ε is used to convert APAR to GPP. NPP is obtained by subtracting maintenance respiration (MR) and growth respiration (GR) components from living tissue material from the annual integral of GPP. LAI is used to compute living biomass, which is a key component of respiration estimation. The meteorological conditions and the IPAR required for the NPP calculation were derived as

46

an average of the 1980-1997 1-km spatially interpolated surface weather observations

(Thornton et al., 1997).
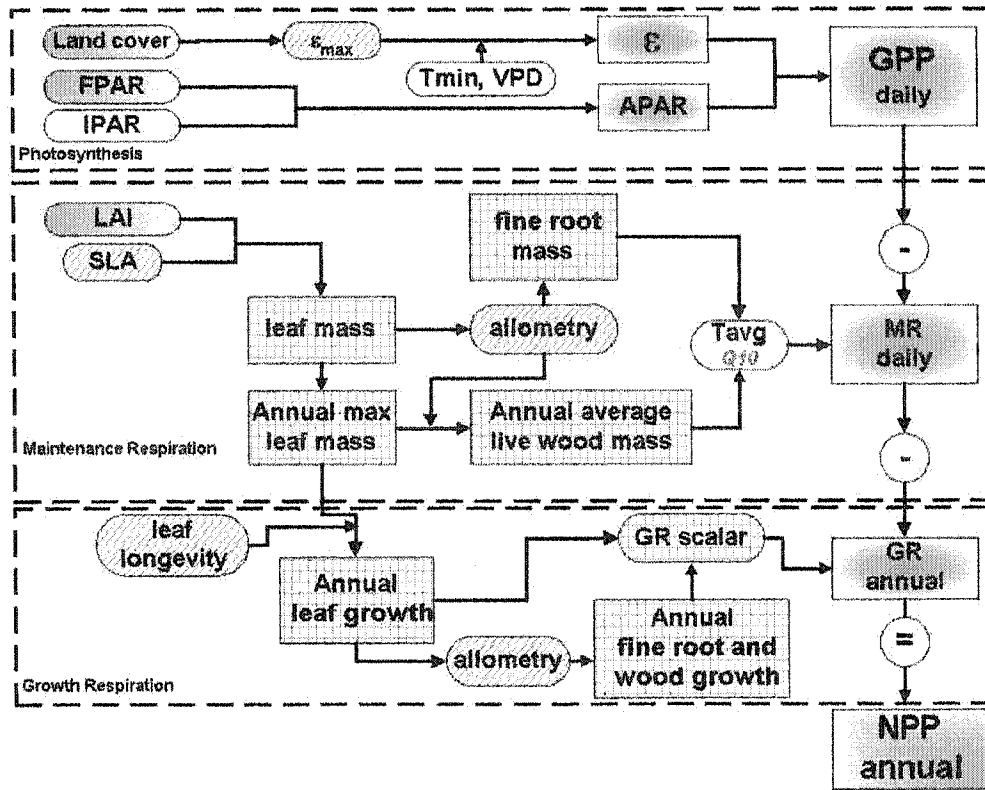
Figure 2.3. MODIS productivity logic.
Key components: 1) remote sensing inputs (land cover, FPAR, LAI), 2) daily surface weather (IPAR = Incident Photosynthetic Active Radiation, T_{min} = minimum daily temperature, T_{avg} = daily average temperature estimated from T_{min} and T_{max}, and VPD = Vapor Pressure Deficit), 3) a look-up-table containing biome specific coefficients (ε_{max}, biometry, leaf longevity and those used in respiration), generated from an ecosystem model. Based on the land cover, a characteristic radiation conversion efficiency parameter (ε_{max}) is extracted from a lookup table. T_{min} and VPD are used to attenuate ε_{max} to produce ε, which is then used with the Absorbed Photosynthetic Active Radiation (APAR) to predict daily Gross Primary Productivity (GPP = ε * APAR, where APAR = IPAR * FPAR). Specific Leaf Area (SLA) determined by land cover is used to estimate leaf mass from LAI. Fine root mass is assumed to be in a constant fraction of leaf mass for each land cover. In an annual time step logic, annual leaf mass is assessed from daily leaf mass and used to estimate annual average live wood mass. Maintenance respiration costs (MR) of leaf, fine root and live wood mass are calculated daily as exponential functions of daily average temperature (T_{avg}). Leaf longevity from a lookup table is used to determine annual leaf growth and, through allometric relationships, annual fine root and wood growth and the associated annual growth respiration costs (GR). Final estimation of annual Net Primary Productivity (NPP) is obtained subtracting the annual integral of daily MR and annual GR from the annual integral of daily GPP.

47

An estimate of total NPP for the 1992 land cover could be obtained in two ways: 1) as a spatially explicit summation of the NPP values derived for each pixel or 2) by multiplying, for each state, the number of pixels in each land cover by its mean NPP. Because of uncertainties related with the land cover accuracy and with the fusion of data from different sources, the total NPP was calculated with the second method. Mean NPP for each 1992 land cover class was obtained as an arithmetic average of the total NPP by land cover category in each state, including only those pixels that were not lit in the 2000 average nighttime data with a threshold of $DN \geq 50$. An estimate of NPP was calculated also for the barren category, since in the SE-US this land cover type is represented mainly by a transitional class. The NLCD land cover defines transitional those areas with sparse vegetation (less than 25% of cover) that are dynamically changing from one land cover to another, often because of land use activities (i.e. forest clearcuts, transition between forest and agricultural land, etc.). The transitional pixel was assumed to be previously covered with the second most dominant cover in the 1-km unit. The mean NPP of the transitional pixel was then assigned to be 25% of the mean NPP of the second most dominant cover. For example, if the second largest cover in the pixel was deciduous broadleaf, the transitional pixel was assumed to be a clearcut of this forest type and its mean NPP equal to 25% of the mean NPP of the deciduous forest. While these assumptions might be incorrect, they do not have a large impact on the total NPP because of the small surface occupied by this category.

An estimate of the NPP of the recently developed areas was obtained by multiplying the mean NPP for the urban category of each state by the number of newly developed pixels in the state that were not classified as urban in the 1992 land cover.

Results and Discussion

Changes in land cover due to urban sprawl

Figure 2.2 shows the 1992-93 and 2000 average nighttime lights with a threshold of

DN ≥ 50 and a difference image between the two periods. The difference image provides

an estimate of the most intense land development occurring during the 1990s in the SE-

US. It indicates that most of the newly developed land is located at the periphery of the

largest urban areas, as already demonstrated in other regions of the United States by

Imhoff et al. (2000). Large development is present around Atlanta, GA, from Atlanta, GA

to Greensboro, NC, around Nashville, TN and in Florida. It cannot be denied that in the

recent years human presence has significantly increased in the SE-US much beyond the

urban fringe. A comparison between the raw 1992-93 and the 2000 nighttime averages

indicates a dramatic increase in the presence of lower intensity nighttime lights in the

countryside, much higher than the one seen after applying the threshold. While a portion

of this low density lights may be attributed to error, most of them are probably the result

of the significant fragmentation process that is taking place in the SE-US landscape.

Even if the low-intensity nighttime lights in these rural areas are effectively due to the

presence of a built-up structure, it is assumed that they would occupy a very low fraction

of the 1-km pixel, therefore not significantly impacting the regional NPP.

Table 2.3 reports the surface in each land cover class that, according to the nighttime

lights difference between the 2000 and 1992/93, showed the most substantial increase

in human activity. The present study indicates that, between 1992 and 2000, land

development has irreversibly transformed about 1.9% of the SE-US. The largest

increase in lit surface was recorded for the states of Georgia, Florida, North Carolina and

South Carolina. It should be noted that a substantial portion of newly lit areas matches

with land already classified as urban in the 1992 land cover. There are a number of

49

factors that could explain this inconsistency; an inappropriate choice of threshold for the DMSP/OLS data would be a significant factor. As listed in Table 2.2, the total urban area for the SE-US estimated from the DMSP/OLS with a threshold of DN $\geq$ 50 is similar to the estimate derived from the 1992 land cover, but large differences can occur on a state-by-state basis. For example, the 1992/93 DMSP data estimate a urban surface of 12,909 km^2 for the state of Florida, a value 3,038 km^2 lower than the figure from the 1992 land cover, which probably is overestimating the real value. The selected threshold for the DMSP/OLS data estimates a smaller urban area than the 1992 land cover also for the states of Mississippi and North Carolina. Another factor contributing to the inconsistency could be related to the preparation of the 1 km land cover from the NLCD data. Assigning the pixels to the dominant cover in the 1 km unit could overestimate the total urban surface if the built-up surface in the pixel was larger than any other cover but less than 50%. Finally, the inconsistency could be due to geolocation errors in the DMSP data or to inaccuracy of the NLCD cover.

Table 2.3. Surface area developed between 1992/93 and 2000 and percent fractions of total land area based on change detection of thresholded DMSP/OLS data for the two composite periods.

State	Urban (km^2)	Crops (km^2)	Deciduous Forest (km^2)	Evergreen Forest (km^2)	Mixed Forest (km^2)	Grassland (km^2)	Shrubland (km^2)	Transitional (km^2)	Total (km^2)	Fraction (%)
Alabama	160	552	573	220	216	7	-	5	1773	1.3
Florida	1183	444	809	511	10	650	2	20	3629	2.5
Georgia	348	611	1284	463	346	17	-	21	2739	2.0
Mississippi	209	516	313	210	34	13	-	4	1090	1.1
N. Carolina	621	713	1136	520	32	6	-	12	2419	2.4
S. Carolina	325	542	495	472	2	73	-	14	1597	2.4
Tennessee	233	818	642	49	99	0	-	4	1612	1.7
SE-US	3079	4196	5252	2445	739	766	2	80	16559	1.9

51

Overall, overlaying the nighttime change image with the current biome land cover map indicates that most of the new development (50%) is due to the conversion of forest, in particular deciduous broadleaf forest, which is the dominant forest type in the region. About 25% of the new development resulted from the conversion of cropland and almost 5% from the conversion of grassland (mainly in Florida). These statistics are in agreement with the results presented in the Southern Forest Assessment Draft Report (Wear and Greis, 2001). According to the same report, this conversion of forest area into developed land is counterbalanced by a conversion of cropland into forest use. Therefore, it is actually the extent of croplands that is being reduced in the SE-US.

Effects of land cover change on regional primary productivity

Table 2.4 reports mean and total NPP estimates for each of the land covers. The 1992 total NPP for the SE-US is estimated to be 872.57 Tg (Teragrams, 10^{12} g) of carbon per year, 68% in forests and grasslands, 28% in crops and about 3% in urban areas. For the urban class, Table 2.4 shows also the percentage of urban area covered by tree canopies, as measured by Dwyer et al. (2000). Urban areas retain high primary productivity, which correlates well with the tree cover. The highest urban productivity per unit area is reported for Georgia (848 g C m^{-2} y^{-1}), which also presents the highest urban tree cover in the nation. Another factor contributing to this high productivity is the presence of parks and golf courses, which tend to be intensively managed with irrigation and fertilizers. Golf courses are particularly numerous in this region, which is also one of the prime North American retirees destinations.

52

Table 2.4. Estimates of mean and total NPP by current land cover types for the seven southeastern states.

State	Urban*	Crops	Deciduous Forest	Evergreen Forest	Mixed Forest	Grassland	Shrubland	Transitional	Total
				Mean NPP $(g\ m^{-2}\ y^{-1})$					
Alabama	800 (48.2)	993	1065	1085	1115	335	-	269	
Florida	749 (18.4)	1066	975	1038	1056	888	844	234	
Georgia	848 (55.3)	1120	1081	1083	1057	712	-	266	
Mississippi	765 (38.6)	958	1023	1077	1117	675	-	263	
N. Carolina	798 (42.9)	1040	1032	997	1068	361	-	241	
S. Carolina	789 (39.8)	1089	1053	1004	1047	585	-	254	
Tennessee	759 (43.9)	905	987	1016	1002	844	-	231	
				Total NPP $(Tg\ y^{-1})$					
Alabama	1.88	31.51	50.77	27.28	27.89	0.05	-	0.50	139.88
Florida	11.95	20.22	36.69	35.09	1.51	27.98	0.18	1.01	134.63
Georgia	4.49	53.08	54.15	41.14	7.04	1.28	-	0.74	161.92
Mississippi	1.30	46.47	38.44	28.30	8.42	0.22	-	0.35	123.50
N. Carolina	5.00	37.25	62.39	20.40	2.58	0.34	-	0.18	128.14
S. Carolina	2.58	23.80	27.12	25.40	0.53	1.08	-	0.31	80.82
Tennessee	2.78	35.54	57.77	3.82	3.65	0.06	-	0.07	103.69
SE-US	29.98	247.87	327.33	181.41	51.62	31.01	0.18	3.16	872.57

* Between parentheses, the urban tree cover, in percent, reported by Dwyer et al., 2000.

53

Table 2.5 shows the estimates of NPP loss due to new development as estimated from the change detection analysis of the nighttime imagery. We considered that no loss took place over those areas that appear as newly urbanized from the nighttime lights change detection but were already classified as urban in the 1992 land cover. The average loss in annual NPP per unit area is 183 g of carbon per square meter. The total loss amounts to 3.04 Tg of carbon per year, 0.35% of the total NPP in 1992 and apparently due to about 1.9% increase in the urban surface. This seems a modest loss in NPP and in carbon sequestration potential, probably contained by fertilization and irrigation of the urban vegetation. However, this loss becomes relevant if we consider that it was probably accompanied by a large increase in emissions of CO_2 due to the significant growth in population of the SE-US during the years between 1990 and 2000. This growth, according to the U.S. Census, amounted to almost 8.2 million people, a number equal to the current population of Georgia.

Table 2.5. Estimates of NPP lost due to estimated development between 1992/93 and 2000.

State	Unit loss in NPP $(g\ m^{-2}\ y^{-1})$	Total loss in NPP $(Tg\ y^{-1})$
Alabama	221	0.38
Florida	153	0.55
Georgia	204	0.63
Mississippi	196	0.26
N. Carolina	178	0.54
S. Carolina	194	0.37
Tennessee	163	0.30
SE-US	183	3.04

It is also important to understand that changes in land cover due to urban sprawl add to the other changes in land cover that took place in the SE-US, which have left unaltered very little of the original vegetation in the region. Most of the original mixed forest has been replaced by deciduous or evergreen stands for industrial timber production and by cropland. Crops, which contribute to almost a third of the primary productivity, are characterized by fast carbon cycling due to annual or biannual harvest. The harvesting of crops is also associated with carbon release from soils. Similarly, the turnover of the carbon from the timber plantation has been accelerated, also reducing the potential for long term carbon sequestration

The loss in NPP due to development could be reduced with intensive urban forestry programs, as shown for the state of Georgia, which has been the most successful in maintaining a high urban tree cover. Trees not only sequester more carbon per unit area than grasses, but also contribute to reduce surface runoff and evapotranspiration from irrigated lawns. Other benefits (Nowak and Crane, 2000) include emission reductions from air conditioners (trees provide shade to buildings) and general mitigation of the urban heat island effect. Urban forests also increase opportunities for wildlife survival and reduce land fragmentation.

Conclusions

The southeastern states, ecologically important because of their high primary productivity, are undergoing rapid changes in land use and land cover as a result of rapid population growth. In the context of characterizing and quantifying these changes, recent advances in remotely sensed data offer a valuable tool. The integration of advanced products such as NPP from satellite data with a nighttime lights map allows

55

not only rapidly monitoring changes in human settlements, but also estimating their impacts on ecosystem resources. Much of the data used in this study is readily available to the public, and should therefore be a valuable resource for communities world-wide.

The results presented in this chapter provide a coarse assessment of the extent of urban sprawl and its impact on NPP in the SE-US. The spatial resolution and uncertainties of the input data limit the accuracy of the results. Nevertheless, it provides a methodology for understanding regional effects of urbanization on primary productivity.

Other MODIS products that are routinely produced and may be of use in urban studies include surface albedo, surface temperature and aerosol concentration. Their integration with the LAI/NPP products could provide useful information of the impact of urban areas on energy efficiency and other ecosystem variables. Though not widely available as yet, MODIS also produces 250m NDVI data, from which higher resolution NPP could be derived. Once the processing is streamlined, it should vastly enhance the potential for urban studies.

CHAPTER 3

SYNERGISTIC USE OF MODIS AND NIGHTTIME DMSP/OLS DATA FOR THE ASSESSMENT OF THE CLIMATIC EFFECTS OF URBANIZATION

Abstract

As urban areas are continuing to expand globally, there is an increasing need for exploring methods of monitoring the environmental effects of urbanization. In this chapter I explore the synergistic use of the fractional Impervious Surface Area (ISA), a measure of urban development density estimated from the Defense Meteorological Satellite Program/Operational Linear Scanner (DMSP/OLS), and the normalized difference vegetation index (NDVI), a surrogate for vegetation biomass, and the land surface temperature (LST) data from the MODerate resolution Imaging Spectroradiometer (MODIS) to understand how urbanization-induced land cover changes influence the local climate. The analysis was performed over the metropolitan areas of Chicago, Atlanta and Phoenix, U.S.A., representing different climatic regimes and urban development densities. The results indicate that NDVI does not necessarily decrease linearly as the fractional ISA increases, and may eventually increase with the density of development due to vegetation management practices, as in the case of Phoenix. In contrast, the nighttime LST consistently increases with the fractional ISA in the three urban environments. The urban-rural differences in nighttime LST for the three metropolitan areas are similar for equal values of imperviousness, indicating that the fractional ISA from the DMSP/OLS and standard products from MODIS could provide a continental physically-based characterization of the surface that could be used to track the effects of urbanization on the local and regional climate.

Introduction

While globally the total urbanized surface represents a small fraction of the land undergoing conversion, the landscape changes created by the concentration of human settlements have large effects (Shepherd and Burian, 2003; Dow and DeWalle, 2000; Pielke, 1999). For example, it is well known that land cover transformations due to urbanization create air and surface temperatures that are often several degrees warmer than their surrounding rural areas. Among the transformations responsible for the arising of the urban heat islands are a number of factors influencing the local energy and water balance such as: changes in the thermal properties of the surface materials and decreased moisture availability for evapotranspiration, changes in the local topography with the creation of urban canyons and consequent effects on the surface roughness and on the short-wave radiation absorption and long wave radiation emissions (Landsberg, 1981; Oke, 1978). The magnitude of the urban heat island has often being related to the population size of the urban area (Karl et al., 1988; Oke, 1973), because of the long historical records of this parameter.

In recent years numerous research efforts have applied remote sensing to measure aspects of urbanization such as growth and associated land cover changes to study how they relate to the modification of the climate. For example, Gallo and Owen (1999) have related the magnitude of the heat island to satellite measures of the urban-rural contrast in vegetation density, such as the Normalized Difference Vegetation Index (NDVI). The possibility of measuring such a variable consistently on a global scale has been found useful to correct the temperature records from meteorological stations located in urban areas for the urban bias effect. Differences in NDVI from urban and surrounding rural areas (NDVIurb-rur) from the Advanced Very High Resolution Radiometer (AVHRR) have been used to correct the urban bias on minimum air temperatures as a better

58

alternative to corrections based on population size of the urban areas where the stations were located (Gallo and Owen, 1999). The correction of the urban bias based on the urban rural contrast in vegetation biomass assumes that the NDVIurb-rur is negatively related to the differences in urban rural air temperatures. The NDVI has also been used to calculate the impervious surface fraction of an urbanized surface, assuming the vegetation index to be proportional to the fractional vegetation cover (Carlson and Arthur, 2000; Owen et al., 1998a), with the limitation that bare and built-up soil can not be discriminated. This methodology also assumes NDVI to decrease linearly as the fraction of impervious surface increases. Moreover, as the factors responsible for the temperature differences are characterized by seasonal variability, the heat island has been found to change seasonally, with the timing of the maximum heat island differing among different cities (Cayan and Douglas, 1984; Landsberg, 1981). For example, the difference in urban and rural vegetation density is strongly seasonal in most climates, but whether its seasonality is synchronized with the seasonality of the heat island has not been fully investigated.

The opportunity to better understand the nature of the physical alterations of urbanization affecting the local climate is enhanced by the recent availability of data from new instruments and formerly unexploited potentials of existing datasets. For example, the possibility to obtain NDVI and land surface temperature data from MODIS that present standard state-of-the-art atmospheric corrections and radiance calibration vastly facilitates the comparison of these variables over urban areas across different geographic regions, a task that was much harder with AVHRR data. Also, a measure of the imperviousness of the surface derived from the nighttime citylights data, and therefore that is independent from NDVI, should also improve the analysis of the effect of urbanization on climate.

The nighttime citylights data from the Defense Meteorological Satellite Program/Operational Linear Scanner (DMSP/OLS) have proven useful to map the extent of urbanization across the continental United States (Milesi et al., 2003; Elvidge et al., 1997b; Imhoff et al., 1997b) and at global scale (Henderson et al., 2003; Elvidge et al., 1997a) and have been used to identify urban, suburban, and rural meteorological stations associated with the U.S. Historical Climatology Network (Owen et al., 1998b). In chapter 1, the radiance calibrated nighttime citylights has also been used to produce a 1-km spatial resolution estimate of the fractional Impervious Surface Area (ISA) of the continental United States. Here I analyze the fractional ISA in conjunction with the standard products of NDVI and land surface temperature (LST) derived from MODIS data to understand how land cover changes due to urbanization influence the local climate along gradients of development densities.

Objectives of this chapter are: 1) to evaluate the generality of the assumption that biomass decreases with the urban fractional ISA; and 2) to analyze the seasonality of daytime and nighttime land surface urban-rural temperature contrasts and compare it to the seasonality of the urban-rural contrast in NDVI along gradients of fractional ISA in order to evaluate the potential usefulness of a coarse-resolution remote sensing based measure of imperviousness for tracking urbanization effects on climate. To represent different climatic regimes and urban development densities, the analysis is carried over the metropolitan areas of Chicago, Atlanta and Phoenix and the rural areas surrounding them.

60

Description of the study areas

Chicago, Atlanta and Phoenix are three major urban areas of the continental United
States characterized by contrasting climates (Figure 3.1) and development densities
(Table 3.1).
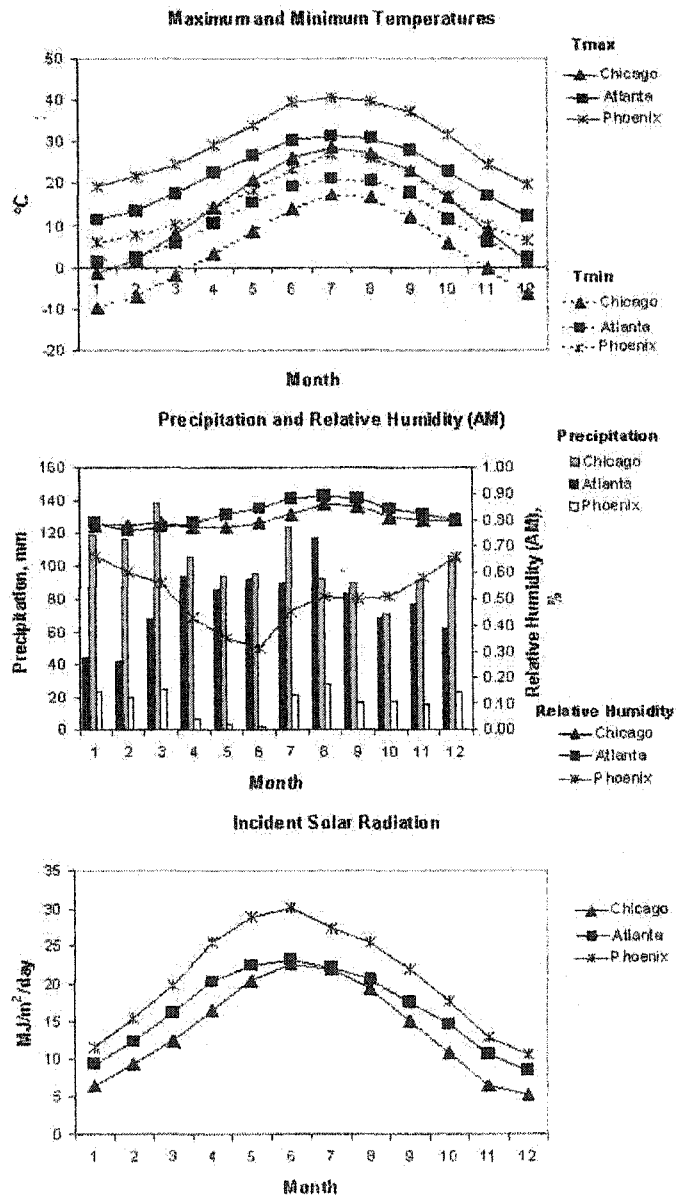
Figure 3.1. Climatic description of the three study areas. Top: maximum (Tmax)
and minimum (Tmin) temperatures. Middle: precipitation (vertical bars, with scale
on the left axis) and relative humidity (lines, with scale on the right axis) (NCDC,
2003). Bottom: incident solar radiation (RReDC, 2003).

61

Table 3.1. Population, surface and population density by fractional impervious surface area (ISA) within the analysis windows of the three metropolitan areas.

Fractional ISA (%)	Chicago Population	Chicago Surface km^2	Chicago Density people/km^2	Atlanta Population	Atlanta Surface km^2	Atlanta Density people/km^2	Phoenix Population	Phoenix Surface km^2	Phoenix Density people/km^2
0-10	364,293	9,048	40	855,618	17,100	50	123,837	12,561	10
11-20	735,755	2,811	262	967,057	2,994	323	225,027	859	262
21-30	1,141,030	1,679	679	834,263	1,322	631	359,437	536	670
31-40	1,122,238	1,019	1,101	269,192	359	750	660,754	562	1,176
41-50	695,536	394	1,765	75,117	79	950	626,263	376	1,665
51-60	584,309	229	2,552	16,934	14	1,210	192,499	104	1,850
61-70	479,900	126	3,809	15,741	10	1,574	65,565	27	2,317
71-80	236,088	55	4,293	14,900	8	1,863			
81-90	122,818	25	4,913	8,926	7	1,275			
>90	145,465	24	6,061	4,746	2	2,373			
Total	5,627,432	15,140		3,062,494	21,895		2,250,382	15,884	

62

The metropolitan area of Chicago (41.6 N, 87.5 W) is located primarily in the State of Illinois, extending into the States of Indiana and Wisconsin, on the shores of Lake Michigan, in the Great Lakes region. Because of its favorable location for lake and river transportation, urbanization of this area started in the first half of 1800 along the lake's shores and proceeded in a radial pattern. The metropolitan area is still growing and has a current population of 8.8 million people (U.S. Census Bureau, 2000b). The dominant land cover of the area surrounding the metropolis is cropland, mainly corn and soybean. The climate is classified as temperate continental modified by the Great Lakes, and is characterized by cold winters, when daily average temperatures tend to remain below freezing, and hot, humid summers, with an average annual temperature of 9.4 °C, and an annual precipitation of 900 mm.

Atlanta, Georgia (33.4 N, 84.2 W), is located in the southeastern United States, in the foothills of the southern Appalachians. This large metropolitan area, situated in a region undergoing massive suburban sprawl, has grown through a process of decentralization and annexation at rather low density. While the City of Atlanta is relatively small (the population in 2000 was 416,500 (U.S. Census Bureau, 2000a), the whole metropolitan area has been one of the fastest growing in the nation, with an estimated population today of more than 3.8 million people (U.S. Census Bureau, 2000b). Mild temperatures throughout the year characterize the humid subtropical continental climate of Atlanta. Annual average temperature is 16 °C and annual precipitation is about 1200 mm, with dry periods in late summer and early fall, and maximum thunderstorm activity in July. In the last 25 years, the Atlanta area underwent a massive transition from forest and agriculture to urban land uses, along with subsequent changes in the land-atmosphere energy balance relationships. Atlanta's heat island has been previously analyzed by the Project ATLANTA (Quattrochi et al., 2000).

Phoenix, Arizona (33.3 N, 112.0 W), is located in the desert environment of the southwestern United States. Phoenix is also among the fastest growing urban areas in the United States. Phoenix had a rapid post WWII urban sprawl, growing mostly through conurbation of its suburban sprawl. The population of the metropolitan area of Phoenix has grown from around 65,000 in 1940 to 3 million people today (U.S. Census Bureau, 2000b). The urban area is surrounded by irrigated agriculture in the valley and Sonoran desert scrub at higher elevation. The climate is that of a midlatitude desert with high temperatures (annual average is 23 °C), low annual rainfall (200 mm) and low humidity. There are two rainy seasons, one from November throughout March and the second one during July and August. The Phoenix urban heat island has been the object of multiple studies, based both on ground measurements and satellite data (Brazel et al., 2000; Lougeay et al., 1996; Stoll and Brazel, 1992; Balling and Brazel, 1987).

Methods

This analysis used MODIS Day and Night Land Surface Temperature (LST) at 1-km resolution (MOD11A2 Version 3) and MODIS NDVI data at 1-km resolution (MOD13A2 Version 3) for the year 2002. Both products are expected to be superior in performance than their predecessors derived from the NOAA/AVHRR due to improved algorithms for atmospheric and, in the case of the LSTs, emissivity corrections of different land covers. I also used MODIS land cover (MOD12Q1 product) to define the type of predominant land cover surrounding the studied areas.

Day (10:30am local time at the equator during the descending orbit) and night (10:30pm local time at the equator during the ascending orbit) land surface temperature from the MOD11A2 product represent 8-days composites calculated as a simple arithmetic average from daily daytime and nighttime LST estimates (Wan, 2001). The

64

MOD11 algorithm applies a view-angle dependent split-window LST algorithm that corrects for atmospheric and land cover dependent emissivity. In most cases, the accuracy of the generalized split-window LST algorithm is better than 1 K (Wan et al., 2002). Each 8-day composited pixel was screened with the corresponding Quality Assessment data set. Because only clear-sky pixels at 99% confidence by the MODIS cloud mask product (MOD35_L2) are processed into the LST algorithm, there will be little or no temperature information for pixels in areas or seasons with persistent cloudiness. To overcome this problem and increase the number of representative pixels of urban and rural LST, simple monthly averages from the 8-day daytime and nighttime LST composites were computed.

NDVI is correlated with vegetation parameters such as the green leaf area, the fraction of the absorbed photosynthetically active radiation and transpiration rates (Running and Nemani, 1988; Tucker et al., 1986). NDVI ranges between –1 and +1, with values greater than 0.2 indicating the presence of a vegetated surface. NDVI data from the MOD13A2 product consist of 16-days composites at 1-km spatial resolution. A maximum-value compositing procedure is used for the production of the 16-day NDVI, which means that each pixel in the final product is assigned the highest value recorded during the compositing period (Huete et al., 2002). This procedure ensures minimal cloud contamination in the 16-day product. As with the LST products, each of the twenty-three 16-days composites for the year 2002 was screened with the Quality Assessment data sets.

The MODIS data were reprojected from the native Integerized Sinusoidal (ISIN) projection to Lambert Azimuthal Equal Area so that they could be overlaid to the fractional cover of ISA. The data were then subset into three analysis windows large enough to contain each of the three metropolitan areas and a portion of their surrounding rural environments (from 105 to 180 km on a side). Urban and rural pixels

65

were discriminated on the basis of the impervious fraction layer and population density data calculated from the Landscan 2001 database (Dobson et al., 2000), a global digital representation of the ambient resident population at 1-km resolution, which was georegistered and overlaid on the fractional ISA and MODIS layers. Rural areas were found to be represented by values from zero to 10% fractional ISA, while urban areas included areas with more than 10% fractional ISA. Suburban areas were included in the urban areas. Statistics of population density along gradients of fractional ISA are presented in Table 3.1. The fractional ISAs of the metropolitan area of Chicago, Atlanta and Phoenix are shown in Figure 3.2.
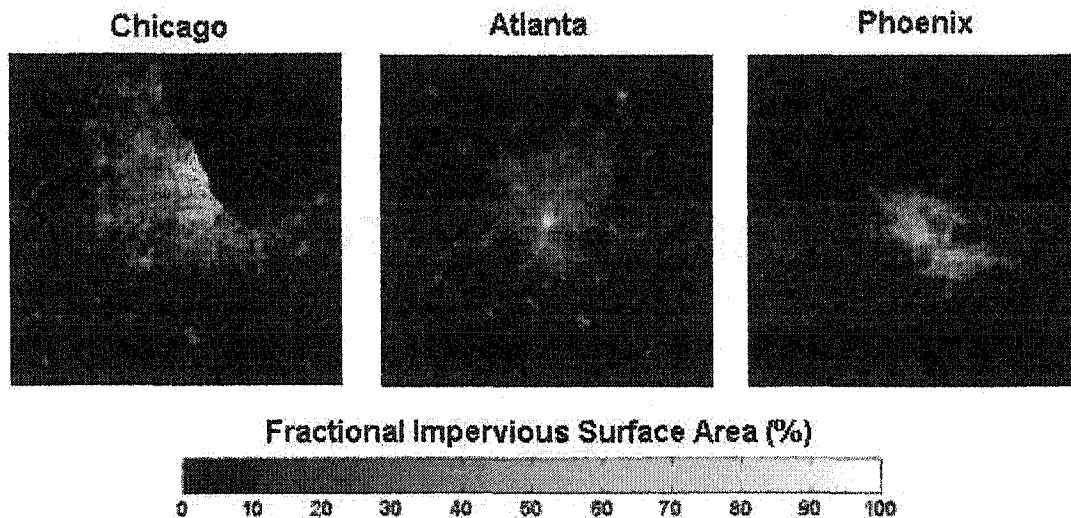
Figure 3.2. Fractional ISA for the metropolitan areas of Chicago, Atlanta and Phoenix.

For each urban area and rural surrounding, monthly average rural and urban daytime and nighttime LST and average NDVI values were calculated as a function of fractional ISA. Since the analysis window containing the metropolitan area of Phoenix included considerable variation in elevation, pixels with more than 500m difference in elevation than the average elevation of the urban area of Phoenix were excluded from the analysis in order to avoid altitudinal bias in the analysis. For representation, the monthly averages

66

were further aggregated into seasonal averages (winter: January through March; spring: April through June; summer: July through September; autumn: October through December), with the maximum and minimum monthly average recorded for each season displayed as error bars. Persistent cloudiness over Atlanta during July and September caused the exclusion of these two months from the analysis at fractional ISA greater than 60%. Excessive cloudiness also determined the exclusion of the months of February and November for Chicago at fractional ISA greater than 50%.

Results and Discussion

Vegetation abundance and imperviousness

Figure 3.3 shows the variation of average seasonal NDVI for three metropolitan areas in relation to the fractional ISA. The month with the highest NDVI in urban environments at all levels of fractional ISA is June both in Atlanta and Chicago, closely followed by May and the other summer months. In Phoenix, the highest greenness is reached in the late fall, peaking in December, when the mild temperatures and surplus water from precipitation contribute to increase the relative humidity, relieving the vegetation from water stress (compare with climate in Figure 3.1). Chicago and Atlanta follow the hypothesized patterns, for which NDVI decreases as the fractional ISA increases. In Atlanta, NDVI decreases steadily as the fractional ISA increases, towards the center of the city. In Chicago, mean monthly NDVI increases up to 20-30% fractional ISA, then decreases rapidly up to 70-80% fractional ISA, after which it decreases more slowly, possibly because of the presence of large parks in the downtown area. In Chicago, the NDVI is more seasonally variable at lower values of fractional ISA, whereas in the densely built downtown the seasonal amplitude of NDVI is probably reduced (White et

al., 2002). Although Atlanta has a higher suburban NDVI, its downtown green biomass is similar to that of Chicago. The higher suburban NDVI in Atlanta can be explained by the type of land cover in the surrounding rural environment, which is dominated by highly productive evergreen needleleaf and mixed forest, while Chicago is surrounded mainly by cropland. While the extensive low density development areas of Atlanta (90% of the urban pixels in the analyzed window have less than 30% impervious surface) maintained a substantial fraction of the trees of the surrounding forests, the tree coverage of the downtown was replenished only more recently (Lowery, 1996). The curve of NDVI for Atlanta is therefore expected to flatten at the higher impervious fraction values in the coming years, as the tree canopies reach full development.
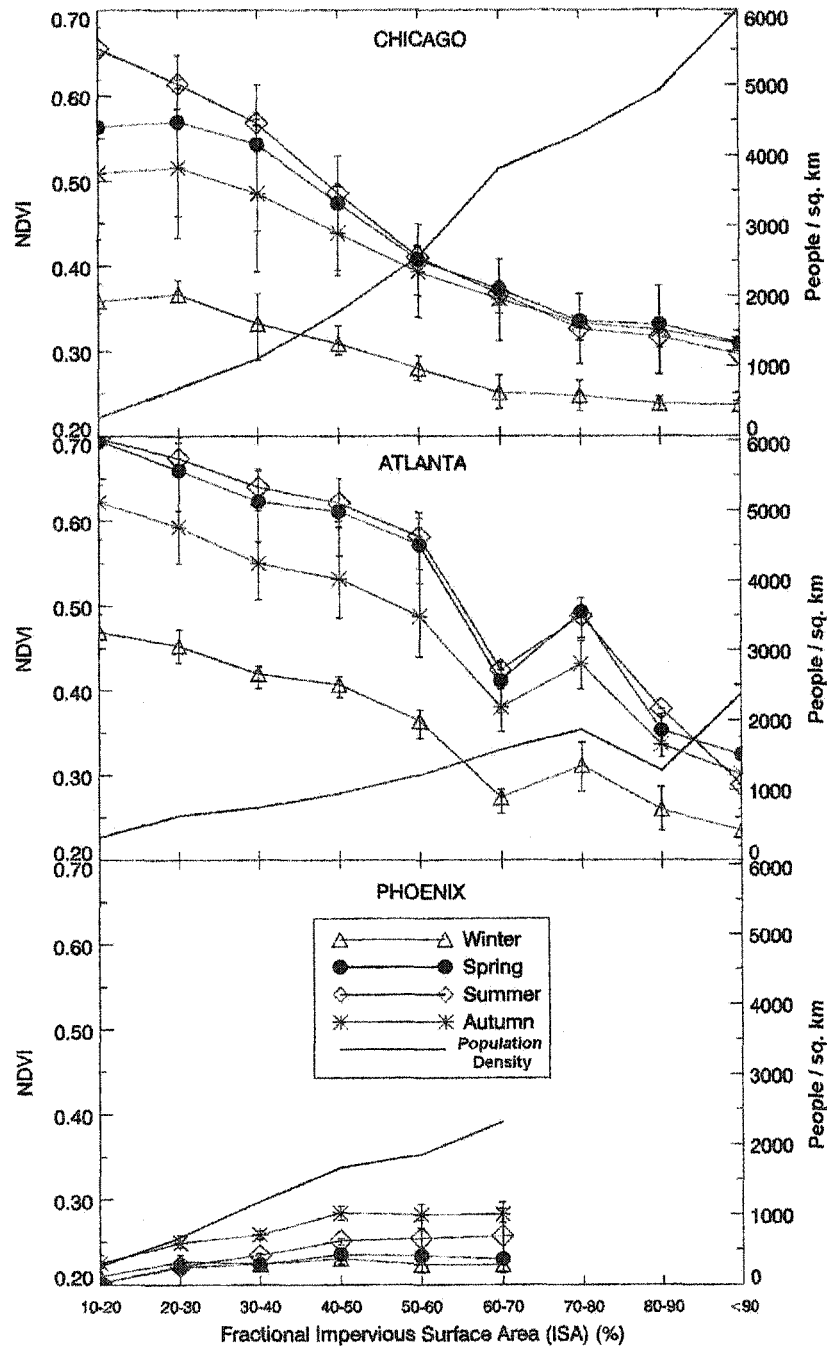
Figure 3.3. Annual variability of NDVI (left axis) and population density (right axis) by fraction of impervious area. The monthly values were grouped into seasonal averages (winter: January through March; spring: April through June; summer: July through September; autumn: October through December). The error bars indicate the upper and the lower monthly average recorded for each season.

69

A substantial increase in biomass per unit area at higher values of imperviousness, with the concentration of irrigated lawns and exotic tree species increasing from the suburbs towards the urban center, could explain the positive relationship between NDVI and fractional ISA observed in Phoenix. The highest level of fractional ISA reached in this city is 70%, leaving 30% of the 1-km pixel surface available for vegetation. The presence of golf courses near the center of the metropolitan area could also contribute to the positive trend of NDVI versus imperviousness. The total variation in NDVI in this urban environment, however, is less than 0.1, remaining lower than 0.3 during all months of the year.

Seasonality of NDVI and LST urban-rural differences

Figure 3.4 shows the differences in urban-rural NDVI (NDVIurb-rur), and daytime (Day LSTurb-rur) and nighttime (Night LSTurb-rur) land surface temperatures for the three metropolitan areas. Table 3.2 reports the values for the month in which the largest differences were observed. In all three metropolitan areas, the NDVIurb-rur and LSTurb-rur generally tend to increase as the fractional ISA increases.

70
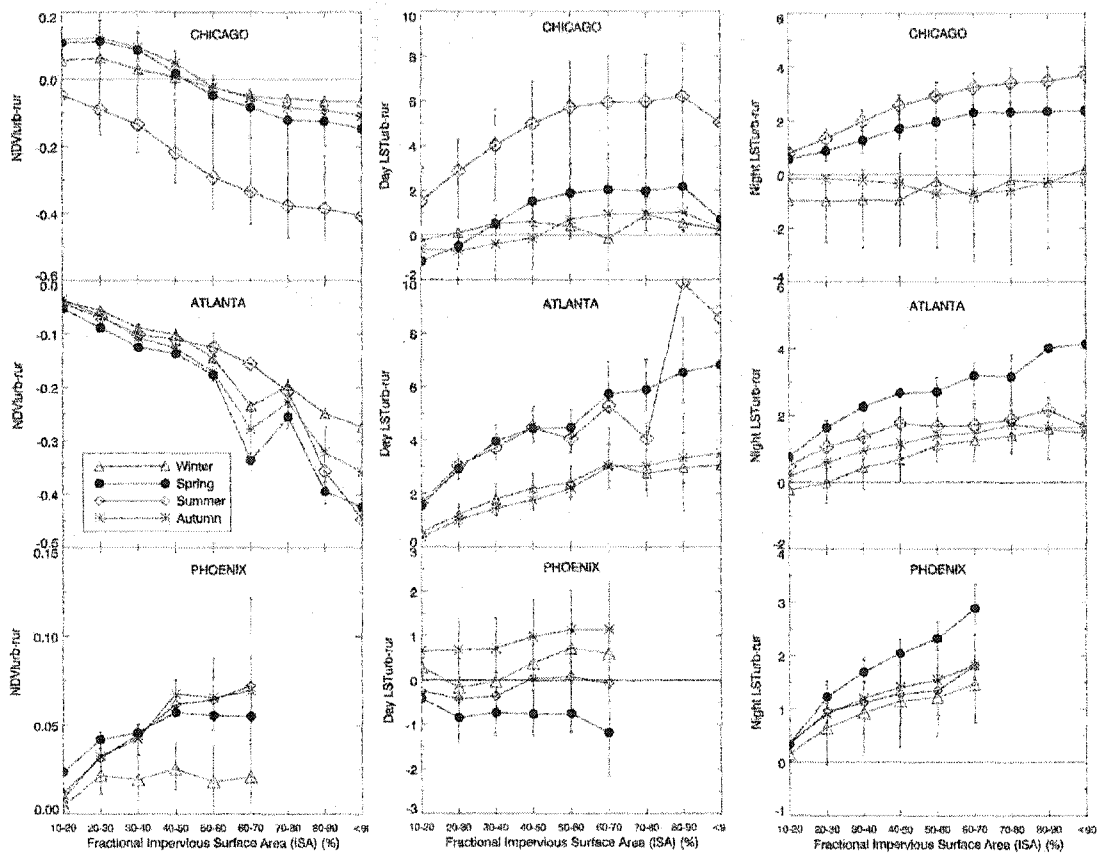
Figure 3.4. Urban-rural differences of NDVI (NDVIurb-rur), daytime LST (Day LTSurb-rur) and nighttime LST (Night LSTurb-rur) by fraction of impervious surface area for the metropolitan areas of Chicago, Atlanta and Phoenix.

71

Table 3.2. Maximum urban-rural differences in NDVI (NDVIurb-rur), daytime LST (Day LSTurb-rur) and nighttime LST (Night LSTurb-rur) and the months in which they were recorded in the year 2002.

Fractional ISA (%)	Chicago			Atlanta			Phoenix		
	Max $NDVI_{urb\text{-}rur}$	Max Day $LST_{urb\text{-}rur}$	Max Night $LST_{urb\text{-}rur}$	Max $NDVI_{urb\text{-}rur}$	Max Day $LST_{urb\text{-}rur}$	Max Night $LST_{urb\text{-}rur}$	Max $NDVI_{urb\text{-}rur}$	Max Day $LST_{urb\text{-}rur}$	Max Night $LST_{urb\text{-}rur}$
Month	August	August	August	June	June	May	November	December	April
11-20	-0.11	2.6	0.9	-0.05	1.9	0.7	0.01	1.0	0.6
21-30	-0.17	4.3	1.7	-0.09	3.5	1.5	0.04	1.4	1.5
31-40	-0.22	5.6	2.4	-0.13	4.6	2.2	0.05	1.4	2.0
41-50	-0.31	6.9	3.0	-0.13	5.1	2.7	0.08	1.8	2.3
51-60	-0.39	7.8	3.4	-0.18	5.1	3.1	0.08	2.0	2.6
61-70	-0.43	8.1	3.8	-0.36	6.9	3.6	0.08	2.2	3.3
71-80	-0.47	8.1	4.0	-0.28	7.0	3.4			
81-90	-0.48	8.6	4.0	-0.42	8.6	4.1			
>90	-0.50	7.4	4.3	-0.44	8.8	4.1			

72

Chicago

In 2002, both Day and Night LSTurb-rur in Chicago were positive for most of the spring and summer months, indicating an urban surface heat island for this period. The LSTurb-rur increases more linearly at night than during day. The presence of a plateau in DayLSTurb-rur at values of fractional ISA greater then 60%, located towards the lake shore, indicates the presence of a strong cooling effect caused by daytime lake breezes and perhaps by the presence of treed parks. The strongest daytime and nighttime surface heat islands were both recorded in the summer (August). During the autumn and winter months, the Night and Day LSTurb-rur were either close to zero or slightly negative, in which case indicating that the surface temperatures in the impervious areas were warmer than in the rural areas. In Chicago, the timing of the NDVIurb-rur is well synchronized with the timing of the Day and Night LSTurb-rur, with the strongest urban rural differences in greenness also taking place during the summer (August). During these months the differences are positive at all levels of fractional ISA. Up to 60% fractional ISA, urban NDVI is actually higher than in the surrounding rural environment, especially during spring and autumn. This is explained by the contrasting vegetation cover in the two environments, represented by lawns and trees in the urban areas (Dwyer et al., 2000) and cropland in the surrounding rural areas (97% of the rural surface according to the MODIS land cover). While the combined effect of fertilization, irrigation and perhaps also higher urban temperatures can extend the growing season of the urban trees and lawns (White et al., 2002), the surrounding crop fields have a low biomass during spring and autumn. On the other hand, in the summer months of July and August, cropland greenness reaches its maximum, and its NDVI becomes much higher than the urban NDVI. This maximum difference in green biomass between urban and rural areas has also a major effect on evapotranspirational cooling and heat storage capacity differences and the timing of maximum NDVIurb-rur coincides with the timing of

73

maximum Day and Night LSTurb-rur. In summary, in the temperate continental climate of Chicago, characterized by strong seasonality, the seasonality of the NDVIurb-rur is indicative of the seasonality of the daytime and nighttime LSTurb-rur. In this case, if the patterns of surface temperature reflect the patterns in air temperature, the NDVIurb-rur could be plausibly interchanged with the fractional ISA to analyze the climatic impact of urbanization.

Atlanta

In Atlanta, the Night and Day LSTurb-rur in 2002 were positive during all months, indicating that the urban surface temperatures were always warmer than the rural ones. However, at low levels of fractional ISA, the Day LSTurb-rur were small during the autumn and winter months and the Night LSTurb-rur remained below 1 K year-round. At higher levels of imperviousness, the Night LSTurb-rur (more than 4 K at fractional ISA greater than 80%) were marked in the spring (April and May), while the Day LSTurb-rur were strong both in the spring and in the summer (highest Day LSTurb-rur for Atlanta were recorded in June and August). The average urban green biomass was lower than in the surrounding rural areas throughout the year, resulting in negative values of NDVIurb-rur at all levels of imperviousness. The strongest differences in NDVI were recorded in the spring and in the early autumn. Irrigation of the urban vegetation might have helped decrease the NDVIurb-rur during the summer. However, because of the evergreen nature of the dominant land cover surrounding the urban areas, the NDVIurb-rur lacks a distinctive seasonality at levels of fractional ISA up to 50-60%. In comparison with Chicago, the timing of the maximum NDVIurb-rur and Day and Night LSTurb-rur in Atlanta is less synchronized. NDVIurb-rur and Day LSTurb-rur are both at their maximum in June. On the other hand, the maximum Night LSTurb-rur occurs in May. During this month, a combination of elevated solar radiation and a relatively dry season

74

(Figure 3.1) directs most of the energy flux into heat storage during the daytime. Because of low thermal inertia of the constructed material, the Night LST of the impervious areas would be warmer at night, when the rural areas surfaces have already cooled off. In the summer months, even though the solar radiation peaks, afternoon thunderstorms help cooling off the impervious surfaces, thus reducing the Night LSTurb-rur.

Phoenix

The least synchronized LST and NDVI urban-rural differences were recorded for Phoenix, where the greatest contrast in urban-rural LST takes place at night rather than during day as in Chicago and in Atlanta. At night the urban surface of Phoenix is up to 3.5 K warmer than the surrounding rural environments. The Night LSTurb-rur are positive throughout the year and at all levels of fractional ISA, but are not significant at low fractional ISA, where the urban environment encroaches upon the desert. In 2002, the Night LSTurb-rur were lowest in January followed by July and August, when the rainy season dampens the urban rural differences. The Night LSTurb-rur were strongest during April, as recorded by (Brazel et al., 2000), when the frequent occurrence of clear skies intensifies the difference. Day LSTurb-rur for Phoenix were mostly non significant from May through October, with the appearance of a moderate daytime oasis during the spring, at the end of the dry season, when the added humidity from lawn sprinkling and swimming pools in the city contrasts with dryness of the surrounding desert environment. Other studies in the Phoenix metropolitan area, carried out at higher spatial resolution, have found the temperature patterns of the month of June to be strongly correlated with the evapotranspirational sink provided by the presence of open water and biomass (Lougeay et al., 1996). As with the NDVIurb, the NDVIurb-rur increases slightly with imperviousness and is stronger in August, October and November. In contrast to Atlanta

75

and Chicago, the NDVIurb-rur is always positive, since the irrigated lawns present a higher biomass per unit area than the surrounding desert environment all year round. A similar pattern was shown for the urban environment of Denver, Colorado by Imhoff et al., (2000), and is probably expected for most of the cities located in the dry regions of the western United States. While the irrigation of the lawns increases the NDVI of the urban areas and creates a moderate surface oasis effect during day, it does not avoid the development of a marked nighttime heat island. In this type of arid environment it seems therefore that a correction of air temperature based solely on NDVIurb-rur would be unsuccessful.

The timing of the maximum NDVIurb-rur, Day LSTurb-rur and Night LSTurb-rur does not necessarily coincide in the three urban areas. In general, the absolute values of the urban-rural differences in NDVI, Day and Night LST increase with the fractional ISA, towards the center of the urban areas. In the case of urban areas surrounded by dense forests or cropland, as the fractional ISA increases, the fraction of vegetated surface decreases and the biomass per unit surface becomes generally smaller than the biomass of the surrounding rural environment. The reduction in vegetation biomass and its replacement by buildings and paved surfaces implies a reduction in moisture availability for evapotranspiration and a great increase in heat storage capacity, changes that make the urban surface warmer than the surrounding rural areas. The warming of the surface temperatures as the fractional ISA increases and the vegetation biomass decreases is most probably reflected in a warming of the air temperatures, as found in other studies (Unger et al., 2001). Except in Phoenix, where we observe a daytime oasis effect, the Day LSTurb-rur is up to 4 K higher than the Night LSTurb-rur. The warming of the air temperature probably lags behind the daytime surface warming, and is likely to be more closely related to the nighttime surface warming (Stoll and Brazel, 1992).

76

The monitoring of changes in climate resulting from the expansion of urban areas based on relating the urban-rural contrast in NDVI to brightness temperatures generally assumes that the NDVIurb-rur is negatively related to the difference in urban-rural temperatures (Gallo and Owen, 1999). The present study indicates that this is the case for Chicago and Atlanta, but not for Phoenix. Census statistics (U.S. Census Bureau, 2000b) show that many rapidly urbanizing regions of the United States are located in the western semi-arid and arid regions, where a correction based solely on vegetation indices is impractical. On the other hand, in this study the Night LSTurb-rur differences detect an urban heat island in all three of the urban areas examined, independent of correlation and synchronization with the NDVIurb-rur. It is also noteworthy that the magnitude of the maximum heat island is proportional to the fractional ISA, as seen from Figure 3.4 and Table 3.2. Both in Chicago and in Atlanta, the maximum Night LSTurb-rur of 4 K is recorded at fractional ISA greater than 90%, although the two metropolitan areas differ largely in terms of population density structure. Atlanta has a much smaller surface area with high fractional ISA than Chicago, and a smaller population density in the downtown area (Table 3.1). The fractional ISA in Phoenix does not reach values higher than 70%. However, the maximum Night LSTurb-rur of 3.5 K at impervious fractions of 60-70% in Phoenix in April compares well with the Night LSTurb-rur at similar values of fractional ISA in the months of August in Chicago and May in Atlanta. This similarity in maximum Night LSTurb-rur across contrasting climates might be explained by a similarity in heat storage capacity and albedo of the constructing materials. Potential future analysis should include urban areas of other countries, where the use of different constructing materials might change the relation between Night LSTurb-rur and fractional ISA. A comparison of how urban-rural temperatures scale linearly with the logarithm of city populations (an indication of imperviousness) across continents (Torok et al., 2001) indicates that heat-islands of American cities are

77

generally larger than those of similar-size European cities, which are generally smaller than those of Australian cities. Differences in building material inertial and reflective properties, as well as urban morphology could be at the root of these differences.

Conclusions

This study presented a synergistic use of MODIS and DMSP/OLS data for the study of the effects of urbanization on vegetation biomass and daytime and nighttime surface temperatures in metropolitan areas characterized by contrasting climates and development densities.

The results indicate that it can not be simply assumed that satellite-measured green biomass in urban areas decreases proportionally as the impervious surface increases. The decrease in biomass is often not linear, and there can even be a modest increase in biomass in urban areas due to vegetation management practices, as is often the case of urban areas located in arid and semiarid regions. In these regions, the more recently developed suburban neighborhoods encroach upon the desert and often practice xeriscaping, while the older central neighborhoods tend to have a higher concentration of irrigated lawns and exotic trees.

The results of this analysis also indicate that the timing of the maximum heat island differs among geographic regions, and does not necessarily take place during the hottest time of the year. Moreover, the maximum difference in NDVIurb-rur, often used as an indicator of the air temperature heat island, is not necessarily synchronized with the surface daytime or nighttime heat island. It remains to be demonstrated whether the LSTurb-rur heat island is synchronized with the air temperature heat island. In all three urban environments, the amount of fractional ISA appears to be a major driver of the urban rural differences in nighttime LST, which seems to be independent of climate, the

78

size and the development density of the metropolitan area. At least in some regions, i.e. the arid and semiarid western United States, the fractional ISA might be a better indicator of the climatic impact of urbanization than NDVI.

The global availability of standard NDVI and LST data from MODIS and the potential to extend the estimation of the fractional ISA to other countries offers the possibility to establish consistent monitoring of the environmental effects of urbanization and eventually provide insights for ways to curb some of these effects. This possibility will be enhanced as longer time series of data from the MODIS instrument onboard the Aqua satellite will provide with another set of NDVI and LST data (1:30 pm and 1:30 am). The fractional ISA product from the DMSP/OLS could also used be used in conjunction with demographic information to regionally predict patterns of energy consumption, particularly for cooling, during the warmer periods of year, and better define vulnerability to heat wave conditions.

CHAPTER 4

THE DISTRIBUTION OF HUMAN POPULATION IN RELATION TO TERRESTRIAL NET PRIMARY PRODUCTIVITY AND ITS VARIABILITY

Abstract

Human domination of ecosystems has been pervasive over the last century, with nearly half of the Earth's surface transformed by human actions. It is widely accepted that humans appropriate nearly 50% of global net primary production (NPP), the energy base of all the trophic levels on the land surface. Yet, knowledge of the spatial relation between NPP and population is limited because of the lack of gridded global datasets of both NPP and human population. I used recently available satellite-based NPP estimates, along with gridded population at 0.5-degree resolution, first to identify the global distribution of human population with reference to NPP and to the various climatic constraints (temperature, water and cloud cover) that limit NPP, second to analyze recent trends in global NPP in relation to population trends, and third to identify populations that are vulnerable to changes in NPP due to interannual variability in climate. Over half of the global human population is presently living in areas with above the average NPP of 490 g C m^{-2} year^{-1}. By 1998, nearly 56% of global population lives in regions where water availability strongly influences NPP. Per capita NPP declined over much of Africa between 1982 and 1998, in spite of the estimated increases in NPP. On average, the NPP over 40% of the total vegetated land surface has shown significant correlations with ENSO (El Niño-Southern Oscillation)-induced climate variability affecting over 2.8 billion people. Recent availability of 1-km NPP and population datasets will vastly improve our ability to monitor and respond to changes in habitability that require concerted efforts.

Introduction

During the 20th century, a fourfold growth in human population to 6 billion people and remarkable increases in fossil fuel and industrial emissions, land cover changes, and agricultural activities have resulted in several changes in the Earth system, including changes in climate, hydrologic cycling, biodiversity and general degradation in environmental quality (WRI, 2003; IPPC, 2001; Chapin et al., 2000). A number of global efforts have been characterizing these changes at regular intervals, but the joint analysis of these changes with socially relevant variables is still at its infancy (Clark and Dickinson, 2003; Rindfuss and Stern, 1998). The different spatial scales at which social and biophysical changes are being measured and made available at the global scale is among the reasons for the frequent lack of analysis of the interactions between environmental and social conditions (Tobler et al., 1995). The availability of global gridded population data, with recently improved and updated data sets such as the Gridded Population of the World (CIESIN, IFPRI and WRI, 2000) and LandScan (Dobson et al., 2000) provide a starting point towards a spatially explicit incorporation of a human dimension in the interpretation of the changes the biosphere is undergoing.

One of the biophysical variables that serves as a good indicator of the climatic, ecological, geochemical, and human influences on the biosphere but that has not yet been analyzed in relation to the distribution of human population is terrestrial net primary production (NPP), the net amount of carbon fixed by plants. Terrestrial NPP has direct relevance to humankind since it not only satisfies our immediate needs for renewable food, fuel and shelter, but also provides the energy to sustain the life of the other organisms we depend on and controls a number of ecosystem services (Field 2001; Daily, 1997). For example, terrestrial NPP integrates the annual carbon flux from the atmosphere to the land and, together with the ocean NPP, is the main driver of seasonal

81

fluctuations in atmospheric CO_2 concentration (Keeling et al., 1996). Terrestrial NPP contributes to the regulation of the water cycle by maintaining soil moisture and surface air humidity, reducing the risks of floods, landslides, and soil erosion. Moreover, terrestrial NPP contributes to the regulation of nutrient cycling, limiting groundwater pollution and maintaining soil fertility, providing opportunities for floral and faunal biodiversity (Daily et al., 1997).

Repeatable and consistent measures of NPP over the globe are today possible with satellite-based measurements of vegetation properties, and at the time of this writing a continuous record is available for the years 1982-1999. The first measurements of global changes in NPP used the Normalized Difference Vegetation Index (NDVI), a satellite based measure of vegetation greenness, as a proxy (Tucker and Seller, 1986). More recent advances in the remote sensing data applications and ecosystem modeling have brought to the translation of the satellite measures into NPP (Goward and Huemmrich, 1992; Field et al., 1995; Running et al., 2000; Running et al., 2004), opening the potential to more directly relate changes in this variable to the anthropogenic influences on the Earth system.

According to Nemani et al. (2003), during the years 1982-1999, the combination of changes in climate and, possibly, land management practices (including nitrogen applications, irrigation, and reforestation) have resulted in an increase in NPP over large regions, globally averaging 6%. The same study also indicates that the increase was characterized by strong interannual variability, averaging 9% over the two decades, but with extremes of 20-30%. How did this long term and interannual changes in terrestrial NPP compare with the recent growth in global human population and what can we infer about the effects of these changes on Earth's habitability?

To help answer this question, the following points are analyzed in this chapter: 1) How was population distributed with respect to average NPP and to the various climatic

82

constraints (temperature, water and cloud cover) that limit vegetation productivity ? 2) How did recent trends in global NPP compare to population trends? 3) How was the population distributed in terms of the geographic distribution and intensity of the interannual variability in terrestrial NPP?

Materials and Methods

Population Data

A digital representation of the global human population distribution was obtained from the LandScan 1998 data set (Dobson et al., 2000). The layer was resampled from the original 30- by 30-arc second (approximately corresponding to 1- by 1-km grid cells) to 0.5-degree spatial resolution to match the resolution of the NPP data. The resampled grid cells cover an area on the land surface of approximately 56- by 56-km at the equator and 56- by 19-km at 70° N. The total population for the year 1998 estimated at 0.5-degree resolution (Figure 4.1a) was 5 920 million people (comparable to the 5 900 million people reported by the World Resource Institute).

Unfortunately, there was no population distribution data set with a resolution comparable to LandScan for the early 1980's and the only available population maps were country based. Even for coarse resolution studies, as is the case of the present work, country level population data lack the required detail in those regions covered by the largest countries (e.g., Russia, China, Australia, Brazil, or United States), where people are not homogeneously distributed within the national borders. To circumvent this limitation, an approximated 0.5-degree gridded population map for the year 1982 was derived from the resampled 1998 LandScan data using national and, for the largest countries, subnational census data from the Populstat database (Lahmeyer, 2003). With

83

the aid of a country mask, and for large countries, subnational administrative borders, I subtracted the national or sub-national 1982-1998 population growth fraction from the 1998 LandScan population of each grid cell falling within the specific administrative unit. This approach suffers from the simplifying assumption that population growth has occurred at a constant pace during the analyzed period, neglecting year-to-year changes in fertility and mortality, and therefore has limited applicability for small scale analysis of population change. Nonetheless, it provides a reasonable approximation of the spatial distribution of population growth at the scale of analysis of this study.

The table in Appendix A shows how the estimates of the total population from this study compare with the estimates reported by the World Resource Institute (available online at: http://www.wri.org).

NPP Data

I used the monthly NPP data estimated by Nemani et al. (2003) from the NOAA/AVHRR (National Oceanic and Atmospheric Administration/Advanced Very High Resolution Radiometer) NDVI data sets for the period 1982-1999 [Pathfinder AVHRR Land (PAL; James and Kalluri, 1994), and Global Inventory Monitoring and Modeling System (GIMMS; Zhou et al., 2001) data set], using a production efficiency model designed for the MODerate resolution Imaging Spectroradiometer (MODIS; Running et al., 2000).

Using the two NDVI data sets, Nemani et al. (2003) obtained two estimates of global NPP distribution for the period 1982-1999. In this study, global population distribution is analyzed with respect to the NPP calculated as an arithmetic average of the two estimates (Figure 4.1b).

84

Dominant climatic controls on NPP

Dominant climatic controls on NPP were defined by Nemani et al. (2003) using long-term (1960-1990; Leemans and Cramer, 1991) monthly climate data of maximum/minimum temperatures, cloudiness, and rainfall, and developing scaling factors (0-1) to indicate the reduction in growing potential from its maximum in each month. In most regions, precipitation, radiation and temperature co-limit and interact in controlling yearly NPP, changing seasonally their geographic distribution. The Indian Monsoon region, for example, can be limited by water during the dry season and radiation during the overcast wet season. However, in general, one of the three factors has a prevailing influence in diminishing NPP from its potential (it is precipitation in the case of the Indian Monsoon), and identifying the dominant limiting factor for every pixel results in the aggregation of spatially contiguous grid cells into large regions, generally analogous to the temperate (temperature-limited), inter-tropical (water-limited) and tropical-equatorial (radiation-limited) regions, offering a more physically based alternative to a characterization of the population distribution than one based on latitudinal bands.

Because of the strong interannual variability in NPP, the distribution of human population was compared with an average of the late 1990s NPP rather than with the NPP of 1998 or 1999. The late 1990s average NPP was calculated by averaging in each grid cell the values for the years 1996 through 1999.

The relationship between the 1998 population and the 1996-1999 average NPP was analyzed by means of joint frequency distributions calculated for the occupied land areas and total land areas, both as global totals and disaggregated by climatic zones.

85

The spatial distribution of the changes in NPP over the period 1982-1999 was mapped by subtracting the average 1982-1985 NPP from the average 1996-1999 from each grid cell. The spatial distribution of the changes in population occurred during the same period was mapped by subtracting the estimated 1982 population from the 1998 population in each grid cell. A percent change in per capita NPP was also mapped to compare the effect of the long-term changes in local NPP with local population changes.

Due to the coarse spatial resolution of the analysis presented here, several types of land covers and topography are included in most of the 0.5- by 0.5-degree grid cells so that the NPP of each grid cell is an averaged estimate. Therefore, the relative differences in NPP between the populated and the inhabited land areas, as well as the differences in productivity under the different climatic constraints should be deemed more important than the absolute values of NPP.
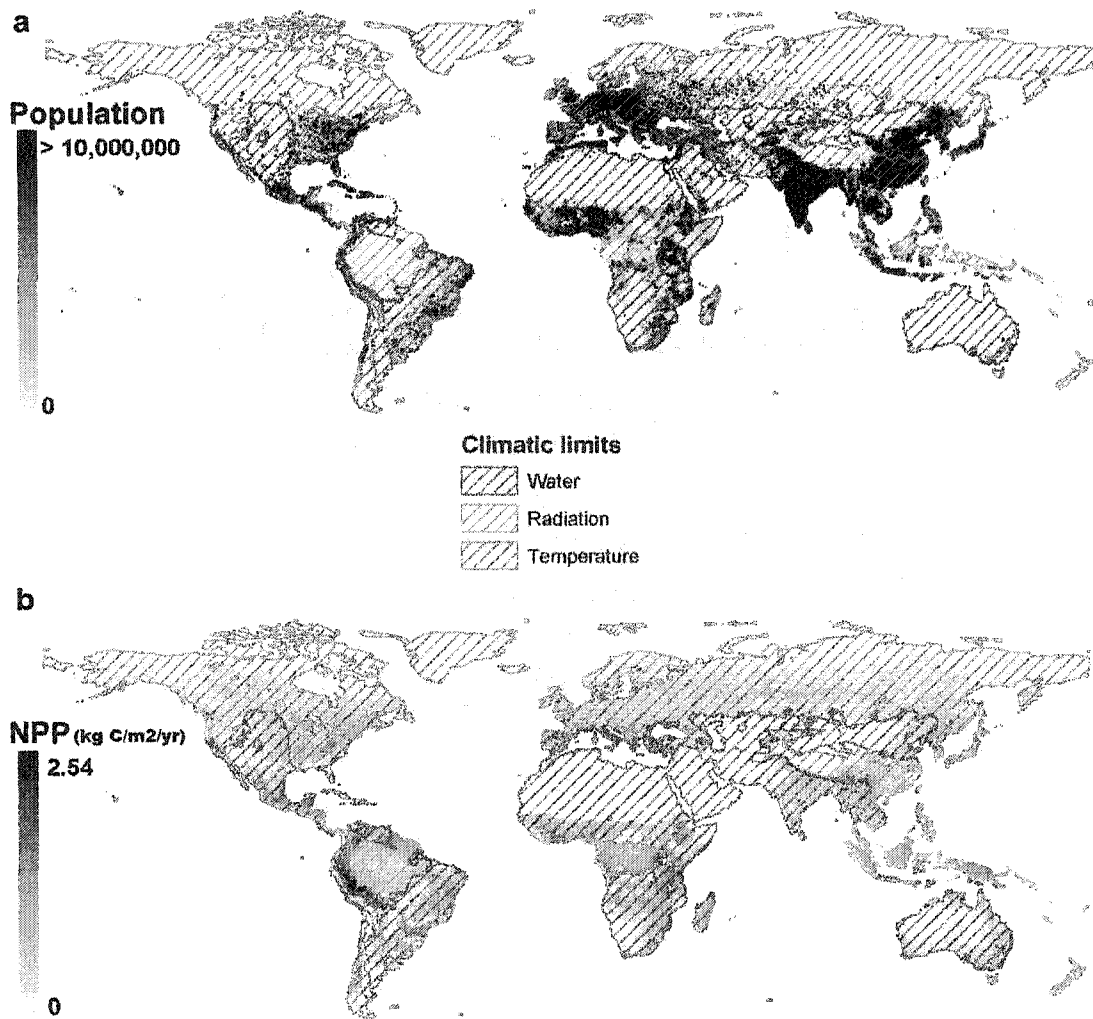
Figure 4.1. a) 1998 population derived from LandScan 1998. b) 1982-1999 average NPP at 0.5 by 0.5 degree spatial resolution. A map of the climatic limits on NPP is superimposed on both maps.

87

Population distribution with respect to interannual variability of terrestrial NPP

While the overall increase in NPP recorded during the period 1982-1999 can be attributed both to long term changes in climate that helped easing constrains on plant growth and to changes in land management, the strong interannual fluctuations are dominated by year to year climatic variability.

On a global scale, the major coupled ocean-atmosphere forcing mechanism on interannual climatic variability is exerted by the ENSO (El Niño-Southern Oscillation) phenomenon (Philander, 1990). The Southern Oscillation, representing the atmospheric component of the ENSO, is determined by the difference in atmospheric pressure between Indonesia/North Australia (Darwin) and the southeast Pacific (Tahiti). El Niño is used to refer to the warming of the surface waters of the eastern equatorial Pacific that occurs at irregular intervals of 2-7 years. During an El Niño, sea level pressure tends to be lower in the eastern Pacific and higher in the western Pacific. La Niña is the counterpart of El Niño and is characterized by cooler than normal sea surface temperatures across much of the equatorial eastern and central Pacific. During La Niña, sea level pressure patterns across the eastern and central Pacific are reversed with respect to the ones observed during El Niño.

Teleconnections, the atmospheric interactions that take place between widely separated regions during ENSO events, are generally closely followed on land by changes in NPP and can be identified through statistical spatial and temporal correlations with climatic indexes.

To map the geographic distributions of populations inhabiting regions sensitive to recurrent ENSO-induced swings in vegetation growth, the monthly NPP values for the period 1982-1999 were regressed on the corresponding time series of the Multivariate

88

ENSO Index (MEI) (Wolter and Timlin, 1988). The MEI is a multivariate measure of the ENSO signal expressed as the first principal component of six main surface climatic variables observed over the tropical Pacific including sea level pressures, wind, sea and air temperatures. Negative values of MEI indicate a cool ENSO event (La Niña) while positive values signify a warm ENSO event (El Niño conditions). By regressing the eighteen year monthly NPP values over the MEI values with a 6 months time lag between the data sets, and isolating the grid cells displaying correlations with p-values < 0.05, the regions where vegetation productivity is most strongly associated with ENSO-related climatic variability are identified. The number of people living in regions where NPP is strongly affected by climatic variability is estimated by overlaying the human population layer on the regression results.

Results

Distribution of population with respect to average NPP and dominant climatic limits to NPP

Distributions of NPP and human population display similar spatial patterns (Figure 4.1). Regions with higher vegetation productivity also have higher concentration of people, while deserts are generally sparsely populated.

The statistics on the distribution of the population and the land area as a function of NPP are summarized in Table 4.1. While these values are likely to change with the use of higher resolution data, they provide a framework to define average present conditions and set a reference for monitoring changes. The statistics indicate that the global human population tends to live in areas characterized by average to above-average values of vegetation productivity. While the populated areas and the total land area have the same

89

mean NPP, the median person lives at higher than average NPP (590 g C m^{-2} year^{-1} versus a global mean of 490 g C m^{-2} year^{-1}). The median land pixel has an NPP of 460 g C m^{-2} year^{-1}. Large land areas (51.6 million km^2 or 35% of the total) are bare or very sparsely vegetated, with an NPP of less than 50 g C m^{-2} year^{-1}, and thinly populated (212 million people, on average 4 people km^{-2}). On the other hand, 2.4 million km^2 of surface possesses very high vegetation productivity (NPP greater than 1500 g C m^{-2} year^{-1}). These high productivity areas are inhabited by 89 million people (on average 36 people km^{-2}).

The dominant climatic limits on NPP superimposed on both maps in Figure 4.1, show that temperature is the climatic limiting factor at high latitudes, from the poles to 40-30 degrees, depending on the longitude, affecting 45% of the total land surface. Suboptimal levels of precipitation constrain vegetation growth over an additional 45% of the land area, in the tropical and subtropical areas and much further north than that in both North America and Asia. Regions where vegetation growth responds predominantly to a reduction in cloudiness (i.e. an increase in radiation) are mostly confined to equatorial areas and to southeastern China, amounting to 10% of the total land surface. Table 4.1 also reveals that, while the largest percentage of the global population in 1998 was living in water-limited regions (56% of the total), the highest density (more than 70 people km^{-2}) is found in the radiation-constrained areas, which also possess the highest rates of vegetation productivity. Here, the mean NPP of the populated grid cells is 870 g C m^{-2} year^{-1}, followed by the water-limited and the temperature-limited areas. While the mean NPP of the populated areas in each of the climatic regions is generally not higher than the mean land NPP, the median person of the water- and temperature-limited areas lives in areas characterized by a higher NPP than the median land grid cell under the same constraining climatic factor.

90

Table 4.1. Distribution of 1996-1999 average NPP (g C m^{-2} year^{-1}), 1998 population over populated areas and total land area.

NPP (gC m^{-2} yr^{-1})	Populated Land				Total Land			
	Global	Precipitation	Radiation	Temperature	Global	Precipitation	Radiation	Temperature
Minimum	0	0	0	0	0	0	0	0
First quartile	420	440	470	390	250	280	550	70
Median	590	630	600	490	460	550	780	270
Third quartile	770	780	880	640	750	800	1 090	440
Maximum	2 550	2 490	2 550	2 170	2 550	2 490	2 550	2 170
Mean	490	490	870	380	490	570	890	340
Standard Dev	400	410	450	270	380	380	450	260
Population								
1998 Population (10^6)	5 900	3 300	1 100	1 500				
1998 Population density (people km^{-2})	40	50	71	22				

91

1982-1999 trends in population versus trends in NPP

Figure 4.2 maps the distribution of the 1982-1999 changes in NPP and in population, and the combined relative effect of these changes on per capita NPP. Figure 4.3 plots the changes in per capita NPP against the changes in NPP and population. Figure 4.4 summarizes the changes in NPP and population by dominant climatic limits.

During the years 1982-1998, the world population increased globally by about 26%. Population growth presented strong spatial heterogeneity, with the strongest growth, 34%, in water-limited areas, which, including most of India and southeastern China, also hosts the largest population. In radiation-limited regions, population grew by 26% whereas the smallest growth (12%) was recorded for temperature-limited regions, where, during the analyzed period, many countries had very limited population growth. Only a few regions show a net decrease in population over the analyzed period, and are mostly represented by eastern Europe countries and an area of eastern China, the latter being possibly due census counts inconsistencies.

While overall population has risen linearly, NPP has increased with large interannual fluctuations and with a lower pace. The largest increase has been observed over the radiation-limited areas (11%), followed by temperature- (5%) and, lastly, water-limited areas (3%), with a global average of 6%. Wide regions in all continents have recorded net decreases in NPP, although less significant than the increases (Nemani et al., 2003).
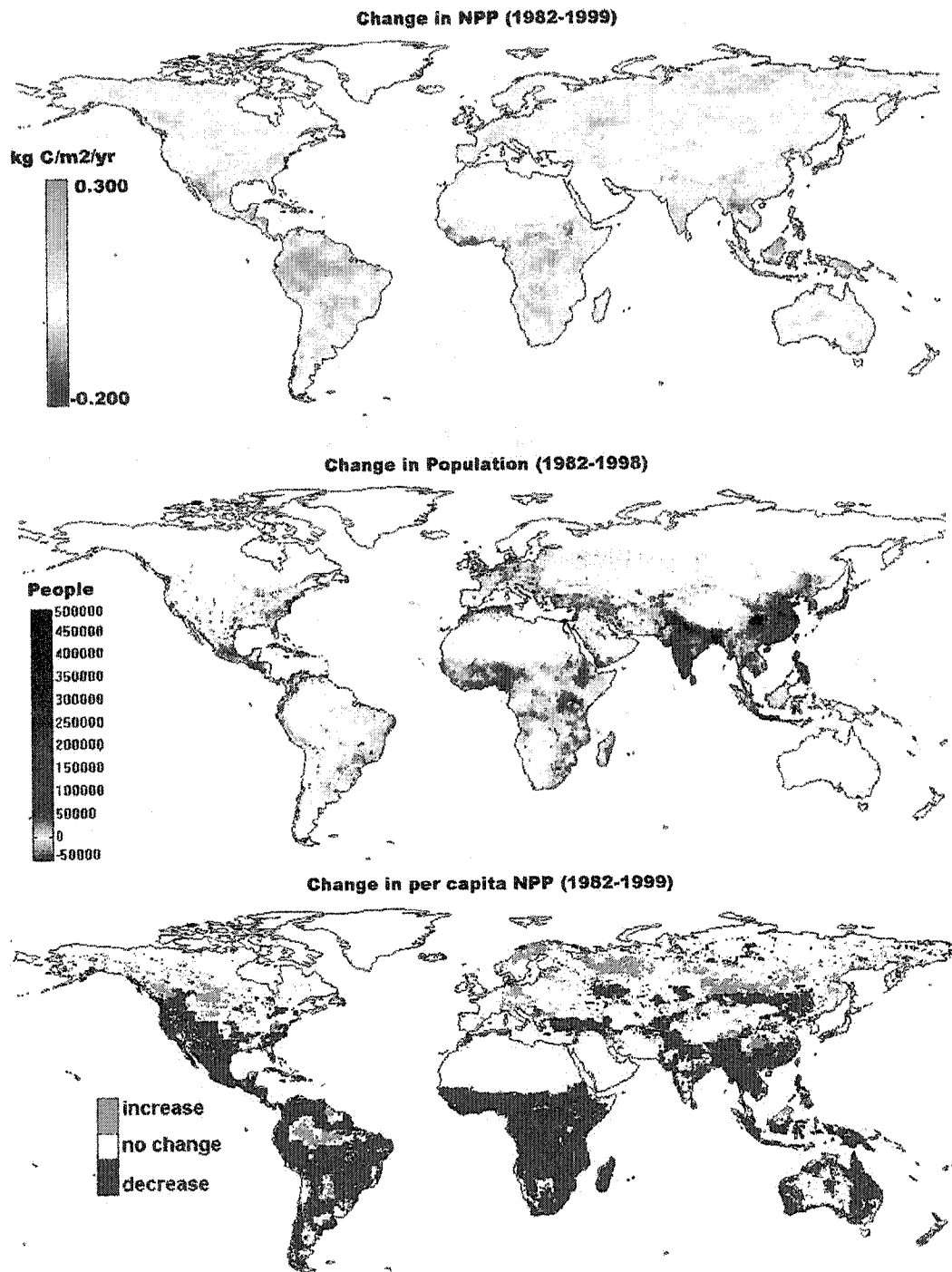
Figure 4.2. Spatial distribution of the changes in total NPP, population and per capita NPP observed during the period 1982-1999.

93

The per capita change in NPP (Figure 4.2) for the period 1982-1999 calculated as the ratio between the changes in NPP and the changes in population indicates that for 47% of the vegetated pixels the combined demographic and vegetation productivity dynamics resulted in a decrease in per capita NPP. For only 7% of the vegetated pixels the increase in vegetation productivity surpassed population growth. From Figure 4.3 we can infer that the modest increase in NPP per capita was generally the result of a combination of increased NPP and decreased or little increase in population.
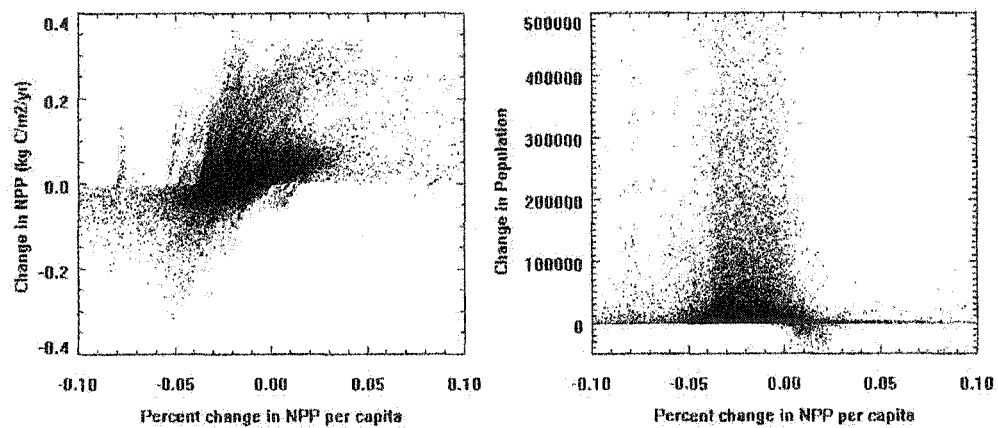
Figure 4.3. Changes in NPP per capita over the period 1982-1999 graphed against changes in NPP and changes in population. Positive changes in NPP per capita took place only where NPP increased and population declined or had only a modest increase.

94
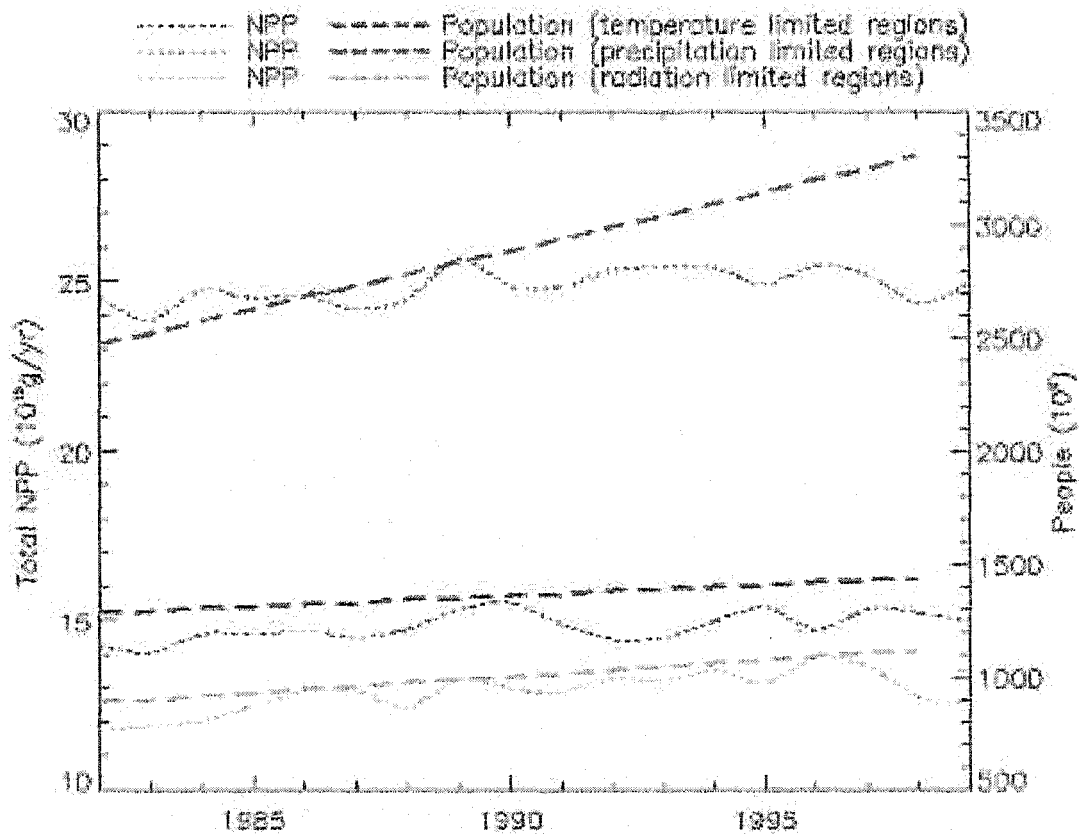
Figure 4.4. Times series of population (dashed line) and NPP (dotted line) for the period 1982-1999 by climatic constraints on NPP. Rates of population growth in the precipitation-limited regions were the highest and accompanied by the smallest positive trends in NPP. In all regions, population growth was steady, while NPP time series showed large interannual variability.

In all the grid cells where NPP per capita decreased, population increased and NPP either also decreased or increased too little to compensate for population growth, such as in water-limited areas (Figure 4.4).

Population distribution in relation to interannual variability in NPP

The monthly NPP regressed upon the monthly MEI values with a 6 months lag, filtered to show only the grid cells where the p-value <= 0.05, is displayed in Figure 4.5.

95

The regression depicts the 18-year average effect of ENSO-related climatic variability on NPP through altered patterns in precipitation, temperature and/or radiation availability.

Significant correlations between MEI and NPP (p-value <=0.05) are found over a total of 64 million km^2 (63% of the total vegetated surface), with changes in NPP per unit variation in MEI of up to 30 g $C/m^2/yr$. This surface is populated by a total of 3 350 million people. Negative correlations between MEI and NPP represent by far the prevailing pattern, being found over 78% (50 million km^2) of the surface showing significant teleconnections and 2 800 million people. The strongest decreases in NPP per unit variation in MEI in Central America, Venezuela, Guayana, Suriname and large portions of both the dominantly radiation limited and precipitation limited regions of Brazil, large portions of the sub-Saharan regions of Africa (with the exception of most of Angola, Zambia, Tanzania, Kenya and South Africa), east-central India and most of Southeast Asia and Southeastern Australia.

Positive variations per unit variations in MEI are stronger in western Canada and western United States, Peru, central Argentina, some portions of eastern Africa (mainly in Ethiopia and Kenya).

(gC/m²/yr)/MEI

-50   +50

Figure 4.5. Variations in NPP per unit variations of MEI. El Niño teleconnections affect more than 60% of the total vegetated areas and declines in NPP are the most common effect.

For more than 90% of the area displaying significant correlations between NPP and MEI, the relative variation in NPP per year is generally within ±10% of the average 1982-1999 NPP. Greater relative variations in NPP per unit variation in MEI take place in areas with progressively lower NPP.

Analyzing the spatial extent of the MEI-NPP relationship by climatic limits, it appears that 47% of the total affected area falls within water-limited regions, followed by 35% in the temperature-limited areas and 18% in the radiation-limited areas. Of the total population living in the affected areas, 53% is in the water-limited areas, followed by 23% in temperature- and 24% in radiation-limited areas.

Discussion

The distribution of population as a function of NPP indicates that humans are localized in areas with average to slightly above-average NPP. Because of the several ecosystem services associated with NPP, such as access to water and high soil fertility, many of these regions have been civilized for thousands of years. Some of the above-average productivity areas would probably show even higher NPP if less densely populated. The conversion of forests or grasslands into croplands and urban areas tends to lower the NPP (Houghton, 1999). It is noteworthy to observe that the regions of the world with the highest NPP, such as the tropical rainforests (radiation-limited areas) are still relatively sparsely populated. The fact that in these regions, the median land grid cell has a higher NPP than the median populated grid cell (Table 4.1) could indeed indicate that an increased human presence could decrease NPP. In less productive regions, on the other hand, the conversion of non-forested land into cropland has increased the NPP above the potential levels with the aid of irrigation and fertilization (DeFries, 2002). Examples can be found in some of the water-limited regions of China and India, which rely heavily on irrigation for 40% and 24% of their respective croplands (FAO, 2000). Humans, therefore, by increasing NPP above potential levels where it is low and reducing it below potential levels where it is high, create an intermediate productivity environment where they localize and maximize their activities. This phenomenon has an analog in nature, where woody species have been found to have highest species richness in intermediate productivity environments (Waring et al., 2002).

Although the changes in NPP observed during the period 1982-1999 probably helped mitigate the effects of increased human activities that took place during the same period, the results of the analysis presented in this chapter show that the per capita changes in NPP were heavily influenced by changes in population, which in most regions were by

98

far larger than the increase in vegetation productivity, especially in the water-limited regions (Figure 4.4). Among these, it is noteworthy that the African continent, which also has among the poorest populations, appears to have benefited the least from changes in NPP per capita over the period 1982-1999 (Figure 4.2).

The moderate increase in NPP observed during the past decade has come with a strong interannual variability, which in most of the years has surpassed in magnitude the global average increase in NPP. While it is too early to say whether the increasing trend in NPP will continue in the future, it is highly probable that the interannual variability will remain strong or even intensify (IPCC, 2001), and potentially continue to affect the regions currently inhabited by more than half of the global human population. As more than half of the total population living in regions with significant MEI-NPP correlations is found in water-limited areas, which also had the fastest population growth in 1982-1998 period, we can expect that the number of people living in regions sensitive to ENSO-related variability in vegetation productivity will continue to grow. The regions with the strongest variations in NPP associated to ENSO-related climatic variability were characterized by below average vegetation productivity, mostly grasslands and savanna (Potter et al., 2003), a characteristic that probably made the local population even more sensitive to climatic fluctuations. The analysis presented here identifies *potentially* sensitive populations to ENSO events because it defines the regions where NPP has displayed significant correlations with MEI over an 18-year period. How these changes in NPP impact societies is highly variable and depends also on a number of other predisposing factors, such as government policies, human diseases, dependence on regional water and power supply, conflicts, unfavorable markets, lack of credit, unavailable storage and shipping facilities, and many others (Glantz, 2001a).

Decreases in NPP, mostly caused by droughts and wildfires, were the most frequent result of this variability. The decreases in NPP resulting from ENSO teleconnections

observed over most of the African continent, which also showed widespread decreases in NPP per capita over the period 1982-1999 (Figure 4.2), indicate that here populations may have a higher potential sensitivity to future intensifications of interannual climatic variability. Even where the variability was associated with an increase in NPP, this may not have been always a positive event since it could have come along with floods, causing losses of lives and destruction of infrastructure. Heavy rains during ENSO events have also been associated with the outbreaks of waterborne and vector transmitted diseases (Epstein, 1999; Linthicum et al., 1999).

ENSO events are never exactly the same even in regions strongly influenced, because they interact with other components of the local climate, which can vary from year to year. Nonetheless, mapping average teleconnections and identifying how many people live in the areas potentially affected could be used for improving the preparedness of both international aid agencies and of local populations, which could benefit of an unbiased early-warning system (Glantz, 2001b). For many regions of the world, where the climatological network is sparse and data require manual collection rather than being distributed online, it is otherwise difficult to estimate the spatial impact of climatic variability in an objective way, without relying on local officials, which may have the interest to inflate or deflate this type of information. Even when climate data are available to be analyzed in real-time, an integrated ecological measure such as NPP is a better parameter than precipitation or temperature alone.

As we continue to improve our understanding of climatic teleconnections and their effect on NPP, enhancing our ability of seasonal or annual forecasting, it is important that we keep monitoring human population dynamics. By further incorporating other types of socio-economic information into the monitoring process, the vulnerable portion of the population (i.e., likely to be exposed to and adversely affected (Cutter, 1996)),

could also be identified and this information could be potentially highly valuable to policy makers.

A continuous monitoring of the global NPP distribution at a 5-10 year is part of taking the Earth's pulse and evaluating the effect of direct (land cover conversions) and indirect (human induced climatic changes) anthropogenic effects on ecosystems. The analysis presented in this chapter makes use of a global NPP data set calculated at 0.5-degree spatial resolution, but standard yearly NPP data from the Earth Observing System at 1-km resolution will vastly enhance the detail of this analysis and the potential for future monitoring (Running et al., 2004; Running et al., 2000). Incorporating population data, already available as a gridded data set at 1-km resolution, into the regular monitoring of global NPP is the first step toward the regular integration of socio-economic information into the spatial analysis of ecological variables and long term measures of per capita NPP could perhaps contribute as an unbiased, easy to measure, sustainability index. A remote sensing based detection of an anomaly in NPP, while not sufficient to identify the cause of a disturbance nor the consequence in terms, for example, of pollution or biodiversity, could also serve as an unbiased measure for the validation of a problem of anthropogenic pressure detected on the ground, and help identifying its spatial extent. Moreover, the satellite-based monitoring of NPP could also serve to raise a red flag before widespread ecological effects of an alteration in vegetation productivity are sensed on the ground although insight into setting priorities for mitigation requires the incorporation of further socio-economic information. Future work should also include the standard translation of NPP into variables holding more tangible economic and societal meaning, such as crop yield and timber production.

Appendix A

Estimates of global population reported by the World Resource Institute (WRI) and estimated in this study by resampling the LandScan 1998 data and subtracting the average 1982-1998 population growth.

Year	Global Population (WRI)	Global Population (this study)
	Million of people	Million of people
1982	4 582	4 702
1983	4 661	4 778
1984	4 742	4 854
1985	4 824	4 929
1986	4 909	5 005
1987	4 995	5 081
1988	5 082	5 157
1989	5 169	5 233
1990	5 255	5 309
1991	5 334	5 385
1992	5 420	5 461
1993	5 501	5 536
1994	5 581	5 612
1995	5 662	5 688
1996	5 741	5 764
1997	5 847	5 840
1998	5 900	5 921

REFERENCES

Alig, R.J. and Healy, R.G., 1987. Urban and built-up land area changes in the United States: An empirical investigation of determinants. Land Economics, 63(3): 215-226.

Balling, R.C. and Brazel, S.W., 1987. Time and space characteristics of the Phoenix urban heat island. Journal of the Arizona-Nevada Academy of Science, 21: 75-81.

Bandaranayake, W., Qian, Y.L., Parton, W.J., Ojima, D.S. and Follett, R.F., 2003. Estimation of soil organic carbon changes in turfgrass systems using the CENTURY model. Agronomy Journal, 95: 558-563.

Beard, J.B., 1973. Turfgrass: science and culture. Prentice Hall, Englewood Cliffs, NJ, 658 pp.

Berry, B., 1990. Urbanization. In: B.L.T. II et al. (Editors), The Earth as transformed by human action. Cambridge Univ. Press with Clark University, Cambridge, NY, pp. 103-119.

Brazel, A., Selover, N., Vose, R. and Heisler, G., 2000. The tale of two climates - Baltimore and Phoenix urban LTER sites. Climate Research, 15: 123-135.

Carlson, T.N. and Arthur, S.T., 2000. The impact of land use - land cover changes due to urbanization on surface microclimate and hydrology : a satellite perspective. Global and Planetary Change, 25: 49-65.

Cayan, D.R. and Douglas, A.V., 1984. Urban influences on surface temperatures in the southwestern United States in the recent decades. Journal of Climate and Applied Meteorology, 23: 1520-1530.

Center for International Earth Science Information Network (CIESIN), Columbia University; International Food Policy Research Institute (IFPRI); and World Resources Institute (WRI), 2000. Gridded Population of the World (GPW), Version 2.

Chapin, F.S., III, Zavaleta, E.S., Eviner, V.T., Naylor, R.L., Vitousek, P.M., Reynolds, H.L., et al., 2000. Consequences of changing biodiversity. Nature, 405: 234-242.

Clark, W.C., and Dickson, N.M., 2003. Science and Technology for Sustainable Development Special Feature: Sustainability science: The emerging research program. PNAS, 100:8059-8061.

Cutter, S.L., 1996. Vulnerability to environmental hazards. Progress in Human Geography, 20:529-539.

Daily, G. (Editor), 1997. Nature's Services: Societal Dependence on Natural Ecosystems. Island Press, Washington, DC, 412 pp.

Daily, G. Dasgupta, P., Bolin, B., Crosson, P., du Guerny, J., Ehrlich, P. et al., 1998. Global Food Supply: Food Production, Population Growth, and the Environment. Science, 281(5381): 1291-1292.

Daily, G.C. Alexander, S., Ehrlich, P.R., Goulder, L., Lubchenco, J., Matson, P.A. et al., 1997. Ecosystem services: benefits supplied to human societies by natural ecosystems. Issues in Ecology, 2: 1-16.

DeFries, R.S., Field, C.B., Fung, I., Collatz, G.J. and Bounoua, L., 1999. Combining satellite data and biogeochemical models to estimate global effects of human induced land cover change on carbon emissions and net primary productivity. Global Biogeochemical Cycles, 13(3): 803-815

DeFries, R.S., 2002. Past and Future Sensitivity of Primary Production to Human Modification of the Landscape. Geophysical Research Letters, 10.1029/2001GL013620.

Dobson, J.E., Bright, E.A., Coleman, P.R., Durfee, R.C. and Worley, B.A., 2000. Landscan: a global population database for estimating population at risk. Photogrammetric Engineering & Remote Sensing, 66(7): 849-857.

104

Doll, C.N.H., Muller, J.-P. and Elvidge, C.D., 2000. Night-time imagery as a tool for global mapping of socioeconomic parameters and greenhouse emissions. Ambio, 29(3): 157-162.

Dow, C.L. and DeWalle, D.R., 2000. Trends in evaporation and Bowen ratio on urbanizing watersheds in eastern United States. Water Resources Research, 36: 1835-1843.

DPRA Incorporated, 1992. Benefit analysis of insecticide use on turf: Preliminary biological and economic profile report., Manhattan, Kansas.

Dwyer, J.F., Nowak, D.J., Noble, M.H. and Sisinni, S.M., 2000. Connecting people with ecosystems in the 21st century: an assessment of our nation's urban forests. PNW-GTR-490, U.S. Department of Agriculture, Forest Service, Pacific Northwest Station, Portland, OR.

Easterling, D.R., 2002. Recent changes in frost days and the frost-free season in the United States. Bulletin of the American Meteorological Society, 83(9): 1327-1332.

Elvidge, C.D., Baugh, K.E., Hobson, V.R., Kihn, E.A., Kroehl, H.W., Davis, E.R. and Coceros, D., 1997a. Satellite inventory of human settlements using nocturnal radiation emissions: a contribution for the global toolchest. Global Change Biology, 3: 387-395.

Elvidge, C.D., Baugh, K.E., Kihn, E.A., Kroehl, H.W. and Davis, E.R., 1997b. Mapping city lights with nighttime data from the DMSP Operational Linescan System. Photogrammetric Engineering & Remote Sensing, 63(6): 727-734.

Elvidge, C.D. Baugh, K.E., Dietz, J.B., Bland, T., Sutton, P.C. and Kroehl, H.W., 1999. Radiance calibration of DMSP-OLS low light imaging data of human settlements. Remote Sensing of Environment, 68(1): 77-88.

Elvidge, C.D., Imhoff, M.L., Baugh, K.E., Hobson, V.R., Nelson, I. and Dietz, J.B., 2001. Nighttime lights of the world: 1994-1995. ISPRS Journal of Photogrammetry and Remote Sensing, 56(ER2): 81-99.

Elvidge, C.D., Milesi, C., Dietz, J.B., Tuttle, B.J., Sutton, P.C., Nemani, R., and Vogelmann, J.E. U.S. Constructed Area Approaches the Size of Ohio. Eos, Transactions, American Geophysical Union. *In press.*

EPA, E.P.A. 2003. Municipal Solid Waste in the United States: 2001 Final Report. EPA530-R-03-011. Office of Solid Waste and Emergency Response, 170 pp.

Epstein, P., 1999. Climate and health. Science, 285: 347.

Falk, J.H., 1976. Energetics of a suburban lawn ecosystem. Ecology, 57: 141-150.

FAO, FAOSTAT database. Land, Available online at: http://apps.fao.org/.

Field, C.B. 2001. Sharing the garden. Science, 294: 2490-2491.

Field, C.B., Randerson, J.T. and Malmström, C.M., 1995. Global net primary production: Combining ecology and remote sensing. Remote Sensing of Environment, 51:74-88.

Fulton, W., Pendall, R., Nguyen, M. and Harrison, A., 2001. Who sprawls the most? How growth patterns differ across the U.S., The Brookings Institution Survey Series, pp. 24.

Gallo, K.P. and Owen, T.W., 1999. Satellite-based adjustments for the urban heat-island temperature bias. Journal of Applied Meteorology, 38: 806-813.

Glantz, M.H., 2001a. Currents of change: Impacts of El Niño and La Niña on climate and society. Cambridge University Press, Cambridge, 266 pp.

Glantz, M.H. (Editor), 2001b. Once Burned, Twice Shy? Lessons Learned from the 1997-98 El Niño. UN University Press, Tokyo, Japan, 294 pp.

Goward, S., and Huemmrich, K., 1992. Vegetation canopy PAR absorptance and the Normalized Difference Vegetation Index: An assessment using the SAIL model. Remote Sensing of Environment, 39:119-140.

Grounds Maintenance, 1996. Turf acreage. Grounds Maintenance, 31(5):10.

Harivandi, M.A., Hagan, W.B. and Elmore, C.L., 1996. The use of recycling mowers in grasscycling. California Turfgrass Culture, 46(1-2): 4-6.

Heckman, J.R., Liu, H., Hill, W., DeMilia, M. and Anastasia, W.L., 2000. Kentucky bluegrass responses to mowing practices and nitrogen fertility management. Journal of Sustainable Agriculture, 15(4): 25-33.

Heimlich, R.E. and Anderson, W.D., 2001. Development at the urban fringe and beyond. Agricultural Economic Report No. 803, U.S. Department of Agriculture, Economic Research Service, Washington, D.C.

Henderson, M., Yeh, E.T., Gong, P., Elvidge, C.D. and Baugh, K., 2003. Validation of urban boundaries derived from global night-time satellite imagery. International Journal of Remote Sensing, 24(3): 595-609.

Houghton, R.A., 1999. The annual net flux of carbon to the atmosphere from changes in land use 1850-1990. Tellus B, 51(2): 298-313.

Huete, A., Justice, C. and van Leeuwen, W., 1999. MODIS vegetation index (MOD 13) Algorithm Theoretical Basis Document, 120 pp.

Huete, A., Didan, K., Miura, T., Rodriguez, E.P., Gao, X. and Ferreira, L.G., 2002. Overview of the radiometric and biophysical performance of the MODIS vegetation indices. Remote Sensing of Environment, 83: 195-213.

Hunt, E.R.J., Piper, S.C., Nemani, R., Keeling, C.D., Otto, R.D. and Running, S.W., 1996. Global net carbon exchange and intra-annual atmospheric CO_2 concentrations predicted by an ecosystem process model and three-dimensional atmospheric transport model. Global Biogeochemical Cycles, 10(3): 431-456.

Imhoff, M., Tucker, C., Lawrence, W. and Stutzer, D., 2000. The use of multisource satellite and geospatial data to study the effect of urbanization on primary

107

productivity in the United States. IEEE Transactions on Geoscience and Remote Sensing, 38(6): 2549-2556.

Imhoff, M.L., Lawrence, W.T., Elvidge, C.D., Paul, T., Levine, E., Privalsky, M.V.and Brown, V., 1997a. Using Nighttime DMSP/OLS images of city lights to estimates the impact of urban land use on soil resources in the United States. Remote Sensing of Environment, 59(1): 105-117.

Imhoff, M.L., Lawrence, W.T., Stutzer, D.C. and Elvidge, C.D., 1997b. A technique for using composite DMSP/OLS "city lights" satellite data to map urban areas. Remote Sensing of Environment, 61(3): 361-370.

IPCC (Editor), 2001. Climate Change 2001: Impacts, Adaptation and Vulnerability - Contribution of Working Group II to the Third Assessment Report of IPCC. Cambridge University Press, Cambridge, UK, 1000 pp.

James, M.E. and Kalluri, S.N.V., 1994. The Pathfinder AVHRR land data set: An improved coarse resolution data set for terrestrial monitoring. International Journal of Remote Sensing, 15(17): 3347-3364.

Jenkins, V.S., 1994. The Lawn: A History of an American Obsession. Smithsonian Institution Press, 246 pp.

Karl, T.R., Diaz, H.F. and Kukla, G., 1988. Urbanization: its detection and effect in the Unites States Climate Record. Journal of Climate, 1: 1099-1123.

Karl, T.R., and Knight, R.W., 1998. Secular trends of precipitation amount, frequency, and intensity in the United States. Bulletin of the American Meteorological Society, 79:231-241.

Keeling, C.D., Chin, J.F.S. and Whorf, T.P., 1996. Increased activity of northern vegetation inferred from atmospheric CO_2 measurements. Nature, 382(6587): 146-149.

Kimball, J.S., White, M.A. and Running, S.W., 1997. BIOME-BGC simulations of stand hydrologic processes for BOREAS. Journal of Geophysical Research, 102(D24): 29043-29051.

Knyazikhin, Y. et al., 1999. MODIS Leaf Area Index (LAI) and Fraction of Photosynthetically Active Radiation absorbed by vegetation (FPAR) product (MOD15).

Kopp, K.L. and Guillard, K., 2002. Clipping management and nitrogen fertilization of turfgrass: growth, nitrogen utilization, and quality. Crop Science, 42: 1225-1231.

Lahmeyer, J., Populstat: historical demography of all countries, their divisions and towns, Available online at: http://www.library.uu.nl/wesp/populstat/populframe.html.

Landsberg, H.E., 1981. The Urban Climate. International Geophysics Series, 28. Academic Press, New York, 275 pp.

Leemans, R. and Cramer, W.P., 1991. The IIASA database for mean monthly values of temperature, precipitation and cloudiness of a global terrestrial grid. RR-91-18, International Institute of Applied Systems Analyses, Laxenburg.

Linthicum, K. et al., 1999. Climate and satellite indicators to forecast Rift Valley fever epidemics. Science, 285: 397-400

Lougeay, R., Brazel, A. and Hubble, M., 1996. Monitoring intraurban temperature patterns and associated land cover in Phoenix, Arizona using Landsat thermal data. Geocarto International, 11(4): 79-90.

Lowery, J., 1996. City of the month: Atlanta, Georgia. City Trees, 32(2).

Mayer, P.W., DeOreo, W.B., Opitz, E.M., Kiefer, J.C., Davis, W.Y., Dziegielewski, B. and Nelson, J.O., 1999. Residential End Uses of Water. American Water Works Association. 310 pp.

McDonnell, M.J., Pickett, S.T.A., Groffman, P., Bohlen, P., Pouyat, R.V., Zipperer, W.C., et al., 1997. Ecosystem processes along an urban-to-rural gradient. Urban Ecosystems, 1: 21-36.

McNaughton, S.J., Oesterheld, M., Frank, D.A. and Williams, K.J., 1989. Ecosystem-level patterns of primary productivity and herbivory in terrestrial habitats. Nature, 341: 143-146.

Milesi, C., Elvidge, C.D., Nemani, R.R. and Running, S.W., 2003. Assessing the impact of urban land development on net primary productivity in the southeastern United States. Remote Sensing of Environment, 86(3): 273-432.

Miller, D.A. and White, R.A., 1998. A Conterminous United States Multi-Layer Soil Characteristics Data Set for Regional Climate and Hydrology Modeling. Earth Interactions, 2.

Myneni, R., Nemani, R. and Running, S., 1997. Estimation of global leaf area index and absorbed PAR using radiative transfer models. IEEE Transactions on Geoscience and Remote Sensing, 35(6): 1380-1393.

National Association of Realtors, 2001. Land use and land loss in the United States: the impact of land use trends on real estate development, The Research Division of the National Association of Realtors. 9 pp.

NCDC, National Climatic Data Center - U.S. Cities Analysis. Available online at: http://lwf.ncdc.noaa.gov/oa/climate/research/cag3/city.html.

Nemani, R., White, M., Thornton, P., Nishida, K., Reddy, S., Jenkins, J. and Running. S., 2002. Recent trends in hydrologic balance have enhanced the terrestrial carbon sink in the United States. Geophysical Research Letters, 29(10.1029/2002GL014867).

Nemani, R.R., Keeling, C.D., Hashimoto, H., Jolly, W.M., Piper, S.C., Tucker, C.J., Myneni, R.B. and Running, S.W., 2003. Climate-Driven Increases in Global

110

Terrestrial Net Primary Production from 1982 to 1999. Science, 300(5625): 1560-1563.

Nowak, D.J., Noble, M.H., Sisinni, S.M. and Dwyer, J.F., 2001. People & trees: Assessing the US urban forest resource. Journal of Forestry, 99: 37-42.

Oke, T.R., 1973. City size and the urban heat island. Atmospheric Environment, 7: 769-779.

Oke, T.R., 1978. Boundary layer climates. Methuen, London, 372 pp.

Oke, T.R., 1989. The micrometeorology of the urban forest. Phylosophical Transactions of the Royal Society of London B, 324: 335-349.

Owen, T.W., Carlson, T.N. and Gillies, R.R., 1998a. An assessment of satellite remotely-sensed land cover parameters in quantitatively describing the climatic effect of urbanization. International Journal of Remote Sensing, 19(9): 1663-1681.

Owen, T.W., Gallo, K.P., Elvidge, C.D. and Baugh, K.E., 1998b. Using DMSP-OLS light frequency data to categorize urban environments associated with US climate observing stations. International Journal of Remote Sensing, 19(17): 3451-3456.

Pacala, S.W., Hurtt, G.C., Baker, D., Peylin, P., Houghton, R.A., Birdsey, R.A., Heath, L., Sundquist, E.T., Stallard, R.F., Ciais, P., Moorcroft, P., Caspersen, J.P., Shevliakova, E., Moore, B., Kohlmaier, G., Holland, E., Gloor, M., Harmon, M.E., Fan, S.-M., Sarmiento, J.L., Goodale, C.L., Schimel, D. and Field, C.B., 2001. Consistent Land- and Atmosphere-Based U.S. Carbon Sink Estimates. Science, 292:2316-2320.

Paruelo, J.M., Burke, I.C. and Lauenroth, W.K., 2001. Land-use impact on ecosystem functioning in eastern Colorado, USA. Global Change Biology, 7: 631-639.

Petrovic, A., 1990. The fate of nitrogenous fertilizers applied to turfgrass. Journal of Environmental Quality, 19(1): 1-14.

111

Philander, S.G., 1990. El Niño, La Niña, and the Southern Oscillation. International Geophysics Series, 46. Academic Press, San Diego, CA.

Pielke, S.R.A., 1999. The influence of anthropogenic landscape changes on weather in south Florida. Monthly Weather Review, 127: 1663-1673.

Potter, C. et al., 2003. Major disturbance events in terrestrial ecosystems detected using global satellite data sets. Global Change Biology, 9(7): 1005-1021.

Priestley, C.H.B., and Taylor, R.J., 1972. On the assessment of surface heat flux and evaporation using large-scale parameters. Monthly Weather Review, 100:81-92.

Qian, Y. and Follett, R.F., 2002. Assessing soil carbon sequestration in turfgrass systems using long-term soil testing data. Agronomy Journal, 94: 930-935.

Quattrochi, D.A., Luvall, J.C., Rickman, D.L., Estes, M.G.J., Laymon, C.A. and Howell, B.F., 2000. A decision support information system for urban landscape management using thermal infrared data. Photogrammetric Engineering & Remote Sensing, 66(10): 1195-1207.

Rindfuss, R.R., and Stern, P.C., 1998. Linking remote sensing and social sciences: the need and the challenges, pp. 1-27, *In* D. Liverman, et al., eds. People and Pixels: Linking Remote Sensing and Social Science. National Academy Press, Washigton, D.C.

Robbins, P., and Birkenholtz, T, 2003. Turfgrass revolution: measuring the expansion of the American lawn. Land Use Policy, 20:181-194.

Robbins, P., Polderman, A. and Birkenholtz, T., 2001. Lawns and toxins: an ecology of the city. Cities, 18(6): 369-380.

Roberts, E.C. and Roberts, B.C., 1987. Lawn and Sports Turf Benefits. The Lawn Institute, Pleasant Hill, TN, 31 pp.

RReDC, Renewable Resource Data Center - Solar Radiation Resource Information. Available online at: http://rredc.nrel.gov/solar/.

112

Running, S.W., 1994. Testing Forest-BGC ecosystem process simulations across a climatic gradient in Oregon. Ecological Applications, 4(2): 238-247.

Running, S.W. and Coughlan, J.C., 1988. A general model of forest ecosystem processes for regional applications. I. Hydrological balance, canopy gas exchange and primary production processes. Ecological Modeling, 42: 125-154.

Running, S.W. and Gower, S.T., 1991. FOREST BGC, A general model of forest ecosystem processes for regional applications. II. Dynamic carbon allocation and nitrogen budgets. Tree Physiology, 9: 147-160.

Running, S.W. and Hunt, R.E.J., 1993. Generalization of a forest ecosystem process model for other biomes, BIOME-BGC, and an application for global-scale models. In: J.R. Ehleringer and C.B. Field (Editors), Scaling physiological processes: leaf to globe. San Diego, Academic Press, Inc., pp. 141-157.

Running, S.W. and Nemani, R.R., 1988. Relating seasonal patterns of the AVHRR vegetation index to simulated photosynthesis and transpiration of forests in different climates. Remote Sensing of Environment, 24: 347-367.

Running, S.W., Thornton, P.E., Nemani, R. and Glassy, J.M., 2000. Global terrestrial gross and net primary productivity from the Earth Observing System. In: O. Sala, R. Jackson and H. Mooney (Editors), Methods in Ecosystem Science. Springer-Verlag, New York, pp. 44-57.

Running, S. W., Nemani, R. R., Heinsch, F. A., Zhao, M., Reeves, M. & Hashimoto, H., 2004. A Continuous Satellite-Derived Measure of Global Terrestrial Primary Productivity: Future Science and Applications. Bioscience. *In press*

Saugier, B., Roy, J. and Mooney, H.A., 2001. Estimations of global terrestrial productivity: Converging toward a single number? In: J. Roy, B. Saugier and H.A. Mooney (Editors), Terrestrial Global Productivity. Academic Press, San Diego, CA, pp. 543-557.

113

Schlesinger, W.H., 1997. Biogeochemistry: An analysis of global change. Academic

Press, San Diego, CA, 678 pp.

Schultz, W., 1999. A man's turf: the perfect lawn. Clarkson N. Potter, New York, 180 pp.

Shepherd, J.M. and Burian, S.J., 2003. Detection of Urban-Induced Rainfall Anomalies

in a Major Coastal City. Earth Interactions, 7(7): 006.

Solley, W.B., Pierce, R.R. and Perlman, H.A., 1998. Estimated Use of Water in the

United States in 1995. 1200, U.S. Geological Survey Circular 1200, Denver,

Colorado.

Spronken-Smith, R.A., Oke, T.R. and Lowry, W.P., 2000. Advection and the surface

energy balance across an irrigated urban park. International Journal of Climatology,

20: 1033-1047.

Stoll, M.J. and Brazel, A.J., 1992. Surface-air temperature relationships in the urban

environment of Phoenix. Physical Geography, 13(2): 160-179.

Sutton, P., Roberts, D., Elvidge, C. and Baugh, K., 2001. Census from Heaven: an

estimate of the global human population using night-time satellite imagery.

International Journal of Remote Sensing, 22(16): 3061-3076.

Sutton, P., Roberts, D., Elvidge, C. and Meij, H., 1997. A comparison of nighttime

satellite imagery and population density for the continental United States.

Photogrammetric Engineering & Remote Sensing, 63(11): 1303-1313.

Thornton, P.E., 2000. User's Guide for Biome-BGC, Version 4.1.1, Numerical

Terradynamic Simulation Group, School of Forestry, University of Montana,

Missoula, MT.

Thornton, P.E., Running, S.W. and White, M.A., 1997. Generating surfaces of daily

meteorological variables over large regions of complex terrain. Journal of Hydrology,

190: 214-251.

Time-Life Books, 2000. Complete Garden Guide: A Comprehensive Reference for All Your Garden Needs, 992 pp.

Tobler, W., U. Deichmann, J. Gottsegen, and K. Maloy. 1995. The Global Demography Project Technical Report TR-95-6. National Center for Geographic Information and Analysis, Department of Geography, University of California, Santa Barbara CA.

Torok, S.J., Morris, C.J.G., Skinner, C. and Plummer, N., 2001. Urban heat island features of souhtheast Australian towns. Australian Meteorological Magazine, 50: 1-13.

Tucker, C.J., Fung, I.Y., Keeling, C.D. and Gammon, R.H., 1986. Relationship between atmospheric CO_2 variations and a satellite-derived vegetation index. Nature, 319: 195-199.

Tucker, C., and Sellers, P., 1986. Satellite remote sensing of primary production. International Journal of Remote Sensing, 7:1395-1416.

U.S. Bureau of the Census, 1999. American Housing Survey for the United States: 1999. Available at: http://www.census.gov/hhes/www/housing/ahs/ahs99/ahs99.html (last update: February 26, 2003).

U.S. Census Bureau, 2000a. County and City Data Book: 2000. U.S. Government Printing Office, Washington DC.

U.S. Census Bureau, 2000b. Metropolitan Area Population Estimates for July 1, 1999 and Population Change for April 1, 1990 to July 1, 1999 (includes April 1, 1990 Population Estimates Base), Available online at: http://eire.census.gov/popest/archives/metro/ma99-01.txt.

U.S. Department of Housing and Urban Development, 2000. The State of the Cities 2000: Megaforces shaping the future of the nation's cities. 4th annual report.

U.S. Environmental Protection Agency, 2000. Our built and natural environments: A technical review of the interactions between land use, transportation and environmental quality. EPA 231-R-00-005.

UN, 2003. World Population Prospects: The 2002 Revision. Population Division of the Department of Economic and Social Affairs of the United Nations Secretariat, http://esa.un.org/unpp, (22 August, 2003)

Unger, J., Sümeghy, Z., Bottyán, Z. and Mucsi, L., 2001. Land-use and meteorological aspects of the urban heat island. Meteorological Applications, 8: 189-194.

Van Dersal, W., 1936. The ecology of a lawn. Ecology, 17:515-527.

Vinlove, F.K. and Torla, R.F., 1995. Comparative estimations of U.S. home lawn area. Journal of Turfgrass Management, 1(1): 83-97.

Vogelmann, J.E., Howard, S.M., Yang, L., Larson, C.R., Wylie, B.K. and Van Driel, N., 2001. Completion of the 1990s National Land Cover Data set for the conterminous United States from Landsat Thematic Mapper data and ancillary data sources. Photogrammetric Engineering & Remote Sensing, 67: 650-662.

Wan, Z., 2001. MODIS Land Surface Temperature Products Users' Guide. 75 pp.

Wan, Z., Zhang, Y., Zhang, Q. and Li, Z.-L., 2002. Validation of the land-surface temperature products retrieved from Terra Moderate Resolution Imaging Spectroradiometer data. Remote Sensing of Environment, 83: 163-180.

Waring, R.H., N.C. Coops, J.L. Ohmann, and D.A. Sarr. 2002. Interpreting woody plant richness from seasonal ratios of photosynthesis. Ecology 83:2964-2970.

Wear, D.N. and Greis, J.G., 2001. The Southern Forest Resource Assessment Draft Summary Report.

White, M., Thornton, P., Running, S., and Nemani, R., 2000. Parameterization and sensitivity analysis of the BIOME-BGC terrestrial ecosystem model: net primary production controls. Earth Interactions 4:1-85.

White, M.A., Nemani, R.R., Thornton, P.E. and Running, S.W., 2002. Satellite evidence of phenological differences between urbanized and rural areas of the eastern United States deciduous broadleaf forest. Ecosystems, 5: 260-277.

Wolter, K. and Timlin, M.S., 1988. Measuring the strength of ENSO events - how does 1997/98 rank? Weather, 53: 315-324.

WRI, 2003. World Resources 2002-2004: decisions for the Earth: balance, voice, and power. *WRI; UNEP; UNDP; World Bank*. 400 pp.

Zhou, L., Tucker, C.J., Kaufmann, R.K., Slayback, D., Shabanov, N.V. and Myneni, R.B., 2001. Variations in northern vegetation activity inferred from satellite data of vegetation index during 1981-1999. Journal of Geophysical Research, 106(D17): 20069-20083.